

FOG

Freiberg Online Geology

FOG is an electronic journal registered under ISSN 1434-7512



2008, VOL 19

University Of Dhaka



Seasonal changes in the arsenic distribution of newly drilled wells tapping different aquifers in the Bangladesh delta



Joerg Steinborn

LIST OF FIGURES	IV
LIST OF TABLES	VI
LIST OF APPENDICES	VI
LIST OF ABBREVIATIONS	VII
ABSTRACT	1
1. OBJECTIVES AND DELIVERABLES	2
1.1. OBJECTIVES	2
1.2. DELIVERABLES	3
2. BANGLADESH – A GENERAL INTRODUCTION TO THE GEOGENIC ARSENIC CONTAMINATION	4
3. DESCRIPTION OF THE INVESTIGATION AREA	13
3.1. STUDY AREA - SELECTION CRITERIA AND SPECIFICS	13
3.2. VEGETATION AND LAND USE	14
3.3. CLIMATE	15
3.4. GEOLOGY	16
3.4.1. GEOLOGY AND GEOMORPHOLOGY	16
3.4.2. GEOLOGICAL EVOLUTION OF THE BENGAL BASIN	18
3.4.3. LITHOLOGICAL UNITS – STRATIGRAPHY	20
3.4.4. HYDROGEOLOGY	22
3.5. HYDROGEOCHEMISTRY	24
4. METHODOLOGY	26
4.1. FIELD ACTIVITIES	26
4.1.1. CORE DRILLING AND TEST FIELD SETUP	26
4.1.2. MONITORING	29
4.1.2.1. Electrochemical parameters	30
4.1.2.2. Photometry	32
4.1.2.3. Sample preservation	34
4.1.2.4. Mapping	35
4.2. LABORATORY	36
4.2.1. DOC/ TIC	36
4.2.2. IC – CATIONS	37
4.2.3. IC – ANIONS	37
4.2.4. IC – ICP – MS	38
4.3. REMOTE SENSING	39
4.3.1. TNTATLAS – IMPORTANT TOOLS	41

5. RESULTS AND DISCUSSION	42
5.1. DIGITAL ATLAS	42
5.1.1. GROUPS AND LAYERS	42
5.1.2. LEGENDS OF THE LAYERS	44
5.2. HYDROGEOCHEMISTRY	47
5.2.1. DATA EVALUATION	47
5.2.1.1. Charge imbalance by PhreeqC	47
5.2.1.2. Measured vs. Calculated Specific Conductance after ROSSUM (1975)	49
5.2.1.3. As/P totals vs. sum of As/P species	51
5.2.2. SPATIAL DISTRIBUTION	53
5.2.3 DEPTH DEPENDENT HYDROCHEMICAL CHANGES	63
5.2.4 SEASONAL HYDROCHEMICAL CHANGES	74
6. RECOMMENDATIONS	82
7. ACKNOWLEDGEMENTS	84
8. REFERENCES	85
9. APPENDIX	89

List of figures

Fig.2.1.	Distribution of As in groundwater from shallow tube wells in Bangladesh	5
Fig.2.2.	(a) Arsenite and (b) arsenate speciation as a function of pH	7
Fig.2.3.	Eh-pH diagram for aqueous As species in the system As-O ₂ -H ₂ O at 25°C	8
Fig.2.4.	Eh/pe-pH diagram for aqueous P species	10
Fig.3.1.1.	BGS“special study areas”(left); Satellite Image from study area (right)	13
Fig.3.3.1.	Climate chart for Comilla district, Bangladesh	15
Fig.3.4.1.1.	Main geomorphologic units of Bangladesh	17
Fig.3.4.2.1.	Surrounding regions of the Bengal Basin	18
Fig.3.4.2.2.	Tectonic elements of the GBM delta system	19
Fig.3.4.3.1.	Drilling profile	21
Fig.3.4.4.1.	Hydrogeological cross section from Bangladesh’s North to South	23
Fig.4.1.1.1.	Overview of well configuration at the test field	27
Fig.4.1.1.2.	Well construction by the local „hand flapping“ method	28
Fig.4.1.2.1.	Sampling procedure for village wells	29
Fig.5.2.1.1.1.	Calculated charge imbalances for (a) mapped wells and (b) monitoring wells	48
Fig.5.2.1.2.1.	Comparison of measured conductivity with calculated conductivity	50
Fig.5.2.1.3.1.	Phosphorus (a) and arsenic (b) in comparison to sum of species	52
Fig.5.2.2.1.	Distribution of (a) total arsenic and (b) total phosphorus vs. depth	54
Fig.5.2.2.2a.	Contour line plots for As(tot), P(tot), As(III), As(V)	55
Fig.5.2.2.2b.	Contour line plots for Eh, Fe(tot), Mn(tot), Phosphate	56
Fig.5.2.2.3.	Piper diagram for groundwater characterisation	57
Fig.5.2.2.4.	Ammonia vs. As(tot) as well as As(III)	58
Fig.5.2.2.5.	As(tot) vs. P(tot), Fe(tot), Mn(tot), Eh, HCO ₃ ⁻ and SO ₄	59
Fig.5.2.2.6.	Comparison As(tot) for the (a) test field and (b) mapping against depth	61
Fig.5.2.2.7.	Total arsenic (a) and total phosphorus (b) vs. well-age	62
Fig.5.2.3.1.	Depth profile of the core drilling and the test field	64
Fig.5.2.3.2.	Reduced grey sand vs. oxidised, brown sand	65
Fig.5.2.3.3.	Vertical profile of hydrochemical mean characteristics at the test field	67
Fig.5.2.3.4.	Total As vs. total phosphorus	68
Fig.5.2.3.5.	Total phosphorus vs. NH ₄	69

Fig.5.2.3.6. Total arsenic vs. SO ₄	70
Fig.5.2.3.7. Model of how arsenic pollution occurs in shallow wells	71
Fig.5.2.4.1. Mean monthly P and T over the last 10 years (1997 – 2006) in comparison to the mean monthly precipitation and temperature during the period of investigation	74
Fig.5.2.4.2. Mean groundwater table in comparison to the daily rainfall	76
Fig.5.2.4.3. Seasonal changes of As(tot) in different depths of the test field	78
Fig.5.2.4.4. Seasonal changes of arsenite in different depths of the test field	80

List of tables

Table 4.1.2.4.	Mapped household wells	35
Table 4.2.1.1.	Device-specific attributes for TIC/DOC speciation	36
Table 4.2.2.1.	Detection limits for cation analysis	37
Table 4.2.3.1.	Detection limits for anion analysis	37
Table 5.2.1.2.1.	Wells with charge imbalances > + 10 %	51
Table 5.2.4.1.	Infiltration time of deposition according to HAZEN;	77
Table 5.2.4.2.	Well by well correlation between total arsenic and total phosphorus	81

List of appendices

Appendix 1a:	Comparison of measured conductivity and calculated conductivity	90
Appendix 1b:	Mean percent error between measured and calculated conductance	92
Appendix 2a:	Comparison of total arsenic with sum of arsenic species	92
Appendix 2b:	Comparison of total phosphorus with sum of phosphorus species	93
Appendix 3:	Dendrogram of the hierarchical cluster analysis – MAP	93
Appendix 4:	Distribution of total phosphorus and P-species at mapping wells	94
Appendix 5:	Dendrogram of the hierarchical cluster analysis – TF	95
Appendix 6:	Piper diagram – major cations and anions at the monitoring wells	95
Appendix 7:	Total arsenic vs. (a) total iron	96
Appendix 8:	Averaged kf for the upper aquifer at the core drilling at hospital ground	96
Appendix 9:	Seasonal changes of total phosphorus concentrations	97
Appendix 10a:	Seasonal changes of EC in different depths (9 – 27 m) of the test field	97
Appendix 10b:	Seasonal changes of EC in different depths (115 – 280 m)	98

List of abbreviations

As	Arsenic
As(III)	Inorganic trivalent arsenic
As(V)	Inorganic pentavalent arsenic
As(tot)	Total arsenic
BGL	Bangladesh
BGS	British Geological Survey
DIC	Dissolved inorganic carbon
DOC	Dissolved organic carbon
DOM	Dissolved organic matter
EC	Conductance
Eh	Redox potential
ETP	Potential evaporation
ETR	Evaporation
ETR _{TURC}	Evaporation adapted from TURC
BGM	Ganges – Brahmaputra – Meghna
GIS	Geographical information system
GPS	Global Positioning System
IC-ICP-MS	Ion chromatography-inductively coupled plasma mass spectrometry
ICP-MS	Inductively coupled plasma mass spectrometry
MAP	Mapping wells
OM	Organic matter
PE	Polyethylene
pH	pH-value
R ²	R-square, coefficient of determination
SI	Saturation Index
TC	Total carbon
TF	Test field
TIC	Total inorganic carbon
TOC	Total organic carbon
UTM	Universe Transverse Mercator
WGS84	World Geodetic System 1984

WHO	World Health Organisation
Wt%	Weight in percent
XRD	X-Ray diffraction

Abstract

The study site is located at Comilla in the southeast of Bangladesh, where 60 % of the wells exceed the World Health Organisation (WHO) guideline value for drinking water of 10 µg/L of arsenic, and was chosen based on available nation-wide As surveys to span the entire spectrum of As concentrations in Bangladesh's groundwater. From February to July 2007, a detailed hydrochemical monitoring was performed on 7 newly drilled monitoring wells tapping the upper Holocene aquifer and the deeper Late-Pleistocene aquifer. The deliverables from hydrochemistry were associated to sedimentological characteristics of the depth profile, investigated within another master thesis. Additionally, depth and spatial dependent changes in chemistry at 48 house and irrigation wells were determined once in the dry season and once in the rainy season.

From the recent findings it can be concluded that highest arsenic concentrations in the groundwater are associated with the grey reduced sediments from the upper aquifer (<300 µg/L), where reducing conditions forced the reduction and dissolution of FeOOH and thus the subsequent release of sorbed arsenic into the groundwater. Maximum arsenic levels were observed in depths between 12 and 36 m and increased with the onset of the monsoonal rainfalls due to seasonal occurring stronger reducing conditions. Species analyses revealed that arsenite was the dominant As-species (67 – 99 %) at almost all the wells, while arsenate was detected in minor quantities. Remarkably high ammonium (up to 200 mg/L) and phosphorus (up to 6 mg/L) concentrations in 36 m depth result from the degradation of peat fragments observed within the depth profile. Further phosphorus is also released when FeOOH is reductively dissolved. Sediments from the shallow aquifer were brown in colour and indicate more likely oxidized conditions. In these sediments reduction is incomplete and the resorption of As to residual FeOOH keeps the arsenic concentrations in the groundwater below 70 µg/L. Dissolved Fe(II) is high at these layers (< 150 mg/).

1. Objectives and deliverables

Arsenic contaminates groundwater across southern, central and eastern Bangladesh as well as the Indian region West Bengal. Groundwater from the Holocene alluvium of the Ganges, Brahmaputra and Meghna Rivers (GBM) locally exceeds 200 times the World Health Organisation (WHO) guideline value for drinking water of 10 µg/L of arsenic. Thus millions of people in both Bangladesh and West Bengal are exposed to contaminated drinking water supply, an enormous health risk. Symptoms like skin diseases, losses on blood vessels (Black Foot Disease), skin pigmentation changes and cancer types of skin, lung, liver, and bladder are typical evidences for arsenical poisoning. The aim of this study was to link the arsenic distribution at the study site in Comilla District, Bangladesh, with the arsenic problem in whole Bangladesh. Therefore the study was focused on spatial, seasonal, and depth dependent hydrochemical changes within the studied area.

1.1. Objectives

The objects of the study were to:

- Collect information from previous projects, analysing and partly reinterpreting them
- Map all irrigation and house wells in the study area with well depth, water table, year of installation as well as infrastructure (roads, bridges, schools, hospital, market place, etc.) & land use
- Determine the depth and seasonal dependent changes in chemistry, especially for redox-sensitive elements (Fe[II], total iron, NH_4^+ , NO_2^- , NO_3^- , total Mn, Mn[II], and S^{2-}) at the newly drilled test field considering the different lithologs from the test field, the core drilling, and old drillings
- Determine the depth and spatial dependent changes in chemistry at 56 house and irrigation wells in the dry season and at selected wells in the rainy season
- Determine correlations between arsenic and other trace elements
- Measure groundwater tables and interpret seasonal variations in correlation with rain events considering rainfall data

- Determine associations between sediment properties (e.g., mineralogy, content of organic matter, iron, manganese, and phosphorus) and arsenic concentrations in groundwater.

1.2. Deliverables

Considering the main objectives given above, the major deliverables of this master thesis were aimed to be:

- Presenting a single-layer digital atlas, based on a Quickbird satellite image, combining the digitized features (e.g. house wells, irrigation wells), thematic layers (e.g. roads, boundaries, rivers, infrastructure), a base map and hydrochemical data. Different databases (e.g. locations and characteristics of the analyzed sites, on-site and laboratory data on hydrochemistry, arsenic speciation) are attached to the digital atlas.
- Comparing the recent hydrochemical findings with results from previous projects to confirm the representativeness of the study site with regard to whole Bangladesh.
- Linking the arsenic concentrations in the groundwater with the associated sedimentological characteristics of the depth profile.
- Contrasting changes in the arsenic distribution at different aquifers with seasonal characteristics, such as irrigation in dry season, monsoon rains, etc.

2. Bangladesh – a general introduction to the geogenic arsenic contamination

Bangladesh and the Indian region West Bengal are located within the world's largest delta, formed by the Ganges-Brahmaputra-Meghna River System and are influenced by monsoonal climate. Until the early 1970s the river water was widely used as drinking water. Thenceforward drinking water supply was changed from pathogenic contaminated surface water, which resulted in waterborne diseases such as cholera and dysentery that caused millions of deaths, to groundwater from wells (RAVENSCROFT et al. 2004). From the early seventies till nowadays more than six million hand pump tube wells, typically drilled to between 20 and 70 m, were installed with the help of international organisations, such as the UN (KINNIBURGH et al. 2003) and to provide clean water to the population without thorough investigation of the quality of the groundwater.. Nowadays, over 90 % of drinking and irrigation water is delivered from shallow wells.

One to two decades after changing to groundwater based drinking water supply, disease patterns like skin diseases, losses on blood vessels (Black Foot Disease), skin pigmentation changes and cancer types of skin, lung, liver, and bladder were detected, attendant symptoms for arsenic poisoning. The delivered water from tube wells is seen as the reason for that. Symptoms may take five to fifteen years or longer to develop (RAVENSCROFT et al. 2004). Arsenic was first identified in the groundwater of West Bengal in 1983 (RAVENSCROFT et al. 2004). This information was unknown in Bangladesh until the early 1990s (RAVENSCROFT et al. 2004). The number of patients with typical symptoms for arsenic poisoning has been estimated by a range between 5,000 and 200,000 in the West Bengal region up to the year 2000 (SMITH et al., 2000). The number in Bangladesh is unknown but must be multiple higher.

Nowadays it is assumed that more than 30 % of all wells exceed the Bangladesh drinking water standard of 50 µg/L; 5 – 10 % of the wells exceed that limit by more than six times. So, 50 of the 64 districts of Bangladesh and 9 out of the total 18 districts in West Bengal have drinking water wells above the local level. At least 30 – 35 million people in Bangladesh and 6 million people in West Bengal are assumed to be exposed to arsenic contaminated drinking water at concentrations above 50 µg/L (SMEDLEY and KINNIBURGH, 2001).

The World Health Organisation (WHO) recommended a guideline of 10 $\mu\text{g/L}$ in 1993. According to the WHO standards, more than 50 million people in Bangladesh are exposed to contaminated water (Sharma et al. 2006). The worst affected area is in the southeast of Bangladesh, where in some districts more than 90 % of the wells are affected (SMEDLEY and KINNIBURGH, 2001) (see figure 2.1). Areas with arsenic concentrations exceeding 300 $\mu\text{g/L}$ can be found in the lower catchment areas of the Ganges-Brahmaputra-Meghna (GBM) system.

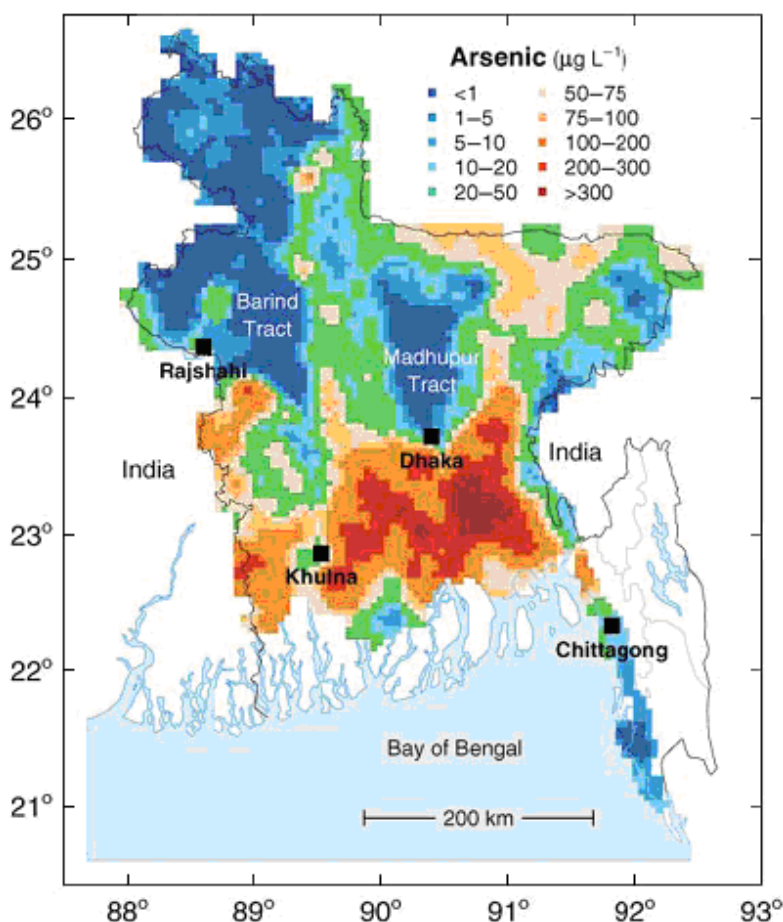


Fig. 2.1. Distribution of As in groundwater from shallow (<150 m) tubewells in Bangladesh (SMEDLEY and KINNIBURGH, 2001)

It has been shown, that especially Holocene alluvial aquifers of the Ganges-Brahmaputra-Meghna River System are highly affected. Due to sea-level rise (from 18 Ka to 7 Ka BP) and higher temperatures, the Holocene sediments are dark-grey, highly micaceous, unweathered and organic matter is present at up to 6 % by weight (see 3.4.4). The affected aquifers are generally shallow (less than 100 – 150 m deep) and in most affected areas, the aquifer sediments are capped by a layer of clay or silt, which restricts exchange with the atmosphere, and thus oxygen supply to the aquifers. In conjunction with organic matter, deposited with the sediments, this phenomenon leads to reducing conditions and favours the mobilisation of As.

Redox changes due to rapid burial of the alluvial and deltaic sediments included the reduction of arsenic to As(III), desorption of As(V) from Fe oxides and reductive dissolution of the oxides themselves. According to SMEDLEY and KINNBURGH (2001), high arsenic concentrations in Bengal aquifers may be associated with:

- areas with relatively low rainfall and high evaporation or runoff, resulting in low recharge;
- very low groundwater flow rates as a result of silts and fine sands within alluvial floodplains and delta areas and an extremely small hydraulic gradient;
- low gradient-areas with flushing times over 200 ka per pore volume;
- areas of low flow like inside river meanders and in closed basins

Low arsenic concentrations are associated with:

- coarse sands in fluvial areas at the base of incised channels;
- medium porosity and high hydraulic conductivities;
- relatively rapid flushing of 2-10 ka per pore volume;
- high groundwater gradients;

Pleistocene aquifers, older alluvial sediments and deeper aquifers (> 150 m) can be seen to be free of arsenic that is why they are preferred for irrigation and drinking water since a couple of years. But there is the risk to suck arsenic contaminated groundwater into the deeper aquifers as a result of excessive exploitation of deeper aquifers.

The transported and deposited sediments derived from the upland Himalayan catchments and from basement complexes of the northern and western parts of West Bengal. Major arseniciferous minerals are ore minerals and their alteration products which are relative rare in natural environments. They are found in close relation with the transition minerals as well as Cd, Pb, Ag, Au, Sb, P, W, and Mo.

Arsenic can occur in the environment in several oxidation states (-3, 0, +3 and +5) (RAVENSCROFT et al., 2001). Organic arsenic is produced by biological activities but can be neglected for groundwaters in the Bengal Basin because it is generally linked to industrial pollution or partially reducing conditions in organic carbon rich zones (SEMDLEY and KINNIBURGH, 2001). GAULT et al. (2004) found no evidence of significant concentrations of thioarsenate species which can be an important form of dissolved arsenic in groundwaters that contain moderate sulphide concentrations.

In natural waters with pH typically between 6.5 and 8.5, arsenic appears usually in the inorganic form as oxyanions of zero-charged trivalent arsenite ($\text{H}_3\text{As}^{\text{III}}\text{O}_3^0$) at reducing conditions or negatively charged pentavalent arsenate ($\text{H}_2\text{As}^{\text{V}}\text{O}_4^-$ or HAsO_4^{2-}) under oxidising conditions (fig. 2.3). However, groundwaters with high concentrations of arsenic are dominated by arsenite, ranging between 70 and 100 % (ZHENG et al., 2004), as it is regarded as the most mobile form of arsenic.

The redox potential is a dominant factor for controlling the arsenic speciation and the arsenic mobilisation into groundwater over a wide range of redox conditions. High arsenic concentrations are always associated with reducing conditions. The mobility, toxicity and bio availability is strongly regulated by the oxidation state of the arsenic complex. Arsenite seems to be much more mobile and toxic than arsenate.

Following speciations are controlled as a ratio of pH and redox potential (fig. 2.2. and 2.3.):

- H_2AsO_4^- is dominant at low pH (<6.9) and under oxidising conditions;
- HAsO_4^{2-} becomes dominant under oxidising conditions but increasing pH;
- uncharged H_3AsO_4^0 at extremely acidic (pH<2.0) and AsO_4^{3-} at extremely alkaline conditions (pH>12) under oxidising conditions;
- uncharged H_3AsO_3^0 under reducing conditions at pH less than 9.2;
- H_2AsO_3^- at pH > 9.2 and HAsO_3^{2-} at about pH > 12;

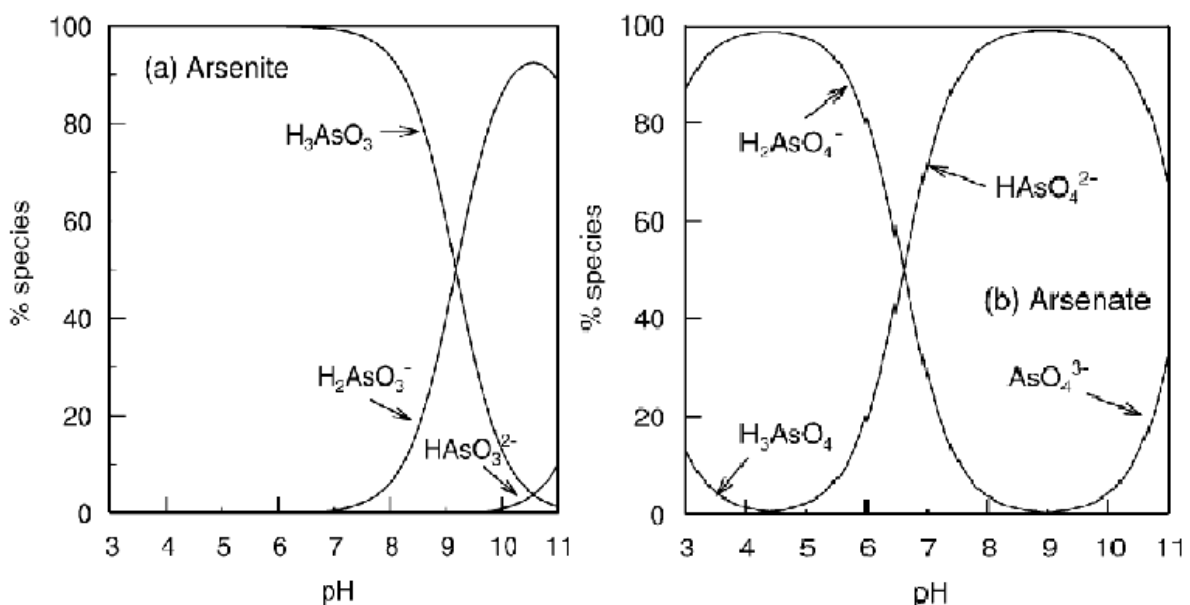


Fig.2.2. Arsenite (a) and arsenate (b) speciation as a function of pH with an ionic strength of 0.01 M (SMEDLEY and KINNIBURGH, 2001)

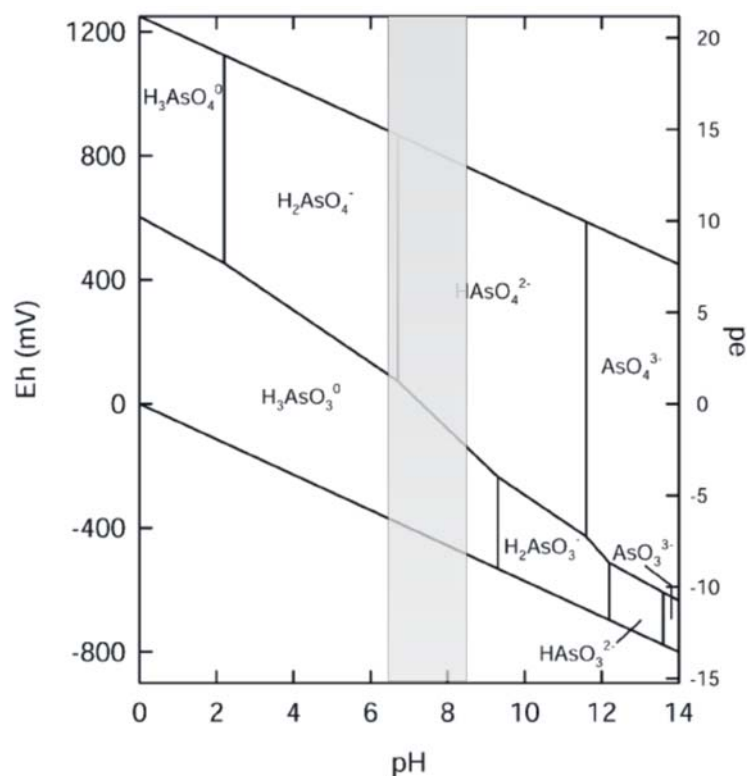


Fig. 2.3. Eh-pH diagram for aqueous As species in the system As-O₂-H₂O at 25°C and 1 bar total pressure; pH-values, typically for natural water are grey-shaded (SMEDLEY and KINNIBURGH, 2001)

Three main theories of arsenic mobilisation might explain the pollution of groundwater in the Bengal Basin and have been confirmed in several studies (RAVENSCROFT et al., 2001; RAVENSCROFT et al., 2004; SMEDLEY and KINNIBURGH, 2002):

I. Pyrite oxidation and irrigation drawdown

Oxidation of arsenic containing pyrite as a reason for arsenic contamination in Bangladesh was rejected by several authors.

Arsenic has a high affinity to sulphide minerals, where Sulphur can be substituted in the crystal structure. Arsenian Pyrite (Fe(S, As)₂), Arsenopyrite (FeAsS), Realgar (AsS) and Orpiment (As₂S₃) are important minerals resulting from such a substitution. Besides being an important component of ore bodies, pyrite can be also formed in low temperature sedimentary environments under reducing conditions and plays an important role in recent geochemical cycles (SMEDLEY and KINNIBURGH, 2001). It can be found especially in river sediments, lake and marine sediments. Pyrite is being primarily formed under reducing conditions in conjunction with organic deposits. Soluble arsenic can be incorporated in the crystal structure during the formation.

The oxidation of pyrite is seen in relation with the drawdown of the water table as a result of intensive irrigation. Oxygen can find its way into previously anoxic aquifer sediments. Within aerobic systems, pyrite isn't stable and oxidises to Fe oxides under formation of Sulphate (SO₄), acidity and trace constituents like arsenic. That is the cause for arsenic problems and acidification of mine drainages around sulphide rich coal mines.

RAVENSCROFT et al. (2001) attempted to relate the distribution of arsenic contamination to that of irrigation but they have not shown any relation to each other. Another reasons for rejecting pyrite oxidation as a mechanism is based on the fact, that the concentrations of arseniciferous pyrite at the sediments are too little to be important. Both pyritic and organic sulphur has been detected in several studies (NICKSON et al., 2000; AAN, 1999; J.M. MCARTHUR, unpublished; DPHE, 1999) with maximum contents less than 0.3 %. Furthermore, the release of sulphate during the oxidation of pyrite should correlate with the dissolved As. In reality, iron and sulphate are mutually exclusive in solution (Ravenscroft et al. 2001; Kinniburgh and Smedley 2001). But the sulphate concentration does not match with that of arsenic because arsenic concentration > 50 µg/L occur only where sulphate concentrations are less than 30 mg/L. Lastly, shallow tube wells (< 10 m) are most exposed to atmospheric oxygen and would be affected highest, if arsenic would be originated from pyrite. But normally, the shallow wells are affected less. In conclusion, pyrite is a sink, but not a source of arsenic (RAVENSCROFT et al., 2001).

II. Competitive exchange of phosphate from fertilizer

Phosphorus commonly occurs almost exclusively in the environment as fully oxidised phosphate (primarily H₂PO₄⁻ and HPO₄²⁻, where the oxidation state of phosphorus is +5) [HANRAHAN et al., 2004]. Inorganic P can occur in the environment in five different oxidation states (-3, 0, +1, +3 and +5), similar to arsenic. In the main, geogenic sources of phosphorus are the minerals Apatite (magmatic), Phosphorite (sedimentary), and seaspray. Additionally, the use of phosphate fertilizers in Bangladesh has been increased immensely within the last 15 years because cropping was switched from one crop to three crops per year. This lead to the assumption, that the arsenic contamination could be a result of increased phosphate input at least in part.

The fertilizer phosphate displaces arsenic from FeOOH as a result of competitive anion exchange (ACHARYYA et al., 2000), owed to the fact that both, arsenic and phosphorus, form similar anionic complexes. For illustration see fig. 2.2. in comparison with fig. 2.4.:

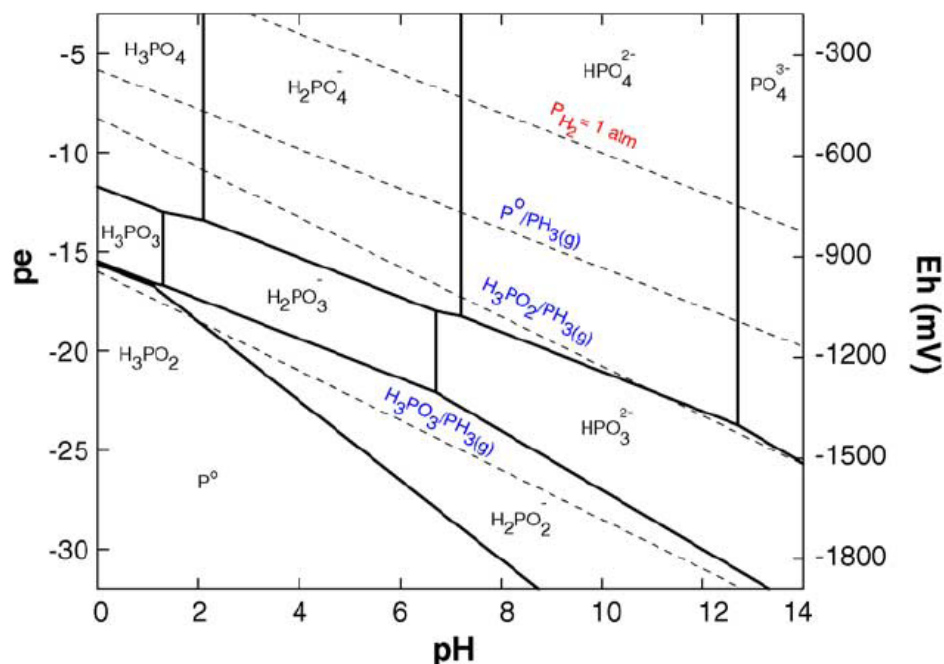


Fig. 2.4. Eh/pe-pH diagram for aqueous P species. For calculations involving equilibrium between reduced P species and phosphine (i.e., dashed lines including PH_3), an equilibrium concentration of 10^{-6} M for the reduced P compound was assumed. (HANRAHAN et al., 2004)

Nevertheless, phosphorus as a displacement for Arsenic was rejected by several authors (RAVENSCROFT et al., 2001; HANRAHAN et al., 2004; Acharyya et al., 2000). On the one hand the use of phosphorus is ubiquitous but on the other hand amounts used are not high in a worldwide comparison. According to RAVENSCROFT et al. (2001), there are largely areas of Bangladesh, where groundwater is free of both arsenic and phosphorus. But especially at these regions irrigation is most intense and also use of fertilizer is highest. Based on this fact, any link between arsenic and fertilizer seems incoherent.

A study of MANNING and GOLDBERG (1996) has shown that phosphorus in a concentration of 5 mg/L would desorb at most 2 $\mu\text{g/L}$ of arsenic to mineral surfaces.

Another argument seems the content of uranium at phosphate fertilizers, used as a tracer for fertilizer phosphate (RAVENSCROFT et al., 2001). But in Bangladesh concentrations of uranium are high where concentrations of phosphorus are low to zero. Furthermore, concentrations of uranium decrease in greater depth (no uranium was found in depths > 41 m) whilst concentrations of phosphorus increase with depth.

III. Reduction of arsenic-rich hydrous iron oxides (FeOOH)

The third theory, known as the reduction of arsenic-rich hydrous iron oxides hypothesis, is now accepted as the principal mechanism of arsenic mobilization in the anoxic surface- and groundwater of the alluvial aquifers in the Bengal Basin (e.g. AHMED et al., 2004; RAVEBSCROFT et al., 2001; MCARTHUR et al., 2001, KINNIBURGH and SMEDLEY, 2001). Microbial oxidation of organic carbon (concentrations may reach up to 6 % in aquifer sediment) forms the basis of FeOOH reduction:



This process is accompanied by microbial reduction of arsenate [As(V)], which is strongly sorbed onto iron hydroxides, to arsenite [As(III)], when anoxic conditions ($E_h < 200$ mV) develop during sediment burial (NICKSON et al., 1998; NICKSON et al., 2000). This is shown in the fact, that arsenic is present basically as arsenite (RAVENSCROFT et al., 2001). The reduction of iron hydroxides is widespread and strong in organic rich and fine-grained deltaic sediments, shown by high concentrations of dissolved iron up to 80 mg/L, primarily present as Fe^{2+} (NICKSON et al., 2000). Due to the reduction process, arsenic-rich hydrous iron oxides are dissolved and release both Fe^{2+} and the sorbed load of the hydrous iron oxides, which includes arsenic. Arsenic accumulates as a result of an extremely low regional hydraulic gradient that caused low flushing rates (KINNIBURGH et al. 2003). High arsenic concentrations might be associated with high iron concentrations. In addition, HCO_3^- ions are generated which explains the relationship between arsenic and HCO_3^- . NICKSON et al. (2000) and various authors (RAVENSCROFT et al., 2001; NICKSON et al., 1998; APPELO et al., 2002; SAFFIULLAH, 1998) mentioned that in most cases poor correlations existing between Fe^{2+} and As. Presumably, poor correlations could arise from re-precipitation of iron, re-adsorption of arsenic onto fresh hydrous iron oxides (FeOOH) or precipitation of Fe^{2+} as siderite FeCO_3 (WELCH and LICO, 1998). Wells with high amounts of HCO_3^- and Fe^{2+} are oversaturated with siderite and slightly with calcite and dolomite.

The spatial distribution of phosphorus in tube wells corresponds to that of arsenic; however the well by well correlation of arsenic and phosphorus is insignificant. This can be explained by a shared diagenetic origin for both arsenic and phosphorus (RAVENSCROFT et al., 2001). Moreover, both arsenic and phosphorus form anions that sorbs strongly to hydrous iron oxides, even though phosphorus was rejected as a

displacement for Arsenic by several authors (RAVENSCROFT et al., 2001; HANRAHAN et al., 2004; ACHARYYA et al., 2000).

It seems to be obvious that high concentrations of arsenic occur in groundwater where microbial reduction of FeOOH has released and reduced sorbed arsenic. Organic matter is required as trigger, the so called redox driver (MCARTHUR et al., 2000). Therefore, the distribution of organic matter (OM) in the aquifer sediments is the main control on the distribution of arsenic contamination and may be present in several forms (RAVENSCROFT et al., 2001):

- Concentrations of less than 0.5 % TOC (total organic carbon) are typical for **disseminated organic matter** of the fluvial sands in the Bengal Basin (NICKSON et al., 1998). During transport at receiving streams, organic matter is being reduced before it gets incorporated into the sediment. After dissemination through the sands, organic matter will be left cellulose rich and unfavourable for bacterial metabolism. Disseminated organic matter at fluvial sands seems to be irrelevant in contribution to FeOOH reduction. Higher concentrations of arsenic may occur where pyrite has formed and scavenged arsenic from solution. But this theory can be mostly rejected for Bangladesh, as aforementioned.
- **Peat beds** are common beneath the Old Meghna Estuarine Floodplain in Greater Comilla, Sylhet, Gopalganj-Khulna Peat Basin, and the shallow aquifer system in Lakshmipur (MCARTHUR et al., 2001). Peat has been found in Holocene sediments and occurs extensively beneath arsenic contaminated areas (RAVENSCROFT et al., 2001). Indicators for peaty sediments are increased concentrations for TOC (up to 8 %), biogenic methane and the presence of ammonium in wells in concentrations up to 24 mg/L (DPHE, 2000; HOQUE, 1998). In addition, there is a strong correlation between ammonium and phosphorus (MCARTHUR et al., 2001). According to RAVENSCROFT et al., (2001) the spatial distribution of peat corresponds with that of arsenic.

3. Description of the investigation area

3.1. Study area - selection criteria and specifics

The study area with an extent of approximately 10 sq km is located 50 km south-east of the capital Dhaka at Titas, Daudkandi Upzilla, Comilla District (UTM WGS84, Zone 46N: 274000E 2613000N – 276000E 2609000N, Atlas Bangladesh 2007). The site at Titas, Comilla was shortlisted along with the British Geological Survey “special study areas” named Chapai Nawabganj (25 % of the wells > 50 µg/L As), Faridpur (41 % of the wells > 50 µg/L As) and Lakshmiপুর (55 % of the wells >50 µg/L).

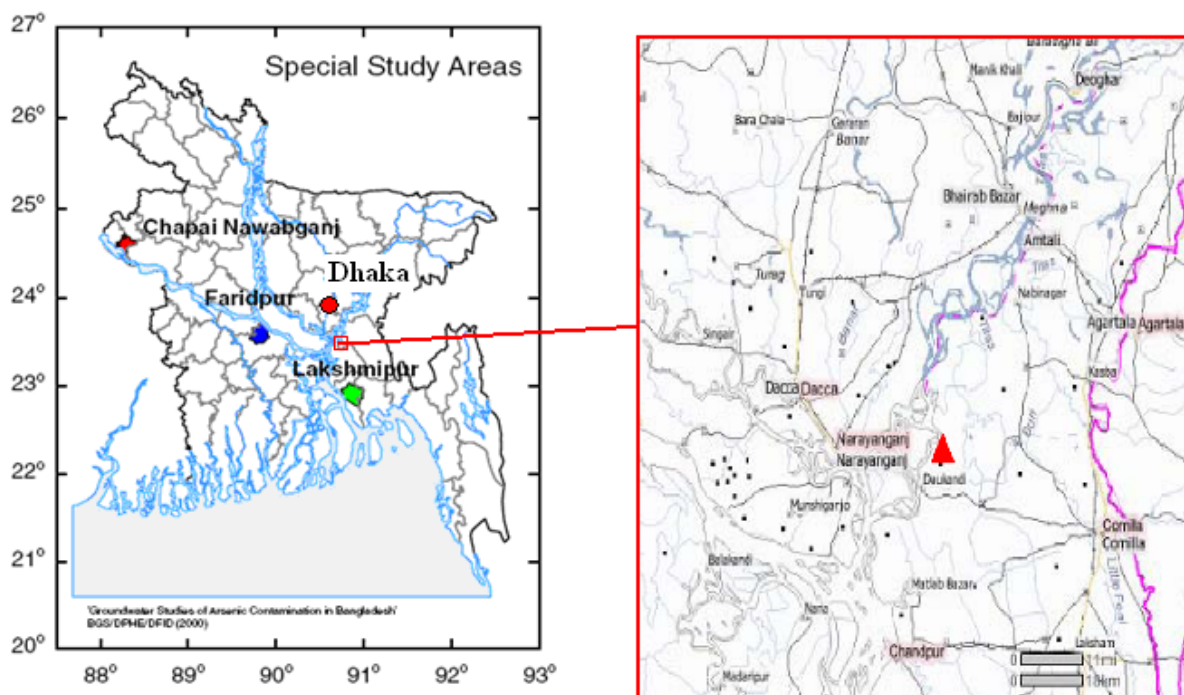


Figure 3.1.1. British Geological Survey “special study areas” (left); Satellite Image from the investigation area (right); modified according to KINNIBURGH and SMEDLEY (2001)

Finally, the site at Comilla has been chosen, because according to the “national guideline for drinking water”, 65 % of all shallow wells at this area exceed the local drinking water standard of 50 µg/L for arsenic. Field tests confirmed this; totals up to 420 µg/L were detected. The area was selected, because of the high arsenic level, closeness to the Meghna River and optimal logistic location due to its closeness to the capital.

First samplings of the shallow tube well at the health complex in November 2006 showed that the groundwater chemistry at the test field has a low mineralization compared to the general groundwater composition. The approximately 12 m deep well is labelled with sample code

BGL MAP 02 01. The water is almost pH-neutral (7.13), partially reductive (Eh: 84.3 mV), has low dissolved oxygen (0.25 mV) and the conductivity was 255 $\mu\text{S}/\text{cm}$. Major cations are Na^+ (9.7 mg/L), K^+ (2.2 mg/L), Ca^{2+} (27.9 mg/L), Mg^{2+} (8.2 mg/L) and NH_4^+ (0.4 mg/L). The major anions are F^- (0.2 mg/L), Cl^- (11.7 mg/L) and PO_4^{3-} (0.8 mg/L). TIC was measured with 26.58 mg/L and DOC with 0.69 mg/L.

The water can be defined as a Ca- HCO_3 type because of the predominance of calcium and TIC. Total arsenic is 76 $\mu\text{g}/\text{L}$ and total phosphorus 817 $\mu\text{g}/\text{L}$.

3.2. Vegetation and land use

Bangladesh, with the world's largest delta of the Ganges-Brahmaputra-Meghna River System is influenced by monsoonal climate, which is favourable for agriculture. The proportion of agricultural land use of total land area (147,570 sq) is highest in Bangladesh (around 70 %), compared to South Asia in general (ALAUDDIN and QUIGGIN, 2007). Since 1950, the ratio of agricultural land to total land was increasing and declined in the 1990's, because the extensive margin of cultivation may have been exhausted (ALAUDDIN and QUIGGIN, 2007). At present, agricultural areas have a size of 103,299 ha of which 88.9 % is arable crop. The rising population (150 million), with an annual growth of 1.7 %, leads to the intensification of farming by modifying farming techniques in order to increase food production. The land person ratio is estimated at 0.12 ha per person. From between the early 1960's irrigation has increased from rare usage to up to presently 56 % of total arable crop. As a consequence of intensive dry season irrigation, a high degree of intensification of agriculture has developed in Bangladesh, which allowed multiple cropping. Supplementary use of chemical fertilizers increased with 84.7 kg of nutrients per ha of arable crop.

High yielding varieties of rice and wheat were introduced in the course of development. Cultivation of arable crop is subdivided mainly in rice fields (approximately 67 %) and secondarily wheat and field fruits e.g. corn, chilli, potatoes, etc.

Rivers are distributed with a surface ratio of approximately 6,400 sq km, stagnant waters cover 4,245 sq km. Forests have an estimated surface of 19,610 sq km which is about 13.3 percent of the total land area of the country. Rural built-up areas, urban areas and infrastructure extend over an area of approximately 16,100 sq km. Comilla is typical for Bangladesh, approximately 64 % of the land is used for farming, 18 % for settling, and 18 % are divided in rivers, stagnant waters and fallow.

3.3. Climate

Bangladesh has a tropical monsoon climate characterized by two main seasons, a dry season from October to April and a rainy season from June to October (REIMANN, 1993). The mean monthly minimum temperatures in January vary from 10 to 12 °C, from June to August between 20 and 25°. The mean monthly maximum temperatures vary from 25 to 28 °C in January to between 32 and 35 °C in June to August. Temperature and humidity increase during March to May. The period between June to October is characterized by a hot and very wet climate. Potential evapotranspiration rises from 70 to 90 mm in wintertime to about 180 mm from March to May. In monsoon time, evapotranspiration stabilises at between 115 and 145 mm and falling, with the end of the rainy season in November. Up to 85 % of the annual rainfall occurs during the May to September monsoon. Approximately 10 % of the precipitation occurs during the so called “Nor’Westers”, heavy rainfalls originated from the Mediterranean and only 5 % of rainfall occurs during the five month dry season between November and March. During this period, agriculture is not possible without irrigation. The mean annual rainfall ranges between 1,250 mm in the western central region and 5,000 mm in the north-east.

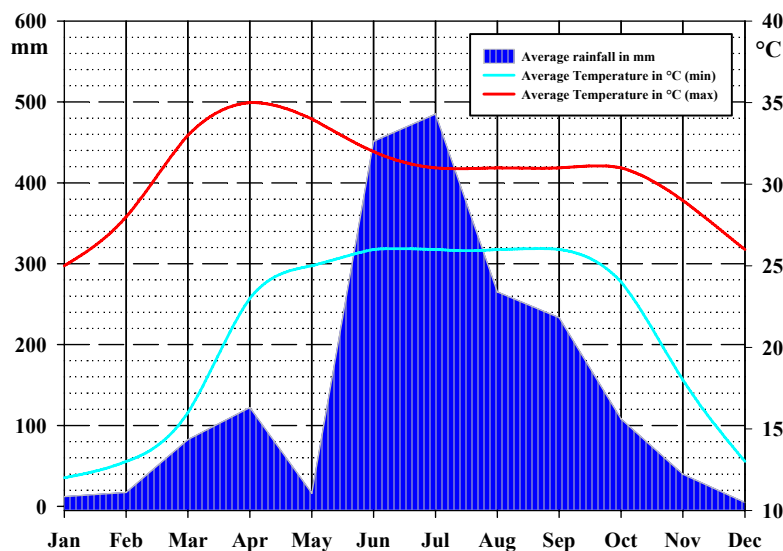


Fig. 3.3.1. Climate chart for Comilla district, Bangladesh. Period of data collection ranges from 01/1994 to 12/ 2004, daily measured values. Station No.: CL356 (Longitude: 91.175; Latitude: 23.462) (Bangladesh Water Development Board (BWDB))

The annual temperature – precipitation distribution for the investigation area is presented in figure 3.3.1.; the mean annual rainfall is of 1838 mm with a maximum of 480 mm in June/July and a minimum in May.

3.4. Geology

3.4.1. Geology and geomorphology

Bangladesh, with a size of 147,570 sq km, is situated in the north-eastern corner of the Indian subcontinent at the head of the Bay of Bengal. The Bengal Basin, which constitutes the major part of Bangladesh and the adjoining part of West Bengal, is bordered by the Himalaya and an uplifted block of Precambrian Shield (Shillong Plateau) to the north (AHMED et al., 2004), a Precambrian basement complex (Indian Platform) to the west, and the Indo-Burman ranges to the east (Morgan and McIntire 1959). More than 16 km thick synorogenic Cenozoic sediments are deposited in the basin derived from the Himalayan and Indo-Burman ranges (Uddin and Lundberg, 1998). According to AHMED et al. (2004), tertiary sediments in Bangladesh mainly comprise sandstone and shale sequences, while Pleistocene sediments are mostly represented by clay, overlain by Holocene alluvium.

The combined deltas of the Ganges, Brahmaputra and Meghna (GBM) river systems lie within Bangladesh (SMEDLEY and KINNIBURGH, 2001). This complex river system can be seen as the driving force for sediment transport and deposition. The source of the sediment loads is glacial and periglacial weathered rock from the Himalaya. The sediment load includes eroded ultramafic rocks from northern parts of the high Himalayas and granitic and high grade metamorphic rock from central and southern parts, with quartz, biotite and feldspar as characteristic minerals.

Sediments from lower altitudes derive from the Damodar and Dareeling coalfields (coals and shales containing high amounts of pyrite), the Rajmahal Traps (basalts with pyrite) and the Gangetic Plains (lateric materials). These sediments are eroded and transported by the GBM system, crossing these areas.

According to SMEDLEY and KINNIBURGH (2001) a characteristic geomorphology has developed as a consequence of a series of glacio-eustatic sea level cycles and long-term tectonic activity. Bangladesh can be divided into two environments of sediment deposition: the continental fluvial environment north of Ganges and lower Meghna and the southern estuarine delta environment (fig. 3.4.1.1).

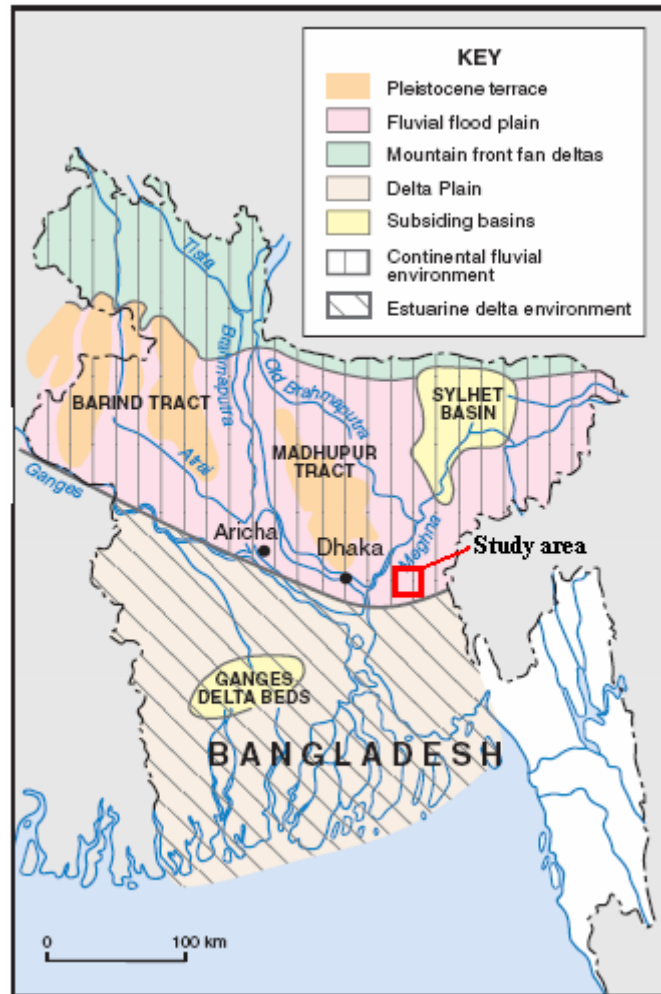


Fig 3.4.1.1. Main geomorphologic units of Bangladesh (SMEDLEY and KINNIBURGH, 2001)

The main geomorphological units (fig. 3.4.1.1) are described by Morgan and McIntire (1959) as:

- Pleistocene terraces in the north-western part of Bangladesh (Barind Tract) and in the north of Dhaka (Madhupur Tract); they locally interrupt the flat topography of central Bangladesh, rising up to 20 m above the adjacent floodplains (RAVENSCROFT et al., 2004). These areas have a dendritic drainage, with channels filled by organic-rich muds of Holocene age (MONSUR, 1995)
- Fluvial flood plains of Ganges, Brahmaputra and Meghna, which is where the study area is located;
- Mountain front fan deltas of the Tista and Brahmaputra;
- Delta plains south of Ganges and Meghna valleys;
- Subsiding basins both at estuarine delta environment (Ganges delta beds) and at continental fluvial environment (Sylhet Basin);

3.4.2. Geological evolution of the Bengal Basin

The **pre-Quaternary** development of the Bengal Basin started in the Permo-Carboniferous, but the significant processes are closely linked to tectonic activities in the Tertiary. Marine sediments were filling the initially passive Bengal Basin during Cretaceous times (SMELDLEY and KINNIBURGH, 2001). In Eocene times, the Indian plate collided with the Burmese Plate, which resulted in the uplift of the Burmese Hills. Eroded sediments from the Burmese hills were deposited in the Bengal Basin. After ALAM et al. (2002), the Bengal Basin evolved from a passive continental margin in the pre-Oligocene to a separated ocean basin at the beginning of the Miocene. The collision of the Indian Plate with the Burma and Tibetan (Eurasian) Plates after the separation of the Indian Plate from the southern continent of Gondwana resulted in a large settling rate into the Bengal Basin, south of the Himalayas and west of the Burmese Hills. The erosional discharge of the Orogen yielded the accumulation of 1–15 km thick clastic sediments in the Bengal foredeep.

Three geo-tectonic provinces developed (fig. 3.4.2.1): the **Stable Shelf**, a passive to extensional cratonic margin in the west, the **Central Deep Basin**, a remnant ocean basin and the **Chittagong – Tripura Fold Belt**.

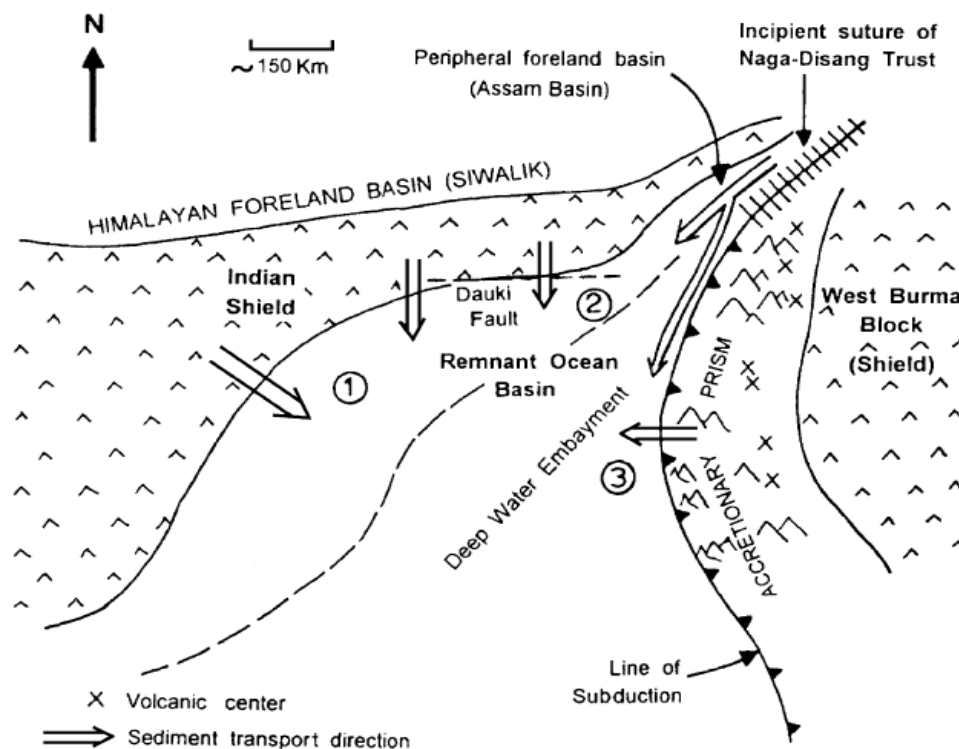


Fig. 3.4.2.1. The Bengal Basin and surrounding regions in the Early Miocene. (1) The Stable Shelf; (2) The Central Deep Basin; (3) The Chittagong – Tripura Fold Belt (ALAM et al., 2002)

Tectonic activities along the Dauki Fault (fig. 3.4.2.1) during the Pliocene resulted in the uplift of the Shillong Plateau and the subsidence of the Garo Rajmahal Gap. The formation of the north-south trending Tripura Chittagong fold belt can be seen in connection with this event. The Brahmaputra entered into the Bengal Basin diverted from the Shillong Hills in the west to the eastern area of Sylhet (fig. 3.4.1.1). The current course of the Brahmaputra, a north-south trending faulted trench, separates Barind and the Madhupur Tracts, two uplifted and tilted blocks (fig 3.4.2.2).

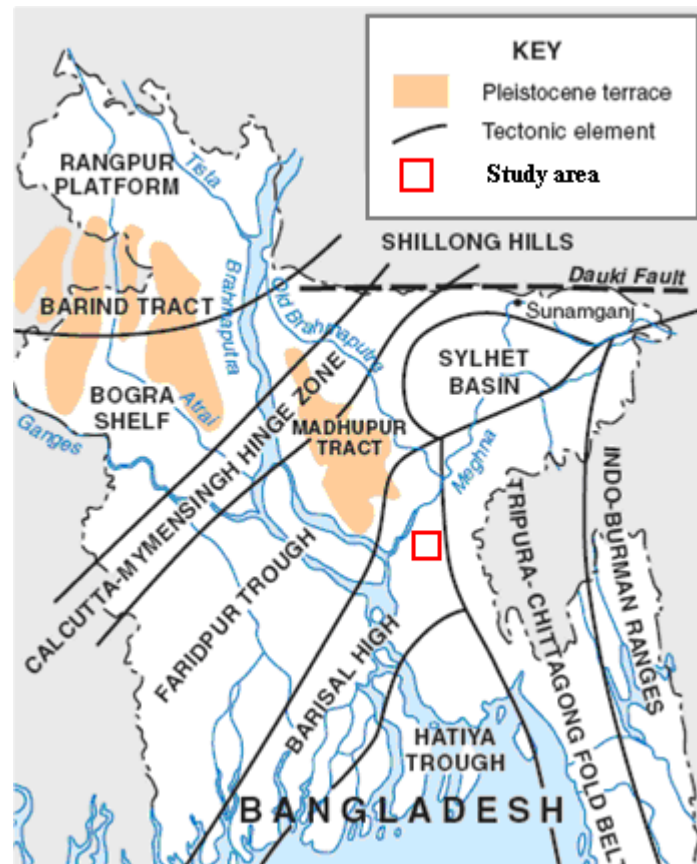


Fig 3.4.2.2. Tectonic elements of the Ganges – Brahmaputra – Meghna delta system (SMEDLEY and KINNIBURGH, 2001)

The south-west to north-east striking Calcutta-Mymensingh Hinge Zone divides the Bengal Basin in two crustal domains (SMEDLEY and KINNIBURGH, 2001). In the north of Bangladesh the basement is formed by the Rangpur Platform and the Bogra Shelf beneath a thin cover of Cretaceous to recent sediments (fig. 3.4.2.2). The areas south of the Hinge Zone (Faridpur, Hatiya and Sylhet Troughs) are underlain by oceanic crust.

The **Quaternary** period is affected by approximately 120 ka of glacio-eustatic cycles (SMEDLEY and KINNIBURGH, 2001), global climatic changes, the uplift of the Himalayas and subsidence in the Bengal basin as a result of huge alluvial sedimentations (RAVENSCROFT et al., 2003). Monsoonal circulations and thereby caused high rainfalls and

river flows were eliminated by Himalayan glaciations. The global sea level was at about 50 m below its present level with a minimum peak of 130 m at 18 ka BP during the Pleistocene (RAVENSCROFT et al., 2004). Consequently, the Ganges, Brahmaputra and Meghna carved deeply into the sediment and left incised channels within a series of terraces. The recent configuration of the Ganges Delta has mainly developed from a Holocene sea-level rise which promoted a landward migration of the system (ALAM, 2003). The sedimentation rate was high and subsidence rates of 1 to 4 mm per year with the maximum in the Sylhet Basin were characteristic for Holocene times. The Pleistocene terraces are now largely buried by Holocene floodplains. Maximum sedimentations on the submarine fan appeared during the postglacial transgression between 12.8 and 9.7 ka BP.

3.4.3. Lithological units – Stratigraphy

The Quaternary in the Bengal Basin is subdivided into the following stratigraphical units, described according to ALAM et al. (1990):

- The **Late Pleistocene to Holocene** forms major aquifers beneath recent floodplains and is represented by the *Chandina Formation* as well as the *Dhamrai Formation*. Maximum thickness is less than 150 m. Upward fining, grey micaceous, medium and coarse sands to silt with organic mud and peat are characteristic;
- The **Lower Pleistocene** is represented by the *Madhupur Clay* and the *Barind Clay* Formations, with a thickness of between 6 and 60 m. Red-brown to grey and silty clay, residual deposits, kaolinite and iron oxides are characteristic. Frequently, the Lower Pleistocene is absent beneath Holocene floodplains.
- The **Plio-Pleistocene** is represented by the *Dihing Formation* as well as the *Dupi-Tila Formation*. Characteristically are unconsolidated yellowish-brown to light grey, medium and coarse sands to clays, depleted in mica and organic matter. The Plio-Pleistocene forms major aquifers beneath Holocene terraces and hills and deeper aquifers beneath the Holocene floodplains. The maximum thickness may reach values up to 6500 m.


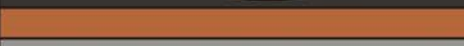
Period	Epoch	Depth [m]	Lithology	
Quaternary	Holocene	0 - 3.0	Filling sand; light grey	
		3.0 - 15.2	Grey fine sand to coarse silt	
		15.2 - 27.4	Grey coarse silt to fine sand	
		27.4 - 36.6	Grey fine sand to coarse silt	
		36.6 - 73.1	Grey silty clay; peat lenses	
	Pleistocene	73.1 - 77.7	Brown medium to coarse sand	
		77.7 - 85.3	Grey coarse silt to fine sand	
		85.3 - 91.4	Grey silty clay	
		91.4 - 103.6	Grey coarse silt, lt. fine sand	
		103.6 - 109.7	Grey fine sand to coarse silt	
		109.7 - 128.0	Grey coarse silt to fine sand	
		128.0 - 137.1	Grey fine sand to coarse silt	
		137.1 - 158.5	Grey medium sand, silty	
		158.5 - 164.6	Grey fine sand	
		164.6 - 182.9	Grey coarse silt to fine sand	
		182.9 - 189.0	Grey fine sand to medium silt	
		189.0 - 195.0	Grey medium sand	
		195.0 - 204.2	Grey fine to medium sand	
		204.2 - 219.5	Grey fine sand to medium silt	
		219.5 - 231.6	Grey fine sand	
		231.6 - 246.9	Grey coarse silt, lt. Fine sand	
		246.9 - 259.0	Grey silty clay	

Fig. 3.4.3.1. Drilling profile from a 259.0 m drilling at the Upazilla Health Complex Titas, Comilla

3.4.4. Hydrogeology

In the following, a generic summary of the hydrogeological situation in Bangladesh is presented (taken from SMEDLEY and KINNIBURGH 2001).

Most data of Quaternary alluvial aquifers were raised during the 1980's by internationally funded irrigation projects.

Bangladesh's topography, geology and hydrology are influenced by the three rivers Ganges, Brahmaputra and Meghna (GBM) and the associated affluents, river branches and connecting channels (REIMANN, 1993). Their deposits of unconsolidated Pleistocene and Holocene alluvial sediments form one of the most productive aquifer systems in the world (SMEDLEY and KINNIBURGH, 2001). Altogether, they have an estimated length of 24,000 km (RASHID 1977). Floods, as a combination of annual monsoon rains, melt water from the Himalayas and tidal-level increase in the Bay of Bengal fully recharge the aquifer system each year. Supplementary to the summer monsoons, heavy rainfalls originated from the Mediterranean (so called "Nor'Westers") can appear in April and May (REIMANN, 1993).

Deeper aquifers are exploited within the coastal regions below shallow zones of saline water intrusions. Freshwater may be also available from older, Tertiary strata in depths of 1,800 m (JONES, 1985). According to UNICEF, large quantities of groundwater exist at shallow depths. Nowadays, more than 95 % of drinking water supply in Bangladesh is abstracted from shallow tube wells.

SMEDLEY and KINNIBURGH (2001) classified the main aquifers of Bangladesh as follows:

- **Late Pleistocene to Holocene** coarse sands, gravels and cobbles of the Tista and Brahmaputra mega-fans and basal fan delta gravels along the incised Brahmaputra channel. Due to sea-level rise (from 18 Ka to 7 Ka BP) and higher temperatures the Holocene sediments are dark-grey, highly micaceous, unweathered and organic matter is present at up to 6 % by weight (fig 3.4.4.1);
- braided-river coarse sands and gravels deposited along the incised palaeo-Ganges, lower Brahmaputra and Meghna main channels from **Late Pleistocene to Holocene** (fig 3.4.4.1);

- At depths > 150 m: stacked fluvial main channel medium to coarse sands from **Early to Middle Pleistocene**, deposited in the Khulna, Noakhali, Jessore / Kushtia and western moribund Ganges delta areas in the subsiding delta basin. Younger **Late Pleistocene to Holocene** sand contains saline groundwater in coastal areas (fig 3.4.4.1);
- Red-brown medium to fine sands from **Early to Middle Pleistocene** underlie grey Holocene medium to fine sands in the Old Brahmaputra and Chandina areas.
- **Early to Middle Pleistocene** coarse to fine fluvial sands of the Dupi Tila Formation (tens to more than a hundred metres thick) underlie the Madhupur and Barind Tracts, an important confined aquifer with low vertical and horizontal permeability in north-west and north-central Bangladesh, capped by deposits of Madhupur Clay Residuum. The Madhupur sediments, deposited during several pre-200 ka BP glacio-eustatic cycles in former channels of Brahmaputra, have undergone several periods of flushing and weathering resulting in the formation of red iron-oxide cements and inter-bedded grey sticky clays. (fig 3.4.4.1)

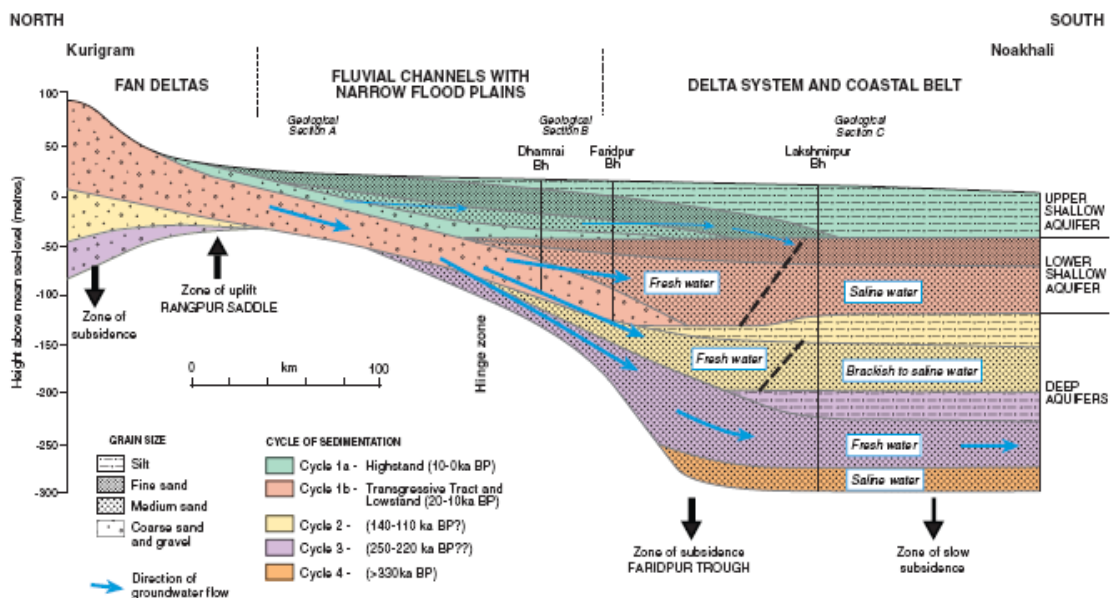


Fig. 3.4.4.1. Hydrogeological cross section from Bangladesh's North to South. Geological structures and groundwater flow patterns are shown. (SMEDLEY and KINNIBURGH 2001)

The headwaters of the Ganges, Brahmaputra and Meghna river system mainly drain parts of the Himalayas and plains of India, Nepal and Tibet. Only 7.5 percent of the total catchment area (1.5 million sq km) lies in Bangladesh. The average annual rainfall ranges between 300 mm in Nepal to 11,615 mm at Cherrapunji on the Meghalaya Plateau, India. The mean annual rainfall in Bangladesh ranges between 1,250 mm in the western central region and 5,000 mm in the north-east.

Floods occur frequently during the period of monsoonal rainfalls, but the degree of flooding is very variable. The expanse of total flooded land area in Bangladesh ranges between 2.1 percent (3149 sq km) in 1982 and 56.9 percent (82,000 sq km) in 1988.

3.5. Hydrogeochemistry

The chemistry of Bangladesh's aquifers has been studied extensively during the last three decades, after the dimension of the arsenic poisoning came to light (e.g. NICKSON et al., 1998; NICKSON et al., 2000; MANNING and GOLDBERG, 1996; SMEDLEY and KINNBURGH, 2001; SMEDLEY and KINNBURGH, 2002, AHMED et al., 2004). AHMED et al. (2004) characterises Bangladesh's groundwater chemistry and geochemical characteristics of the aquifer sediments as follows:

The groundwater pH is generally near neutral to slightly alkaline (6.2 – 7.6). Dissolved oxygen is less than 1 mg/L and Eh values range between 500 and – 400 mV, mildly oxidising to strongly reducing conditions. Bangladesh's groundwater's are mostly from HCO₃ and Ca – Mg – HCO₃ type, in exceptional cases from Ca – Na – HCO₃ or Na – Cl type. The major ion composition seems to be controlled by depth and lithology and is dominated by HCO₃⁻ (ranging between 320 and 600 mg/L). Lower concentrations of SO₄²⁻ (<3 mg/L) and NO₃⁻ (< 0.22 mg/L) are characteristic with a few exceptions. On the other hand, phosphate concentrations are high with values of up to 8.75 mg/L. Major cations are distributed as follows and show variations with depth: Ca (21 – 122 mg/L), Mg (14 – 41 mg/L), Na (7 – 150 mg/L) and K (1.5 – 13.5 mg/L). Variabilities as a function of depth are reflected also in concentrations of total As (2.5 – 846 µg/L), total iron (0.4 – 15.7 mg/L) and Mn (0.02 – 1.86 mg/L). The dominant arsenic species are represented by As(III) with a share between 67 and 99 % and, in some wells, As(V). Highest concentrations are usually in alluvial aquifers of less than 150 m depth and levels of contamination reaches its maximum at depths between 10 and 50 m (HASAN et al., 2008).

Iron shows high correlations with HCO_3^- and PO_4^{3-} but low with total arsenic, even though this might have been expected. Ferrous iron precipitates as siderite (FeCO_3), which shows a positive SI of between 0.42 and 0.75. The SI values for calcite and dolomite are close to equilibrium, which show that Bangladesh's aquifers are not controlled by the dissolution of the carbonates. Furthermore, high levels of HCO_3^- appear to correlate with the concentrations of dissolved organic carbon (DOC = 1.15 – 14.2 mg/L) in groundwater. DOC concentrations indicate trends of variation with both As(III) and total iron. Sources for high concentrations might be organic matter in Holocene aquifers (see chapter 2).

Sulphate and Nitrate concentrations are near detection limit and there is no significant correlation with arsenic. Microbial activities could turn into an increase of sulphide (< 2 mg/L) and ammonia (< 13.2 mg/L). At elevated ammonia concentrations, high concentrations of As(III) were also detected.

The following hydrogeochemical investigations have been conducted in the Comilla district before:

- HASAN et al. (2008) investigated shallow alluvial aquifers in Daudkandi Upzilla up to a depth of 25 m. Water samples were taken for later hydrochemical determinations at laboratory. Sediment-samples were taken for later geochemical and mineralogical investigations. The results show, that the upper part of the aquifer (< 6.5 m depth) is distinguished by low dissolved concentrations of As, Fe and HCO_3^- but relatively high Mn, SO_4^{2-} and NO_3^- concentrations. The lower part of the aquifer is high in As (>10 $\mu\text{g/L}$) coupled with high Fe and HCO_3^- . Manganese is low as well as SO_4^{2-} and NO_3^- .
- ZAHID et al., (2007) did investigations at shallow (25-33 m) and deep (191-318 m) tube-wells at the south-east of Bangladesh (Kachua Upazilla), near the investigation area. The groundwater was divided in two groundwater-types: the Na-Cl type and the Na-Ca-Mg- HCO_3 type. The major ion trends are $\text{Na}^+ > \text{Ca}^{2+} > \text{Mg}^{2+} > \text{K}^+$ and $\text{Cl}^- > \text{HCO}_3^- > \text{SO}_4^{2-}$. The As concentration was detected as 140–585 $\mu\text{g/l}$ down to 33 m depth of upper aquifer in Kachua area, whereas moderate values were detected at the 2nd and 3rd aquifer (< 1– 44 $\mu\text{g/l}$).

4. Methodology

4.1. Field activities

The study area is located in Titas, Daudkandi Upzilla, Comilla District and was selected on the basis of an initial screening undertaken in November 2006 (see 3.1). Field activities undertaken as part of this study comprise an intrusive investigation and subsequent monitoring along with a survey on household and irrigation wells in the study area.

Field activities were undertaken between February, 9th and July, 31st 2007. Cores were used to acquire stratigraphical information and to retrieve undisturbed samples for further detailed classification and sorption tests in laboratory setups (LISSNER, 2008). Stratigraphical information acquired from the cores was used to decide on specific installation designs of the monitoring wells. Following the installation of the monitoring wells, water level and hydrochemical monitoring was undertaken to observe seasonal changes, as explained in section 4.1.2.

Parallel to the monitoring programme, the information was gathered for household and irrigation wells in the area in order to determine the spatial distribution of hydrogeochemical parameters to be presented in a digital atlas. A description of mapping programme is presented in the section 4.1.2.4. Lab analysis conducted in Germany and Canada on the collected samples is described in chapter 4.2.

4.1.1. Core drilling and test field setup

Core drilling was performed by rotary drilling and cable percussion to a final depth of 84 m. Drilling fluid was a bentonite-water mixture. Drilling equipment and handling was arranged by a local company. The drilling was stratigraphically logged and core samples were taken in 2” and 4” PVC liners. Altogether, 37 samples were taken and sealed immediately after extraction with paraffin wax. Samples of broken liners or unconsolidated material that was not retained in the liner were refilled in bags. In an on site glove bag the samples were divided in subsamples and packed in nitrogen filled polyethylene bags to avoid contact with the atmosphere. Sediment classification and laboratory sorption tests with the collected material were performed within another master thesis (LISSNER, 2008). The core drilling was used

for sampling and stratigraphically logging only. After achieving the final depth, the borehole was sealed and abandoned.

On the basis of the stratigraphic information obtained the layout of the future test field was developed. The approximately 20 m long and 5 m wide test field was set up in approximately 55 m distance to the core drilling, where seven individual sampling wells were installed at a depth of 9 m (30 ft), 15 m (50 ft), 21 m (70 ft), 26 m (85 ft), 27 m (90 ft), 35 m (115 ft), and 85 m (280 ft) (fig. 4.1.1.1.). Test well BGL TF 90 was drilled to a depth of approx. 40 m in the hope to catch a supposed sand-layer. However, that was not the case, so the bore hole was screened in a depth of 27 m and the lower part was sealed by a solid pipe. The boreholes were not cored, but the sediment slurry was sampled continuously to observe changes in stratigraphy.

An individual sampling code was given to each monitoring well in order to differentiate the single wells and measuring days. The following format was adapted: BGL- (stands for Bangladesh), TF- (stands for test field) and a number reflecting the depth in feet. The single measuring days are characterised by a consecutive number. For example the first monitoring at the 30 ft well is identified by the sample code BGL TF 30 01. In the following the monitoring wells will be labelled by these sample code.

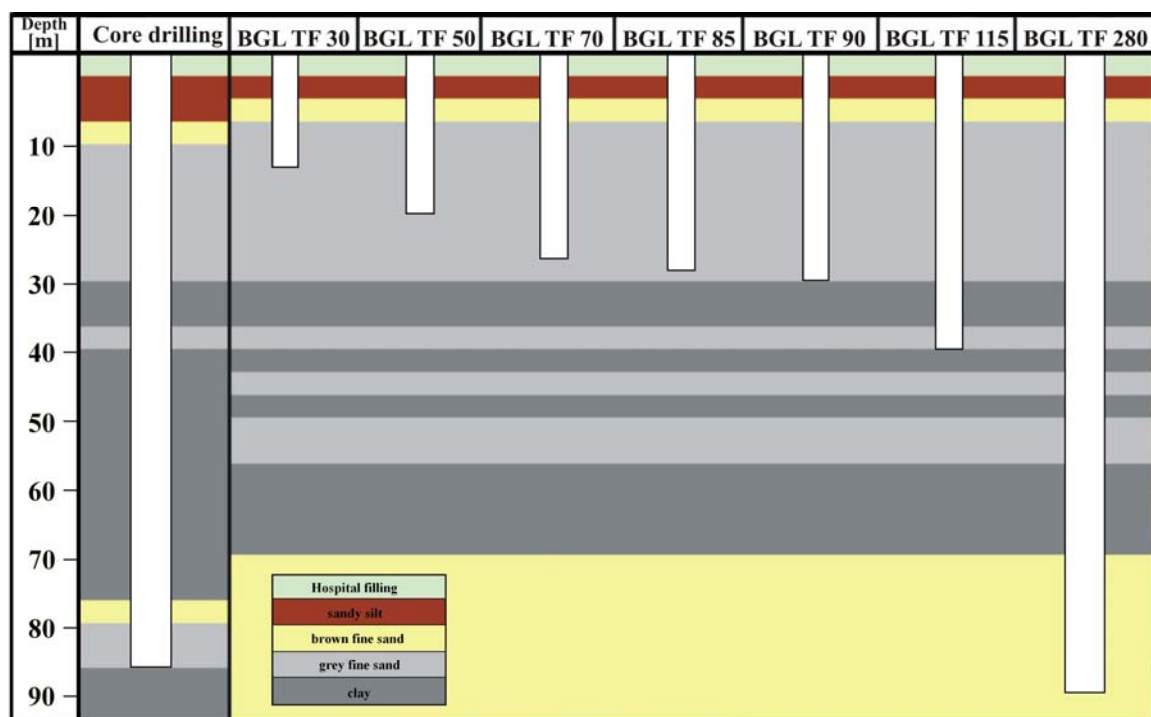


Fig. 4.1.1.1. The monitoring wells TF 30, TF 50, TF 70, TF 85 and TF 90 tapping the upper aquifer. TF 115 is sunken in a sand layer lens immediately below the major upper aquifer and TF 280 is sunken in the lower aquifer. Scale independent diagram

All monitoring wells, apart from TF 280, were constructed by the local „hand-flapping” method (see figure 4.1.1.2). This method involves utilization of a drilling fluid (a mixture of bentonite and water) to the borehole and driving of a cane into the sediment by use of a lever. The hand is used as a low pressure valve at the top of the cane to carry out the sediment laden slurry. The sediment slurry was sampled continuously to observe changes in stratigraphy. After reaching the desired depth, PVC casings were installed. The monitoring wells TF 30 up to and including TF 90 were all screened at the base of the hole with 1.5 m of slotted screen. TF 115 was screened with 3.1 m and TF 280 with 6.3 m at the base of the hole.

The drilling of the 85 m borehole (TF 280) was done by man powered rotary drilling. A drilling rig was raised to keep the drill stem. The rotary motion was done by four employees, moving the rig by pipe tongs. This drilling method did not produce cores either but offered the possibility to sample the drilling fluid which was circulated by means of an electrical powered mud pump.



Fig. 4.1.1.2. Well construction by the local „hand flapping“ method

The water samples were taken by a “low flow sampling” device. In order to be able to use this device, Teflon tubing with a 2 mm diameter was insert into the well down to the depth of the individual screens. The well tops were sealed by caps to avoid air admittance and protected by a lockable casing.

4.1.2. Monitoring

Altogether, 196 groundwater samples were taken: 140 (7 wells x 20 campaigns plus several replicates of the same sample for quality control) samples at the test field and 56 of both village and irrigation wells. Where possible, water table was measured using a light indicator. Samples were taken by low flow pumping, using a portable, battery-powered aspirated Ismatec pump (fig. 4.1.2.1). Irrigation wells were sampled by the farmer's mobile diesel powered irrigation pumps. Village wells were sampled without any exception by the so-called Hand-pump No.5. Since the commonly installed "hand pump No. 5" is a piston pump and thus a sealed system, it was not possible to lower a Teflon tube into the well without removing the entire hand pump. Therefore, a bucket was used as connector (fig. 4.1.2.1). Before sampling, the well was pumped for at least 15 minutes, giving flow rates of 1000 to 3000 ml/min to that amount to the purging of approximately three to five volumes of the well. However, due to the construction of a piston rod hand-pump a complete exclusion of water-air contact is not given.



Fig. 4.1.2.1. Sampling procedure for village wells by connection of a bucket (to avoid oxygen contamination and to connect the Hand-pump NO.5 with the transportable pump)

For sampling, water was continuously delivered to the bucket by hand pumping. Continuous overflow guaranteed exclusion of atmospheric oxygen to a certain extend. The sample was sucked by the peristaltic pump from the bottom of the bucket.

Redox-sensitive parameters and chemical species were measured at the sampling site. Temperature, pH, Eh, conductivity and dissolved O₂ generally were determined in a flow-through cell. Between the flow-through cell and the battery-powered pump, an interconnected T-distribution piece allowed taking water samples at the same time. Water samples were taken for onsite photometry and laboratory analyses. Alkalinity and acidity were determined by titration with NaOH and HCl in the field.

4.1.2.1. Electrochemical parameters

The onsite parameters such as pH, dissolved oxygen, conductivity, redox potential and temperature were measured by electrodes in a flow through cell. The flow through-cell and the electrodes were rinsed by the first litre of sample water over a period of about 10 minutes. Thereafter, the flow-through cell was refilled under continuous circulation of sample water and values were taken in time steps of 5, 10, 20, 30, 40 and 50 min.

The **pH** was measured with a combination SenTix 97/T pH electrode with integrated temperature probe. The displaying measurement instrument was a Hach HQ40d Multi Meter, which was used simultaneously for oxygen. For pH measurement a two point calibration with pH 4 and pH 7 buffer solutions was performed at least once a day. The pH values of the study area were close to neutral, ranging between 6.20 and 7.50. Upon completion of measurements, the probe was secured in a KCl filled protecting cap.

Dissolved **oxygen** was determined with a HACH HQ40d Multi Meter (luminescent based oxygen sensor with an integrated temperature probe). The displaying measurement instrument was, as aforementioned a Hach HQ40d Multi Meter, which was used simultaneously for the pH measurement. The sensor came pre-calibrated from HACH. There was no option for user-defined calibration. Concentrations for oxygen were indicated in percent as well as mg/L.

The **redox potential (Eh)** was determined as **EMF** (in mV) with an Ag/AgCl Pt 4805/S7 probe on the WTW MultiLine P4. Values for EMF ranged approximately between -150 and 200 mV. The EMF values were drifting strongly at the beginning of the measurement; if there was a slight difference between the 40 minutes and 50 minutes values in mV, equilibrium was accepted. Upon completion of measurement, the probe was regenerated and protected by a

KCl filled protecting cap. The following calculation was used to convert the EMF value to the Eh value:

$$E_h = EMF(\text{measured}) + (-0.7443 \bullet \text{temperature}[C^\circ] + 224.98) \quad (\text{eq.1})$$

The **conductivity** was determined with a TetraCon 325 conductivity cell with integrated temperature probe on the WTW MultiLine P4. The equilibration was reached after about 10 minutes. The values at the different wells ranged between 100 and 3200 $\mu\text{S}/\text{cm}$. A direct calibration of the conductivity-probe wasn't possible, but the accuracy was checked by testing a normalised 0.01 mol/L KCl standard solution (0.01 mol/L = 1413 $\mu\text{S}/\text{cm}$). If there was a significant deviation, the possibility was given to adapt the cell constant (c) at the WTW MultiLine P4.

As aforementioned, **water temperature** was determined with three probes: the SenTix 97/T pH electrode, the HACH HQ20 luminescent dissolved oxygen sensor, and the TetraCon 325 conductivity cell. The three measurement instruments showed similar values with deviations less than 0.1 $^\circ\text{C}$. Thus, a mean temperature was calculated from the three determinations.

The titration of inorganic carbon species (CO_2 , HCO_3^-) was done directly at the field site. **Alkalinity** (K_S 4.3) was determined with 0.1 N HCl and **acidity** (K_B 8.2) with 0.1 N NaOH using a digital titrator HACH Acidity Test Kit, Model AC-DT. The **pH** was monitored with the afore mentioned SenTix 97/T pH electrode with integrated temperature probe. From the consumption of acid or base, alkalinity and acidity can be calculated by the following formula:

$$K_S = \frac{V \bullet c}{V_S} \quad (\text{eq.2})$$

$$K_B = \frac{V \bullet c}{V_S} \quad (\text{eq. 3})$$

V = volume of added HCl or NaOH in mL
 c = concentration of HCl or NaOH in mol/L
 V_S = sample volume

The volume of consumed acid or base was displayed in rotation units and can be converted by the following formula in millilitre:

$$V = \frac{\textit{rotations}}{V_s \bullet 1000} \bullet \frac{800 \bullet N}{1000} \quad (\text{eq. 4})$$

N = normality of acid or base

4.1.2.2. Photometry

The redoxsensitive elements Fe^{2+} , Mn^{2+} , NO_3^- , NO_2^- , NH_3^- , and S^{2-} were analyzed in the field by photometry to avoid both chemical and microbial oxidation during storage. Total iron and manganese were also determined on-site. The photometer used in the field was a HACH DR/890 Colorimeter. Before measuring, the photometry vials were first rinsed with distilled water and afterwards rinsed two times with filtered sample water. All samples were filtered by hand, using the Membrex 25 CA filter stacked on top of a PE-syringe (25 ml and 100 ml). Cellulose Acetate filters with a pore size of 0.2 μm were used and replaced for each sample.

Total iron was determined with method 8008 with a detection range of between 0.03 and 3.00 mg/L. The standard deviation for this method is ± 0.017 mg/L. The FerroVer reagent reacts with all dissolved iron species in the sample to form soluble Fe(II). The Fe(II) reacts with the 1,10-Phenanthroline-Indicator in the reagent to an orange-coloured complex. Sample water was used as blank value; the required sample quantity was 10 ml. Concentrations in the study area ranged between lower than detection limit and 150 mg/l, so that dilution was necessary. Interferences may appear at high levels of Cl^- ($> 185,000$ mg/L), Mg ($> 100,000$ mg/L) and S^{2-} .

Method 8146 was used for determining **Fe(II)** with a detection range of between 0.03 and 3.00 mg/L. The standard deviation for this method is ± 0.017 mg/L. The 1,10 Phenanthroline-indicator interacts with the Fe(II) in the sample and forming an orange coloured complex. Sample water was used as blank value; the required sample quantity was 25 ml. Concentrations in the study area ranged between the lower than detection limit and 150 mg/L. Dilution was necessary.

Fe(III) was determined by subtracting Fe(II) from Total Iron.

Total manganese was determined by method 8149 with a detection range of 0.020 and 0.700 mg/L. The standard deviation for this method is ± 0.013 using a standard solution with 0.5 mg/L total manganese. An ascorbic acid reagent is used initially to reduce all oxidised forms of manganese to Mn^{2+} . An alkaline-cyanide reagent is added to mask any potential interference. PAN-indicator is then added to combine with the Mn^{2+} to form an orange-colour complex. Distilled water was used as blank; the required sample quantity was 25 ml. Concentrations in the study area ranged between the lower detection limit and less than 1 mg/L. Interferences can appear at high levels of aluminium (> 20.0 mg/L), copper (> 50 mg/L) and iron (> 5 mg/L).

Mn (II) was determined by a self-modified method 8149 with assuming the same detection limit of between 0.020 and 0.700 mg/L and standard deviation of ± 0.013 . The fundamental idea is to skip the ascorbic acid reagent, which reduces all oxidised forms of manganese to Mn^{2+} and determining originally present Mn^{2+} directly by adding the alkaline-cyanide reagent and the PAN Indicator. As a matter of fact, values with this method were less than values for total manganese. However, the method was not tested with standardized Mn^{2+} -solutions, yet.

Medium concentrations of **Nitrate** were determined by method 8171 with a detection limit of 0.2 and 5.0 mg/L. The standard deviation for this method is ± 0.1 mg/L using a standard solution of 3.0 mg/L NO_3^- -N. Cadmium metal (NitroVer 5) reduces nitrate present in the sample to nitrite. The nitrite ion reacts in an acidic medium with sulfanilic acid to form an intermediate diazonium salt, which couples to gentisic acid to form an amber-coloured product. Sample water was used as blank; the required sample quantity was 10 ml. Interfering substances can be ferric ions, chloride, and nitrite. Concentrations in the study area ranged between lower than detection limit and less than 2 mg/L.

Low concentrations of **Nitrite** were determined by method 8507 with a detection limit of between 0.005 and 0.350 mg/L. The standard deviation for this method is ± 0.001 mg/L using a standard solution of 0.250 mg/L nitrite nitrogen. Nitrite in the sample reacts with sulfanilic acid (NitriVer3 Nitrite Reagent Powder Pillows) to form an intermediate diazonium salt. This couples with chromotropic acid to produce a pink coloured complex directly proportional to the amount of nitrite present. Sample water was used as blank; the required sample quantity

was 10 ml. Interfering substances can be ferric ions, ferrous ions and nitrate. Concentrations in the study area ranged between lower than detection limit and less than 0.200 mg/L.

Ammonia (as $\text{NH}_4^+\text{-N}$) was determined by method 8155 with a detection limit of between 0.02 and 0.5 mg/L. The standard deviation for this method is ± 0.02 mg/L using a standard solution of 0.40 mg/L ammonia nitrogen. Ammonia compounds combine with chlorine to form monochloramine. Monochloramine reacts with salicylate to form 5-aminosalicylate. The 5-aminosalicylate is oxidised in the presence of a sodium nitroprusside catalyst to form a blue-coloured compound. The blue colour is masked by the yellow colour from the excess reagent present to give a final green-coloured solution. Distilled water was used as blank; the required sample quantity was 10 ml. Interfering substances can be iron (all levels), nitrate (> 100 mg/L), calcium (>1000 mg/L as CaCO_3) and nitrite (> 12 mg/L). Concentrations in the study area ranged between the lower detection limit and above 150 mg/L. Dilution was necessary.

Method 8131 was used for determining **Sulphide** (S^{2-}) with a detection limit between 0.01 and 0.70 mg/L. The standard deviation for this method is ± 0.02 mg/L using a standard solution of 0.73 mg/L sulphide. Hydrogen sulphide and acid-soluble metal sulphides react (sulphide reagent 1) with N, N-dimethyl-p-phenylenediamine oxalate (sulphide reagent 2) to form methylene blue. The intensity of the blue colour is proportional to the sulphide concentration. Distilled water was used as blank; the required sample quantity was 25 ml. Concentrations in the study area ranged between the lower detection limit and less than 0.10 mg/L.

4.1.2.3. Sample preservation

For later analyses at the laboratory, water samples were taken for speciation, totals, major cations and anions. All samples were filtered manually using the Membrex 25 CA filter Holder stacked on top of a syringe (25 ml and 100 ml). Cellulose Acetate filter with a pore size of 0.2 μm were used and replaced for each sample. Before collecting the water samples, the new bottles were rinsed with filtered sample water twice, to avoid contaminations. For quality check, triplicates were taken at different wells at intervals of 3 weeks.

Below, all used bottle types are listed, stating bottle size, material, preservation, intended use and the analyzing laboratory:

- 50 ml PE bottle, no preservation → IC (cations, anions; Freiberg)
- 100 ml glass bottle, no preservation → TIC / DOC (Freiberg)
- 50 ml PE bottle, 500 µL 1:1 HNO₃ → ICP-MS (totals; Trent)
- 60 ml HDPE bottle, 500 µL 1:1 HCl → IC-ICP-MS (As+P-species; Trent)

4.1.2.4. Mapping

Mapping as a basis for the digital atlas was done beside the periodical monitoring work at the test field. In an initial inspection, the size of the mapping area was set to approximately 10 km². For orientation, distinctive waypoints such as market-places, bridges, main buildings, transmitters and factory-buildings were located by GPS (Garmin eTrex). Land use and infrastructure were mapped by walking along roads, side roads, footpaths and rivers, using the tracking function of GARMIN handheld GPS.

The next step was to map all irrigation and domestic wells with information such as position, well depth, water-table, year of installation, owner, pipe casing, and use. Hydrochemical information such as arsenic or iron concentration were registered when known by the owner. It was not possible to read depth to groundwater at domestic wells, because the pumps are a closed system. The same problem occurred with irrigation wells when pumping. Sulphide concentrations were measured with on-site photometry when the well water had a rotten egg smell, which is an indication of elevated concentrations. Altogether, 202 domestic and 161 irrigation wells have been mapped within investigation area.

Table 4.1.2.4. Mapped household wells were selected for sampling. Selection criterion was, to sample wells of different depths and ages. The table shows the selection of sampled well

	< 30 ft	30 - 50 ft	50 - 60 ft	60 - 70 ft	70 - 80 ft	80 - 100 ft	100 - 120 ft	> 120 ft
< 1 a	-	MAP43	-	-	MAP06	MAP05	MAP42	-
1 - 5 a	-	MAP30	MAP27	-	MAP41/14	MAP01	-	MAP03
5 - 10 a	MAP26	MAP31/12	-	MAP04/07	MAP29	-	-	-
10 - 15 a	MAP13	MAP44	MAP15	MAP47	MAP46	-	-	-
15 - 20 a	-	-	-	MAP45	-	-	-	-
> 20 a	-	-	MAP28	MAP25	-	-	-	-

Based on the information, 26 domestic wells from different depths and ages were sampled in the dry season and analysed for the complete chemistry program (Table 4.1.2.4.1). Wells with increased arsenic concentrations were re-sampled during the rainy season. Irrigation wells

were sampled, where pumps were in operation. Altogether, 22 irrigation wells were sampled during the dry season; fields were flooded during the rainy season so that resampling was impossible.

The chemistry program was the same as described in former chapters (see chapters 4.1.2.1; 4.1.2.2; 4.1.2.3). Redox-sensitive parameters and chemical species were measured at the sampling site. Temperature, pH, Eh, conductivity, and dissolved O₂ generally were determined in a flow-through cell. Water samples were taken for on-site photometry and laboratory analyses. Alkalinity and acidity were determined by titration.

To distinguish between samples from monitoring and mapping, an individual sampling code was given to each well from the mapping campaign in order to differentiate the single wells. The following format was adapted: BGL- (stands for Bangladesh), MAP- (stands for mapping) and a consecutive number, starting with 01. Repetitive measurements are characterised by the second number, with a maximum of 02. For example sampling at the first well investigated during the mapping campaign is identified by the sample code BGL MAP 01 01.

4.2. Laboratory

4.2.1. DOC/ TIC

For the determination of total inorganic carbon (TIC) and dissolved organic carbon (DOC), filtered samples were sent in 100 ml glass bottles to Freiberg University, Germany without preservation. Speciation was done by the liquiTOC (elementar Analysensysteme GmbH) with a detection limit of between 0.1 and 5000 mgC_{org}/L and a standard deviation of ± 0.05 mgC_{org}/L. Device-specific attributes are described in the following table:

Table 4.2.1.1. Device-specific attributes for TIC/DOC speciation

Device:	"liquiTOC" (Elementar Analysensysteme GmbH)
IR - channels:	IR 1: 2.4 ml sample; detection limit: 0 - 49 mg C _{org} /L IR 2: 5.0 ml sample; detection limit: 50 - 300 mg C _{org} /L IR 3: 10.0 ml sample; detection limit: ≥ 300 mg C _{org} /L
calibration:	TIC: sodium carbonate DOC: potassium hydrogen phalate
detector:	UV detector
carrier gas:	oxygen with 3 bar

4.2.2. IC – cations

The concentrations of the major cations Lithium, Potassium, Sodium, Ammonia, Calcium, and Magnesium were determined by ion chromatography (IC). Therefore, filtered samples were sent in 50 ml PE bottles to Freiberg University, Germany without preservation. The ion chromatograph in use was a Merck HITACHI system model 6000A L5025, equipped with a RT 125-4.6-column. The detector was a Merck HITACHI L3720 Conductivity detector. No suppressor column was in use. The eluent was 2 mM HNO₃ + 0.9 mM Dipicolinacid + 0.75 mM Crown Ether with a flow rate of 1.0 ml/min. In case of high cation concentrations, samples were analyzed at different dilutions. The detection limits for the cations are shown at table 4.2.2.1:

Table 4.2.2.1. Detection limits for cation analysis

	Lithium	Potassium	Sodium	Ammonia	Calcium	Magnesium
detection limit:	0.05 mg/L	0.4 mg/L	0.1 mg/L	0.2 mg/L	0.3 mg/L	0.3 mg/L

4.2.3. IC – anions

The concentrations of the major anions Chloride, Bromide, Nitrate, Fluoride, Phosphate and Sulphate were determined by ion chromatography (IC). Therefore, filtered samples were sent in 50 ml PE bottles to Freiberg University, Germany without preservation. The ion chromatograph in use was an Eppendorf Biotronic IC 2001, equipped with a FGC II AN-P separation column and pre-column. The suppressor column was an Eppendorf Biotronic FGC 1 AG P. Detector was a conductivity detector with a range of 100 µS/cm. The eluent was 1.8 mmol/L Na₂CO₃ + 0.6 mmol/L NaHCO₃ with a flow rate of 1.5 ml/min. In case of high anion concentrations, samples were analyzed at different dilutions. The detection limits for the anions are shown at table 4.2.3.1:

Table 4.2.3.1. Detection limits for anion analysis

	Chloride	Bromide	Nitrate	Fluoride	Phosphate	Sulfate
detection limit:	0.1 mg/L	0.2 mg/L	0.3 mg/L	0.05 mg/L	1.0 mg/L	0.3 mg/L

4.2.4. IC – ICP – MS

For arsenic and phosphorous speciation, acidified samples were sent off to Trent University, Peterborough, Canada. Speciation was done by anion-exchange chromatography (Dionex, Sunnyvale, CA, column: IonPac AS-16) coupled to inductively coupled plasma mass-spectrometry (Elan[®]DRC[®] II, PerkinElmer, Shelton, CT) using a strongly alkaline eluent (0.1 M NaOH) to preserve potentially occurring thioarsenate species. Simultaneous ICP-MS on-line detection of arsenic (as AsO^+ , $m/z = 91$), phosphorous (as PO^+ , $m/z = 47$), and sulphur (as SO^+ , $m/z = 48$) in eluting compounds was accomplished using the dynamic reaction cell (DRC[®]) technology with O_2 as reaction gas as described previously (Planer-Friedrich et al. 2007). Species identification was achieved by retention time match with commercial standards. Arsenite, arsenate, and phosphate were quantified using standard solutions made from solids (NaAsO_2 , J.T.Baker, Phillipsburg, NJ; Na_2HAsO_4 , Sigma-Aldrich, Oakville, ON; $\text{NH}_4\text{H}_2\text{PO}_4$, SCP Science, Bale d'Urfé, QC). Due to the lack of a commercial standard, monothioarsenate was identified via retention time match with a synthesized monothioarsenate standard (Wallschläger and Stadey 2007) and routinely quantified using the arsenate calibration curve. A new phosphorous species was detected with a retention time of approximately 185 s that neither matched the retention times of a phosphite standard ($\text{Na}_2(\text{PHO}_3) \cdot 5\text{H}_2\text{O}$, Riedel-de-Haen, Seelze, Germany; retention time 260 s) nor exactly that of a hypophosphite standard ($\text{H}_2\text{NaO}_2\text{P} \cdot \text{H}_2\text{O}$, Sigma-Aldrich, Oakville, ON; retention time 175-180 s), even though it was close to the latter. Until further identification it is referred to as “unknown P-species” in the following. Its quantification is based on the hypophosphite calibration curve.

Arsenic and phosphorous total concentrations were determined independently from the sum of species by ICP-MS. Correction via an internal rhodium standard ($\text{RhCl}_3 \cdot \text{H}_2\text{O}$, SCP Science, Bale d'Urfé, QC) was applied in case of longer analytical runs to compensate for instrument sensitivity drift. An analytical reference material (TM-DWS, Environment Canada, National Water Research Institute) was included in each run as standard check.

4.3. Remote sensing

The Digital Atlas „Atlas Bangladesh 2007“ is based on the results of hydrogeological and hydrogeochemical field works at Titas, Daudkandi Upzilla, Comilla District, Chittagong Division, Bangladesh. The period of data acquisition was between February 2007 and July 2007 (see chapter 4.1.2.4).

Presentation of the spatial data was done with the GIS software TNTmips, version 2005:71 (MicroImages Inc.). This program includes TNTatlas, free viewing software, which allows the visualization of the digital atlas.

To generate the digital atlas, it was first necessary to import the Satellite Image (QuickBird, ID 1010010005888203, Acquisition Date 20070320, 60 cm 4-band PSM RGBI). The image comprises an area of 5000 * 5000 m and has a ground resolution of 60cm. The image was already georeferenced, so no further refurbishment was necessary. The four channels were combined for true colour displaying. Based on the satellite image, the percentage of land use was determined by a supervised, semiautomatic classification in off-shade mode. The land use areas were summarised in fallow, houses-congested areas, sand- and water surfaces, and farmland. Based on a field survey, land use areas were identified and marked by taking GPS coordinates (located by GPS [Garmin eTrex]). These coordinates were read out with Garmin Map Source software, version 6.13.4, and were imported as reference points into TNTmips. The next step was to import further coordinates into TNTmips, divided in:

- House wells – labelled as HW in field site and marked as red dots in the atlas;
- Irrigation wells – labelled as IRR in field site and marked as blue squares in the atlas;
- Monitoring wells – labelled as TF in field site and marked as green dots in the atlas;
- Infrastructure – marked by individual symbols;
- Roads, Hydrogeology – taken by GPS in tracking mode with a dot spacing of 25 m

These coordinates were imported as vector objects, standardised to the Universal Transverse Mercator System (UTM) Zone 46 North CM93E. Assigned to these vector points, additional tables with information such as well-age, owner, use, features, hydrochemistry, etc. were imported as databases. From these tables, three groups for hydrochemistry were created: Chemistry HW, Chemistry IRR and Chemistry TF. Within these three groups, different notations were chosen to illustrate hydrochemical features, based on the internal feature

tables. TIC/DOC, major anions, major cations, total arsenic/phosphorus, and their species were displayed as pie charts and bar charts, respectively. Therefore, a SML-script was written, defining size, shape, colours and graphic rendition for all charts. Additionally, the concentrations are printed next to the charts, also based on a SML-script. Conductivity, redox-potential, and dissolved oxygen are displayed as bubbles, size and colour depending on the represented concentration: small size with blue colour for low concentrations, medium size with green colour for moderate concentrations, and big size with red colour for high concentrations.

The spatial distribution for each TIC/DOC, total As/P, arsenate, arsenite, phosphate, iron, manganese, and ammonia is shown by contour lines, plotted with Golden Software Surfer 8. Therefore, the coordinates as well as the associated hydrochemical values were imported to the internal excel-table in Surfer. Only wells from depths ranging between 12 m and 25 m, assumed to show the highest effects, were considered. The next step was to create the grid with a lattice spacing of 5 mm per cell with Kriging as gridding method. The grids were exported as grd-files; contour lines were exported as mif-files. Colouring was made in TNTmips, choosing red colour for high values and blue for low values. These raw data were imported separately to TNTmips and regrouped for each element. Those wells, characterising the grid, are shown as a vector layer, divided in house wells (HW), irrigation wells (IRR) with known depths, and irrigations wells (IRR) with unknown depths. Supplementary, those wells with depths lower than 25 m and less than 12 m are presented by size depending pie charts for corresponding elements, based on a SML-script.

4.3.1. TNTAtlas – important tools

Viewing tools

Different viewing tools are available within TNTAtlas. TNTAtlas is a free software product from MicroImages for viewing hierarchical atlases prepared in TNTmips with HyperIndex Linker, or for single-layout atlases. The available atlas is a single-layout.



Redraw: use after selecting a new layer to refresh the view



Full Zoom: to revert from detailed view to general view



Previous View: restore previous view and zoom



Zoom In: enlarge view



Zoom Out: reduce view



Zoom Box: default viewing setting; by holding the left mouse button, a rectangle can be drawn in the region of interest; right mouse button confirms selection

Working tools

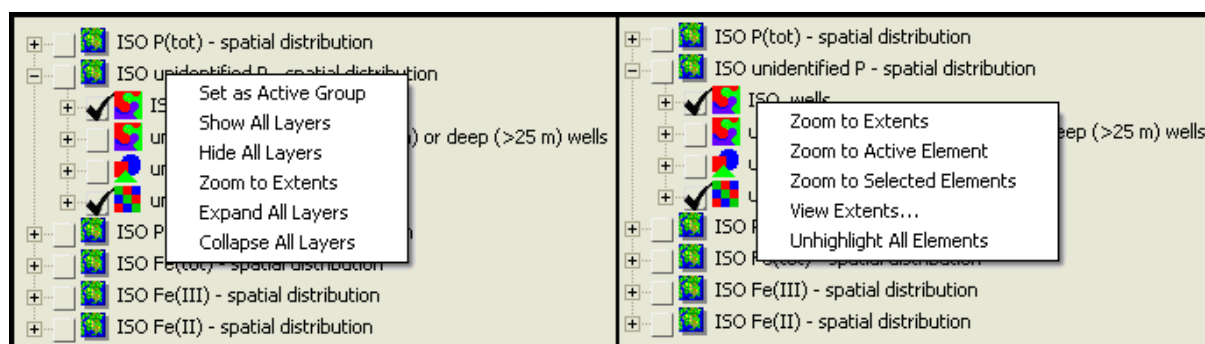


Geo Toolbox: opens an additional window including working tools for measuring lengths, areas or to get point information. Therefore, different geometric types like arcs, polygons etc. are available. Sketches can be drawn.



Select: single vector objects can be chosen by this tool. Click the vector of interest by the left mouse button, go to the associated group and layer and select a feature table. A red dot will mark the selected point information.

Clicking on groups or layers by **right mouse** button provides several functions



5. Results and discussion

5.1. Digital Atlas

The “Digital Maps” layout contains a 5km x 5km Quickbird RGBI Satellite Photo and a georeferenced base map to give an overview about the location. Moreover, detailed information including land use, infrastructure and water supply by irrigation and village wells are given in further layers. Different chart types and contour line-plots present the hydrogeochemical situation at the investigation area and give a spatial and depth dependent summary for groundwater components like anions, cations, redox sensitive elements and field parameters as well as arsenic and phosphorus. These features and additional data are included in tables belonging to the vector objects.

In addition to the data acquisition as the general basis of the digital atlas, a weekly monitoring was done on seven wells within the established test field. A major purpose of the digital atlas was thus to provide background information to relate observations from the test field to a larger context and interpret them considering the overall spatial distribution of hydrogeochemical parameters. The digital atlas should be considered as a snapshot of the whole arsenic problem at one of the most highly affected regions in Bangladesh. TNTmips version 2005:71 provides the basis for the digital atlas.

5.1.1. Groups and layers

The digital atlas is subdivided in several thematic groups that are further separated in different layers. Altogether these twenty groups can be abstracted into three thematic categories: the hydrogeochemistry of sampling points for mapping, the spatial distribution of selected chemical elements, and some basis cartographic information comprising of topography, land use and infrastructure. All layers were georeferenced by the Universal Transverse Mercator (UTM) Zone 46 North CM93E. Below the groups are described in the order of the digital atlas from top to bottom. Navigation is described in chapters 4.3.1 and 4.3.2.

Groups and layers are divided in:

Chemistry HW: contains eleven vector layers with hydrogeochemical features for the mapped house wells (HW) which were sampled between February and April. The layers represent from top down total arsenic, total phosphorus, arsenic species, phosphorus species, total inorganic carbon (TIC) and dissolved organic carbon (DOC), Eh, oxygen, conductivity, pH, and temperature, cations (Li^+ , Na^+ , NH_4^+ , K^+ , Mn^+ , Ca^{2+} , Mg^{2+}) and anions (F^- , Cl^- , NO_2^- , NO_3^- , PO_4^{3-} , SO_4^{2-}). The totals are presented in bar charts. Species, carbon, cations, and anions are displayed in pie charts and the on site parameters represented as different coloured and sized pins (see 5.1.4).

Chemistry IRR: contains eleven vector layers (see chemistry HW) for the mapped irrigation wells, which were sampled between February and April.

Chemistry TF: contains eleven vector layers (see chemistry HW) for the monitoring wells at the test field. Wells in test field were sampled in regular intervals of about one week over a period of six month. The Chemistry TF group displays chemical data from middle of March, to get contemporary and comparable data to the house wells (HW) and irrigation wells (IRR).

WHO/EPA: The three layers show drinking water standards for arsenic, manganese and iron by different coloured and sized pins. As the layer name implies, the standards are derived from the World Health Organisation (WHO) for arsenic (10 $\mu\text{g/L}$) and manganese (0.4 mg/L) and the Environmental Protection Agency (EPA) for iron. The second value represents the local limit for arsenic in Bangladesh.

As(tot) vs. P(tot): In these two layers, pie charts reflect relative concentrations for arsenic and phosphorus by bubble size.

ISO: The ISO groups display the spatial distribution of selected hydrogeochemical compounds in the investigation area. Each group is composed of four layers. Wells with depths between 12 m and 25 m are shown as a black/with contour line map and coloured contour line plots that can be activated independently. Shallow (<12 m) or deep (>25 m) wells are highlighted by pie charts, bubble size reflects relative concentrations for each element.

The digital atlas contains eleven ISO groups for total arsenic, arsenate, arsenite, total phosphorus, unidentified phosphorus, phosphate, total iron, divalent iron, trivalent iron, total manganese, TIC, DOC, and ammonia.

Sampling points for mapping: contains three vector layers with all wells mapped in the investigation area. HW displays all house wells, IRR all irrigation wells and TF refers to the newly tapped monitoring wells at the test field. The coordinates were determined by GPS. In addition, feature tables give information about age, depth, finishing, use, and owner, if the information was available. Wells, which were analysed for their complete chemistry (see the chemistry groups) are labelled by the sample code MAP.

Topography, land use and, infrastructure: The raster layer “Satellite Image” (QuickBird, ID 1010010005888203, Acquisition Date 20070320, 60 cm 4-band PSM RGBI) with a ground resolution of 60cm serves as the general basis of the digital atlas. The raster layer “Land use” is based on the satellite image and was edited by a supervised, semiautomatic classification. The vector layer infrastructure is based on field measurements. Roads and hydrogeology were georeferenced in TNTmips.

5.1.2. Legends of the Layers

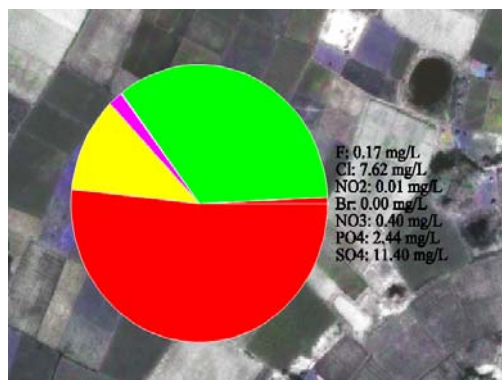
For the most part, the layers of the atlas Bangladesh 2007 are self-explanatory by legends and symbols. In some layers, a legend was not possible due to limited functions of TNTmips. In the following, these layers will be explained, starting from the top to bottom.

- Each individual **ISO** group comprises the same kind of layers, exemplified by the group ISO As(tot), containing ISO wells, an contour line plot and a black/white contour layer. These layers are self-explanatory by legends. The layer **Arsenic(total) in shallow (<12 m) and or deep (>25 m) wells** comprises pie charts for arsenic in shallow or deep wells. The higher the arsenic concentration, the bigger the pie charts. Additionally, the single pie-charts are labelled with the associated well depth.

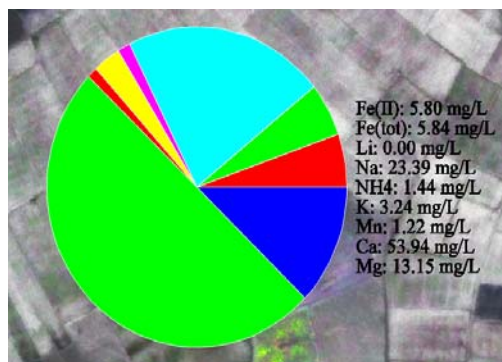
- The layer **As(tot) vs. P(tot)** compares total arsenic concentrations in $\mu\text{g/L}$ to total phosphorus in $\mu\text{g/L}$. For both arsenic and phosphorus, amount dependent pie charts were chosen, based on a SML-script. The pie-chart for arsenic is yellow-coloured, that for phosphorus again is pink coloured.



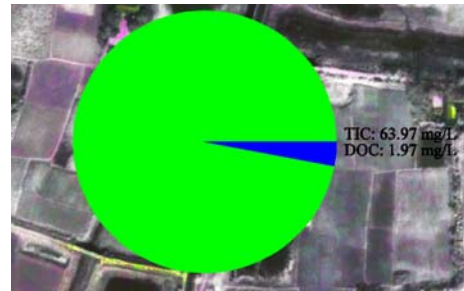
- The TNT atlas contains three chemistry groups: Chemistry HW, Chemistry IRR and Chemistry TF. Each chemistry group comprises the same kind of layers, exemplified by the group Chemistry IRR, containing layers for total arsenic, total phosphorus, arsenic species, phosphorus species, TIC/DOC, Eh, dissolved oxygen, conductivity, pH, and temperature, major cations and major anions. Apart from the layers for Eh in mV, Oxygen in mV and Conductance in $\mu\text{S/cm}$, each layer is based on a SML-script, which excludes an internal legend. In the following, these layers will be explained, starting from the top to bottom:
 - The layer **Anions** contains pie-charts for all major anions. Colouring for each element was chosen as follows: ■ (sulphate), ■ (chloride), ■ (phosphate), ■ (nitrate), ■ (bromide) and ■ (fluoride). Concentrations are listed at the right site;



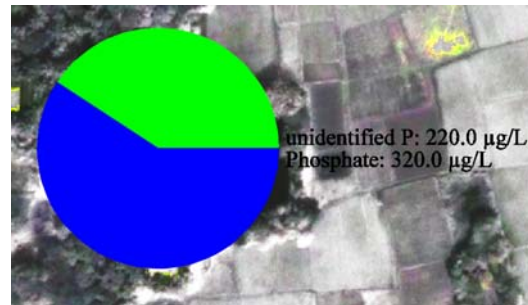
- The layer **Cations** contains pie-charts for major cations. Colouring for each element was chosen as follows: ■ (calcium), ■ (sodium), ■ (magnesium), ■ (potassium), ■ (Fe[III]), ■ (manganese), ■ (ammonia), ■ (Fe[II]), and ■ (lithium). Concentrations are listed at the right site;



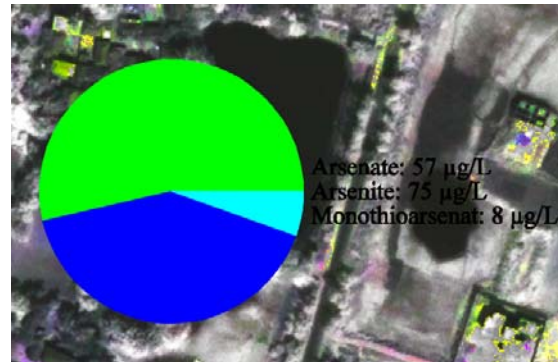
- The layer **TIC/DOC** contains pie-charts for main total inorganic carbon and dissolved organic carbon. Colouring was chosen as follows: ■ (TIC) and ■ (DOC). Values are given at the right site;



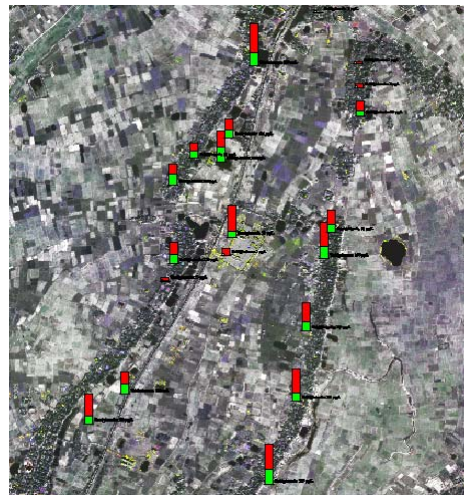
- The layer **Phosphorus species** contains pie-charts, divided in phosphate and unidentified phosphorus species. Colouring was chosen as follows: ■ (phosphate) and ■ (unidentified P). Concentrations are plotted at the right site in $\mu\text{g/L}$.



- The layer **Arsenic species** contains pie-charts. Colouring was chosen as follows: ■ (arsenite), ■ (arsenite) and ■ (Monothioarsenate). Concentrations are given at the right site in $\mu\text{g/L}$.



- Within the layers **P(tot)** and **As(tot)**, concentrations for total phosphorus and total arsenic are shown as bar-graphs. The bar-graph for phosphorus is coloured red, that for arsenic is light green. Additionally, concentrations are plotted at the right site of each chart. If both layers are activated, As and P can be compared with each other.



5.2. Hydrogeochemistry

5.2.1. Data evaluation

During the field activities, 7 sampling sites were investigated at the test field, another 48 in the surrounding area. Altogether, 196 water samples were taken; 140 at the test field and 56 at the mapped sites. Redox sensitive parameters (pH, dissolved oxygen, conductivity, redox potential, temperature), and redox sensitive constituents (Fe^{2+} , Mn^{2+} , NO_3^- , NO_2^- , NH_3^- , S^- plus total Fe and Mn) were measured at the sampling sites (see chapters 4.1.2.1., 4.1.2.2.). Major anions and cations, total inorganic carbon (TIC) and species for arsenic and phosphorus were analysed in different laboratories (see chapter 4.2.). Values below detection limit were replaced by $0.3 * \text{detection limit}$; missing values were labelled by the general code -999.

5.2.1.1. Charge imbalance by PhreeqC

The accuracy check of the water analyses from field site and laboratory was done by calculating the charge imbalance with the hydrogeochemical modelling program PhreeqC version 2.15 using the WATEQ4F-database. The program PhreeqC uses the following equation for calculating the charge imbalance:

$$\text{PercentError} = \frac{100 * (\sum \text{cations}[\text{meq} / \text{L}] - \sum \text{anions}[\text{meq} / \text{L}])}{(\sum \text{cations}[\text{meq} / \text{L}] + \sum \text{anions}[\text{meq} / \text{L}])} \quad (\text{eq. 5})$$

For field measurements with a wide range of error sources, values $\leq \pm 10\%$ are considered as tolerable and values $\leq \pm 5\%$ can be seen as accurate. Potential errors such as inaccurate dilution in the field and laboratory, errors in sample acidification and preservation, etc. might sum up and contribute to the observed charge imbalance besides analytical problems.

Beside the major cations and anions, on-site parameters such as pH, dissolved oxygen, redox potential and temperature were included for error calculation with PhreeqC. The results of the accuracy check are represented in figure 5.2.1.1.1 for (a) mapped wells and (b) monitoring wells at the test field.

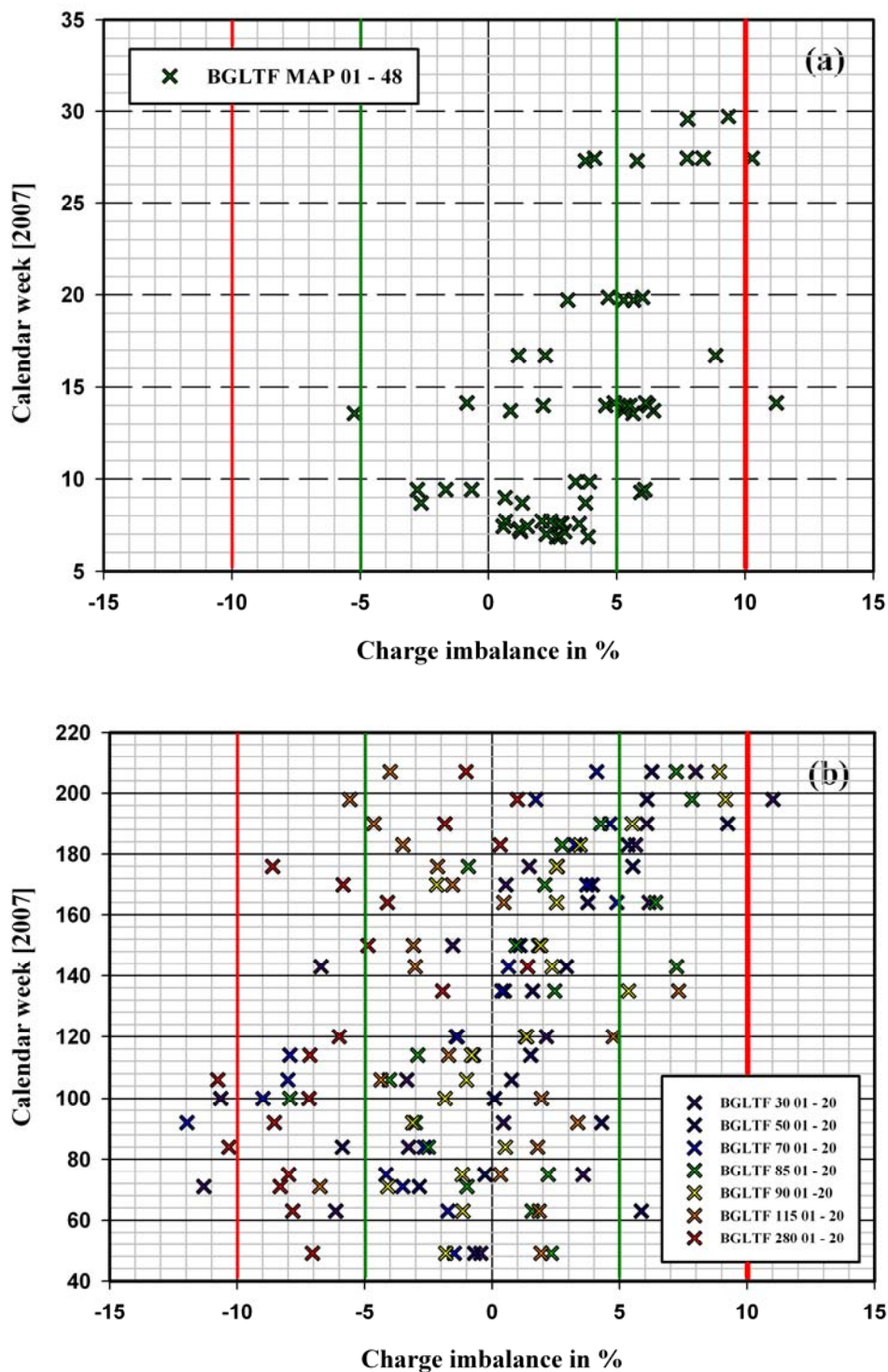


Fig. 5.2.1.1.1. Calculated charge imbalances for (a) mapped wells and (b) monitoring wells at test field. Modelling was done with PhreeqC, version 2.15

Due to a partial instrument failure (HACH HQ40d Multi Meter), values for oxygen and pH were not measured at the monitoring well BGL TF 30 18 on the 08.07.2007. Electrochemical parameters were not taken and photometry was not conducted at the monitoring wells BGL TF

85 19, 90 19 and 280 19 due to heavy monsoonal rains. These parameters were interpolated for the accuracy check by linear regression based on the remaining data from the same well at different sampling times. The interpolated values will not find attention for further evaluations.

The accuracy check with PhreeqC (PARKHURST, 1995) resulted for the most part in errors $< \pm 5\%$. But especially at the BGL TF 280 series, a deficit of cations with charge imbalances less than -5% was recognized in most cases. This could be due to high dilution ratios (up to 1:500) for ammonia (>100 mg/L) and Fe[II] (> 100 mg/L) in the field with correspondingly high potential for inaccuracies. Dilutions in the laboratory with ratios of up to 1:15 were necessary for carbon (> 120 mg/L), chloride (> 500 mg/L) and sodium (>200 mg/L), a further source of error.

5.2.1.2. Measured vs. Calculated Specific Conductance after ROSSUM (1975)

As the charge balance as described before only gives the information on either deficit of cations or excess of anions, an additional parameter is needed to determine the source of error. Thus, conductivity was calculated based on the sum of specific conductances for individual species as calculated by PhreeqC and compared with the measured conductivity. The calculation was done in an Excel-file considering specific conductances for CO_3^{2-} , HCO_3^- , SO_4^{2-} , Cl^- , NO_3^- , F^- , Br^- , HSO_4^- , Ca^{2+} , Mg^{2+} , Na^+ , K^+ , Li^+ , Fe^{2+} , Al^{3+} , Ba^{2+} , Fe^{3+} and Sr^{2+} , taken from ROSSUM (1975). In cases where the calculated conductance exceeds the measured conductance, negative charge balance indicates an excess of anions, whereas positive charge balance indicates an excess of cations. If the measured conductance is greater than the calculated conductance, negative charge balance indicates a deficit of cations, whereas a positive charge balance indicates a deficit of anions.

Figure 5.2.1.2.1 shows that the measured conductivity exceeds the calculated conductivity at almost all monitoring wells from test the field with exception of well BGL TF 115 at the measurement-series 01 (23.02.2007), 16 (25.06.2006) and 17 (03.07.2007). Also at the mapped wells, the measured conductance exceeds the calculated conductance without exception. Therefore, a deficit of cations and anions is present at almost all wells. The mean deviations range 18.1 % at well BGL TF 115 and 33.4 % at well BGL TF 85 (see appendix 1b). The calculated specific conductance after ROSSUM is designed for EC-values less than $1000 \mu\text{S}/\text{cm}$. At values $> 1000 \mu\text{S}/\text{cm}$, inaccuracies may appear. However, also values within

the range of calculation were less than the measured values from field site. Problems with the EC electrode were already encountered in the field and thought to have been solved by re-adjustment of the cell constant. Apparently this was not the case and the unacceptable high discrepancies between calculated and measured conductivities are most likely due to wrong values for the latter. Therefore, the calculated conductivity will be used in the following, under the assumption that these values are more exact.

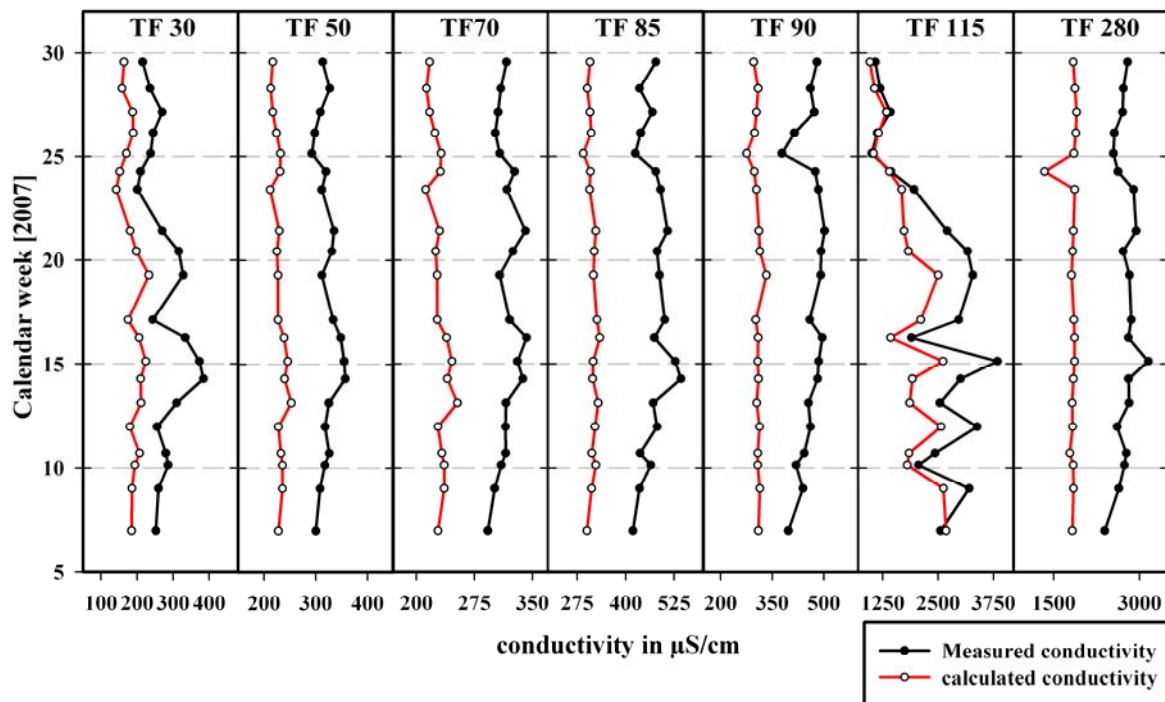


Fig. 5.2.1.2.1. Comparison of measured conductivity with calculated conductivity for each monitoring well at the test field, linear plotting

In spite of re-measurements for cations, anions and TIC/DOC, the limit of tolerance ($\leq \pm 10\%$) was exceeded in the following wells, shown at table 5.2.1.2.1. As shown in table 5.2.1.2.1, the measured conductance exceeds the calculated conductance in all cases, which is why a negative percent error indicates a deficit of cations and a positive percent error indicates a deficit of anions. As aforementioned at chapter 5.2.1.1, possible sources of error could be high dilution ratios (up to 1:500) for ammonia (>100 mg/L) and Fe[II] (>100 mg/L) in the field with correspondingly high potential for inaccuracies. Dilutions in the laboratory with ratios of up to 1:15 were necessary for carbon (>120 mg/L), chloride (>500 mg/L) and sodium (>200 mg/L). But this is not a reason for high charge imbalances at the wells BGL TF

30 and 70, because dilutions were unnecessary. Presumably, these imbalances might be based on errors in measurement at the field and laboratory respectively.

Table 5.2.1.2.1. Wells with charge imbalances $> \pm 10$ %. The percent error was determined with PhreeqC; the deficit of ions was determined due to a comparison between the measured conductance and the calculated conductance

Sample-code	% error	Measured EC	Calculated EC	Comment
BGLTF 30 03	-11.3	286.2	194.0	deficit of cations
BGLTF 30 07	-10.6	384.0	210.0	deficit of cations
BGLTF 30 19	11.0	236.0	158.0	deficit of anions
BGLTF 70 06	-12.0	315.6	253.0	deficit of cations
BGLTF 280 05	-10.3	2605.0	1833.0	deficit of cations
BGLTF 280 08	-10.8	3150.0	1863.0	deficit of cations
BGLMAP 37 01	11.2	388.0	241.0	deficit of anions
BGLMAP 43 02	10.3	231.5	166.0	deficit of anions

5.2.1.3. As/P totals vs. sum of As/P species

Arsenic and phosphorus species were determined by IC-ICP-MS, totals were determined independently by ICP-MS. On the assumption that all species for phosphorus and arsenic were detected and correctly quantified, the sum of it should give the same values as the independently measured concentrations for arsenic and phosphorus totals. For this purpose, the sum of species was compared with totals by using linear regression (fig. 5.2.1.3.1) and individually for each monitoring well (see appendix 2a and 2b). In comparison to arsenic and phosphorus totals, excess values for the sum of species could reveal errors in measurements either during speciation or determination of totals. If values for the sum of species are less than total As/P, this could also be an indication for an undetected arsenic and/or phosphorus species. Values for the measurement-series 16 (25.06.2006) were not taken into account, because these samples were not acidified in the field and show thus expectedly lower total concentrations due to precipitation.

According to figure 5.2.1.3.1b, the values for total arsenic and sum of arsenic species show a significant correlation ($P \leq 0.05$) and match well at concentrations less than approximately 150 $\mu\text{g/L}$. Between 150 $\mu\text{g/L}$ and 250 $\mu\text{g/L}$, total As exceeds the sum of As-species in the majority of cases, observable at the wells BGL TF 70 and 90 (see appendix 2a). At values > 250 $\mu\text{g/L}$, the sum of As-species exceeds total arsenic in all cases, observable at the wells BGL TF 85 and BGL TF 115 (see appendix 2a). The distribution of total phosphorus vs. sum

of phosphorus species also show a significant correlation ($P \leq 0.05$). The totals-species ratio for phosphorus is balanced at values less than approximately 4000 $\mu\text{g/L}$, as shown in figure 5.2.1.3.1a. At values greater than 4000 $\mu\text{g/L}$, perceptible deviations occur in favour of totals as well as species and can be assigned to BGL TF 115, the only well at such high concentrations (see appendix 2b).

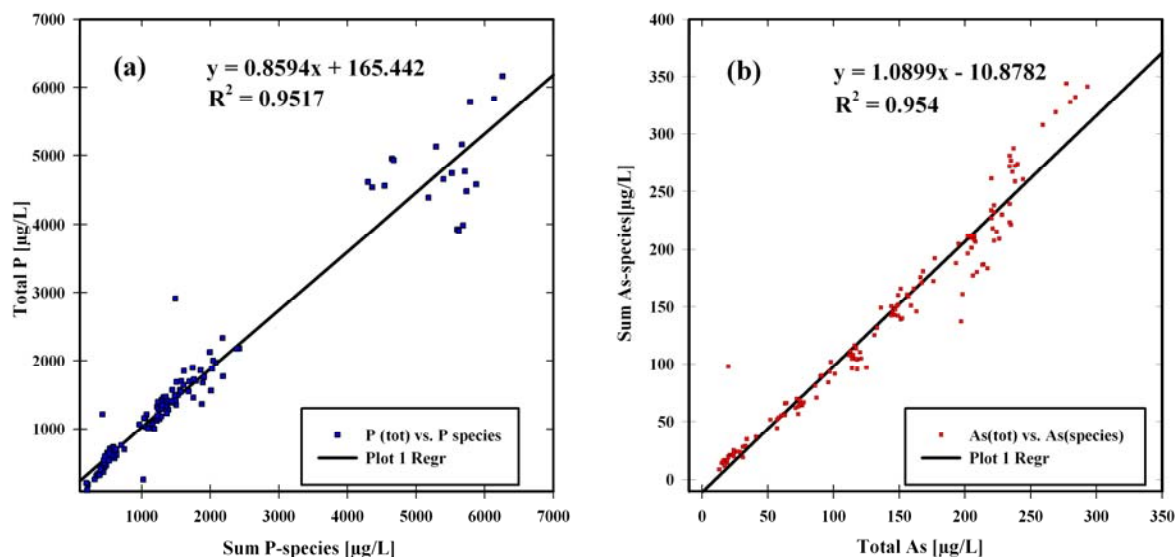


Fig. 5.2.1.3.1. Phosphorus (a) and arsenic (b) in comparison to sum of species

5.2.2. Spatial distribution

As described in chapter 4.1.2.4, mapping was done to put the results from hydrochemical weekly monitoring at the test field site (see chapter 4.1.2) into a bigger context in relation to the spatial distribution of groundwater components like anions, cations, redox-sensitive elements, and field parameters as well as arsenic and phosphorus in the surrounding area. Altogether, 363 wells were registered, 201 house wells (HW) and 162 irrigation wells (IRR). Of these, 26 house wells and 22 irrigation wells were selected for analyses of the complete hydrochemical program. The irrigation wells were chosen randomised by considering working pumps and regular distances to the test field site. Furthermore, house wells were selected to cover a wide range of different ages and depths (see figure 4.1.2.4). Most of the wells are constructed in depths ranging from 12 m to 25 m, apart from two deeper wells (BGL MAP42 = 35 m and BGL MAP 03 = 275 m) and four shallow wells in depths less than 12 m (BGL MAP 13, 26, 30, and 31). Altogether, 9 irrigation wells are unknown in depth because the water table was not measurable with the pumps installed. A later determination was not possible, because re-localization of the well was impossible due to device-specific deviations of GPS and closeness to other irrigation wells. These wells were adopted with depths of between 18.0 m and 21.0 m, usual for irrigation wells. In the following, these wells will be treated equally to wells with known depths.

The hydrogeochemistry of both Bangladesh and West Bengal (India) is summarized in chapter 3.5. In the study area at Titas, Daudkandi Upzilla, Comilla District (see figure 3.1.1), situated in the south-east of Bangladesh, almost all wells are increased in total arsenic and exceed the local drinking water standard of 50 µg/L, some more than fourfold. Only three wells (BGL MAP 22, 32 and 44) are below the local drinking water standard, but exceed the international guideline for arsenic (10 µg/L). From all sampled wells, 57 % exceed 100 µg/L and 6 % exceed 200 µg/L. The dominant arsenic species at nearly all wells is arsenite (the As(III)/As(tot) ratio is between 60 to 92 %) and, at well BGL MAP 18 arsenate at a rate of 68.4 %. The predominance of arsenite was also reported by several authors (SMEDLEY and KINNIBURGH, 2001; BGS; AHMED et al., 2004). An As distribution-map for the study area was prepared with the results of mapping, suggesting that arsenic is increased at most of the shallow wells (see figure 5.2.2.2). AHMED et al. (2004) describes that maximum of arsenic concentrations occur at depths between 20 and 50 m, whereas samples shallower than 10 m and deeper than 150 m are basically As free. This was confirmed by several authors

(SMEDLEY and KINNIBURGH, 2001; HASAN et al., 2008; ZAHID et al., 2007; ZHENG et al., 2004; RAVENSCROFT et al., 2001; RAVENSCROFT et al., 2005). In the study area, arsenic is increased at depths between 12 and 35 m, whereas shallow wells (< 10 m) can be seen as less affected or arsenic-free respectively (see figure 5.2.2.1). Apart from BGL MAP 03 (275 m), depths less than 35 m were not sampled during the mapping campaign, so that a general statement in consideration of water quality can't be made (see figure 5.2.2.1). As figure 5.2.2.2 suggests, high concentrations of arsenic are equally distributed through-out the study area as well as phosphorus.

Phosphorus commonly occurs in study area and at the test field as fully oxidised phosphate with rates between 76 and 99.8 %; remaining rates belong to unidentified phosphorus species, which is dominant at BGL MAP 03, 20, 26, 30 and 31 (see appendix 4). Total phosphorus ranges from approximately <100 to 1400 $\mu\text{g/L}$ (see figure 5.2.2.1). Phosphate as dominant species was also reported in several publications (BHATTACHARYA et al., 2002; AHMED et al., 2004; HANRAHAN et al., 2004)

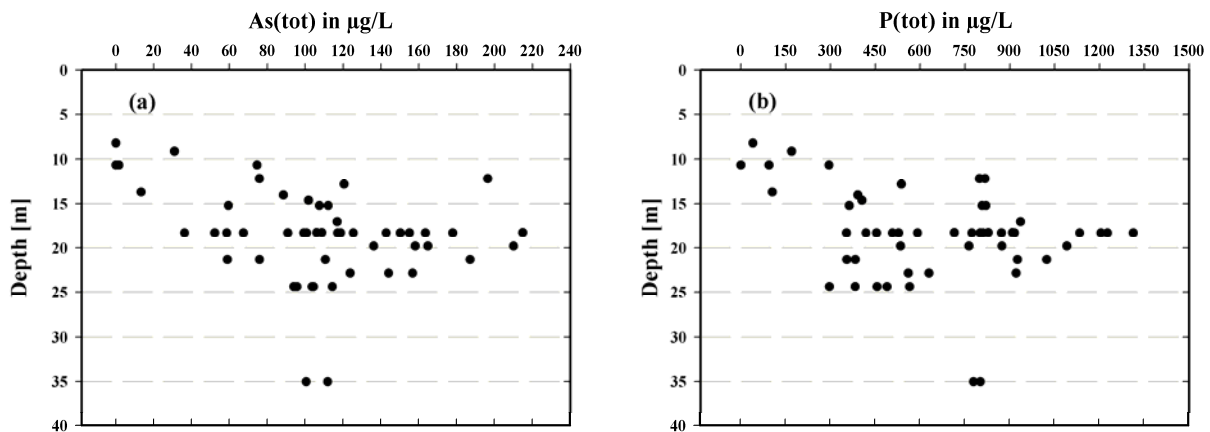


Fig. 5.2.2.1. Distribution of (a) total arsenic and (b) total phosphorus vs. depth

Eh values were determined to be in the range of mildly oxidising conditions (100 – 350 mV), typically for arseniciferous groundwaters (ZHENG et al. 2004; BHATTACHARYA et al., 2002; AHMED et al., 2004). Several authors reported redox potentials typically less than 100 mV (SMEDLEY and KINNIBURGH, 2002; BGS and DPHE, 2001). The groundwater pH at all wells is in the near-neutral range (6.5 – 7.3). For the most part, iron occurs as reduced Fe(II) with values of between 0.2 and 14.1 mg/L so that concentrations of total iron are almost similar distributed (0.8 – 20 mg/L). Fe(III) is less than 1 mg/L. High concentrations were determined for manganese (0.28 – 1.34 mg/L), HCO_3^- (<500 mg/L), SO_4^{2-} (< 30 mg/L). Chloride (< 30 mg/L), Ammonia (<1 mg/L), Nitrate (< 0.8 mg/L), Nitrite

(< 0.03 mg/L), Bromide (< 0.01 mg/L) and Sulphide (< 0.04 mg/L) are generally low. With respect to whole Bangladesh, this was also reported by several authors (SMEDLEY and KINNIBURGH, 2002; MC ARTHUR et al., 2000; RAVENSCROFT et al., 2003; NATH et al., 2007; ZAHID et al., 2007; HASAN et al., 2008). Total inorganic carbon (TIC) concentrations mainly ranging between 26.0 and 56.0 mg C/L, dissolved organic carbon (DOC) is generally low (< 3.7 mg/L). The spatial distribution of As(tot), arsenite, arsenate, Fe(II), Mn and Eh in the study area is represented at figure 5.2.2.2.

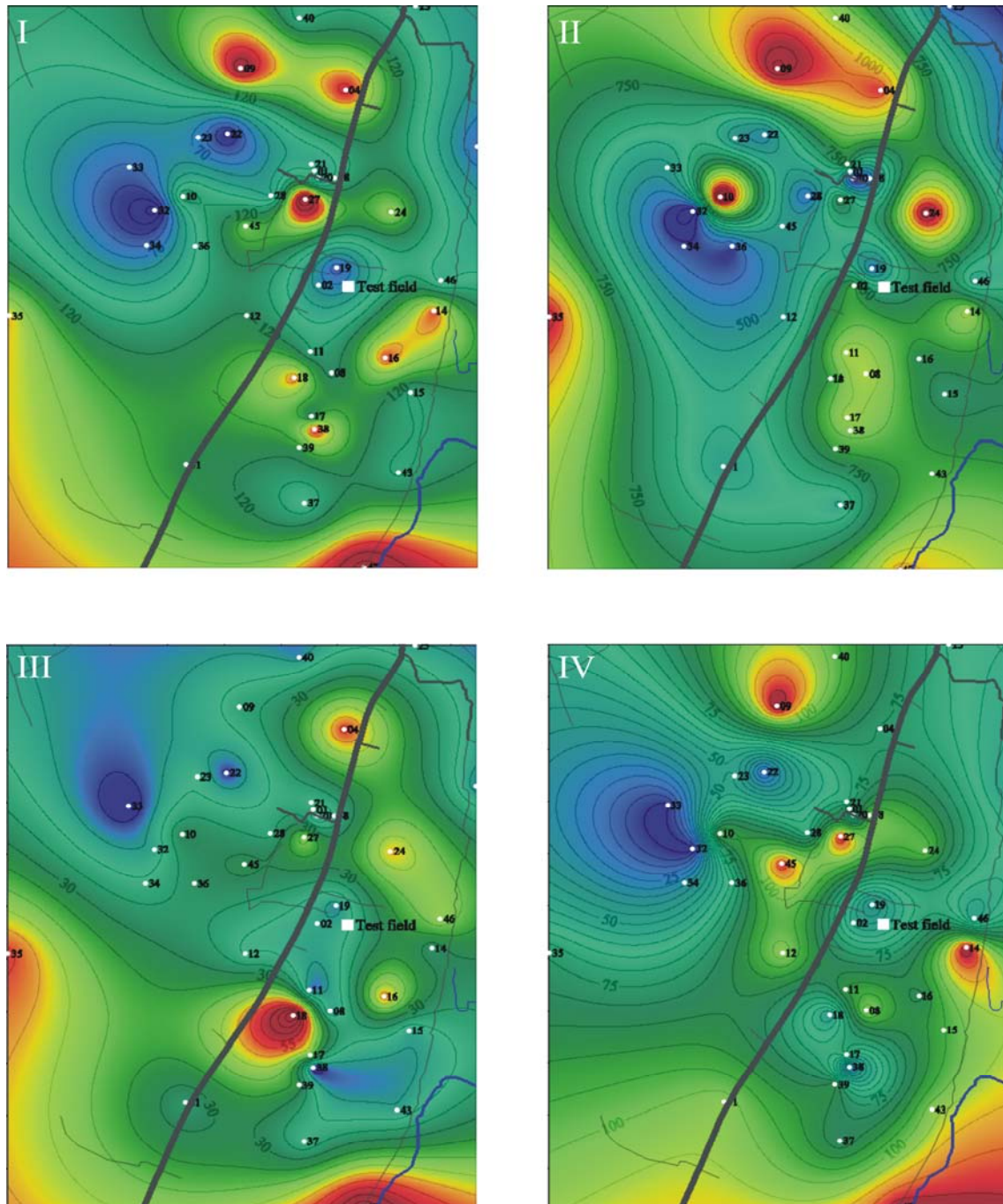


Fig. 5.2.2.2a Contour line plots showing the spatial distribution of (I) total arsenic, (II) total phosphorus, (III) arsenate and (IV) arsenite; (continued at Fig. 5.2.2.2b)

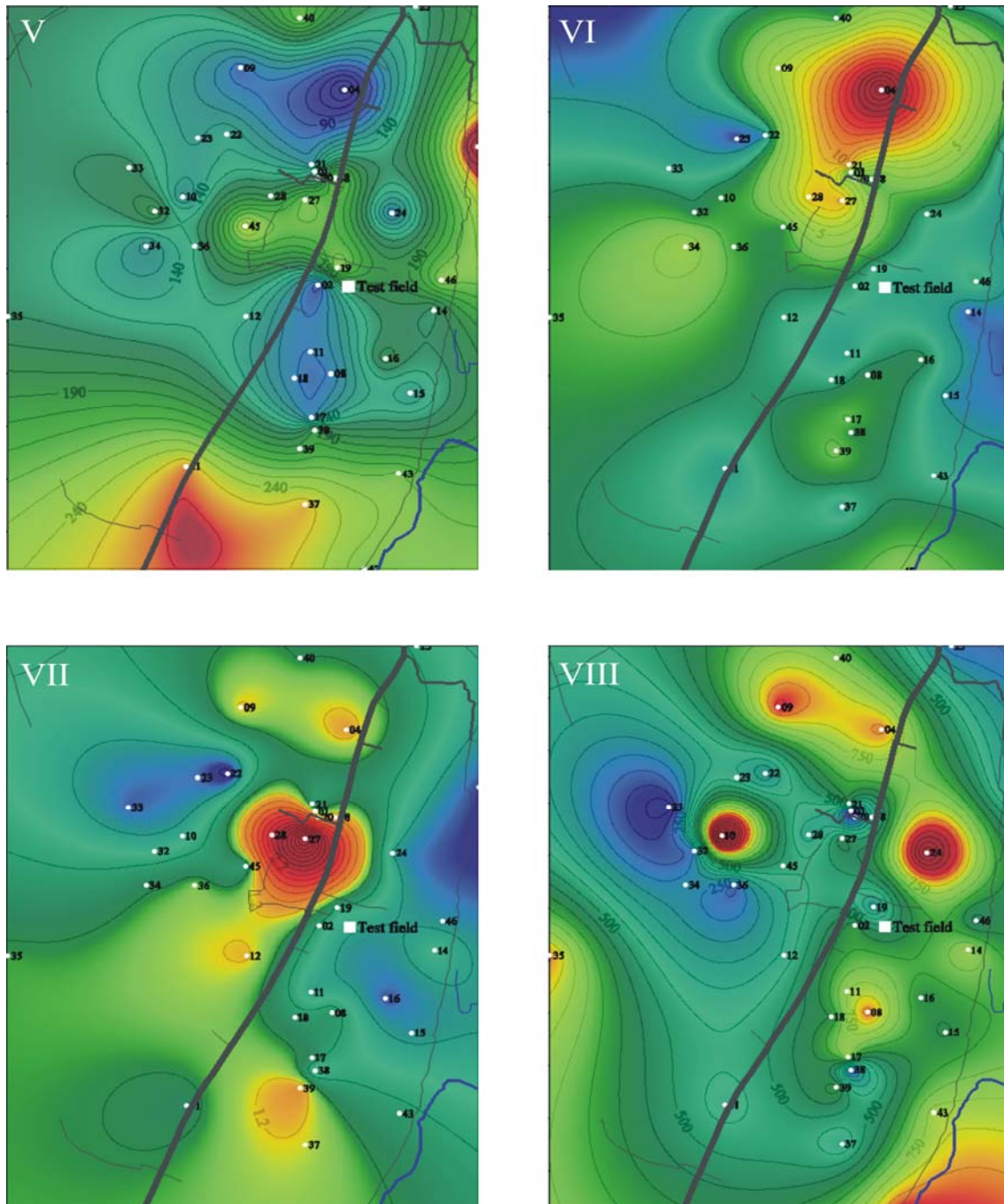


Fig. 5.2.2.2b Contour line plot showing the spatial distribution of (V) redox potential, (VI) total iron, (VII) total manganese and (VIII) phosphate; screenshot from Atlas Bangladesh 2007; mapping wells are displayed as white dots, the sample code is shortened; main streets are displayed grey, rivers blue

As aforementioned, the hydrochemistry shows a relative homogeneous composition at the study area and the groundwater can be defined as a Ca – HCO₃ type, because of the predominance of calcium and HCO₃⁻ at almost all wells, shown at figure 5.2.2.3. This water type was reported also in other studies (AHMED et al., 2003; ZHENG et al., 2004; RAVENSCROFT et al., 2004; MCARTHUR et al., 2000). An exception is shown at the six

high mineralized house wells (BGL MAP 04, 26, 30, 40, 31, 44). Dominant ions are represented by HCO_3^- , sodium + potassium and calcium; chloride is increased. Therefore, the groundwater from these wells can be distinguished as Ca – Na – HCO_3^- type (AHMED et al., 2003; RAVENSCROFT et al., 2004). A reason could be that these high ionised waters are influenced by a source of Na^+ and Cl^- . According to ZHENG et al.(2004), the source of elevated Na^+ and Cl^- at relatively shallow depths (14 and 34 m) might come from seawater intrusion, sea salt aerosol deposition or remnant seawater. Seawater intrusions seem to be implausible, due to the fact that the coastline is far (approx. 100 km) from study area. Increased Na^+ and Cl^- concentrations might be explained by the fact that the study area is situated at the fringe of the estuarine delta environment, southern of Ganges and lower Meghna (fig. 3.4.1.1). Thrusts of saltwater at exceptionally flooding events could be a potential explanation. Traces of bromide (0.1 – 0.4 mg/L) supporting this assumption.

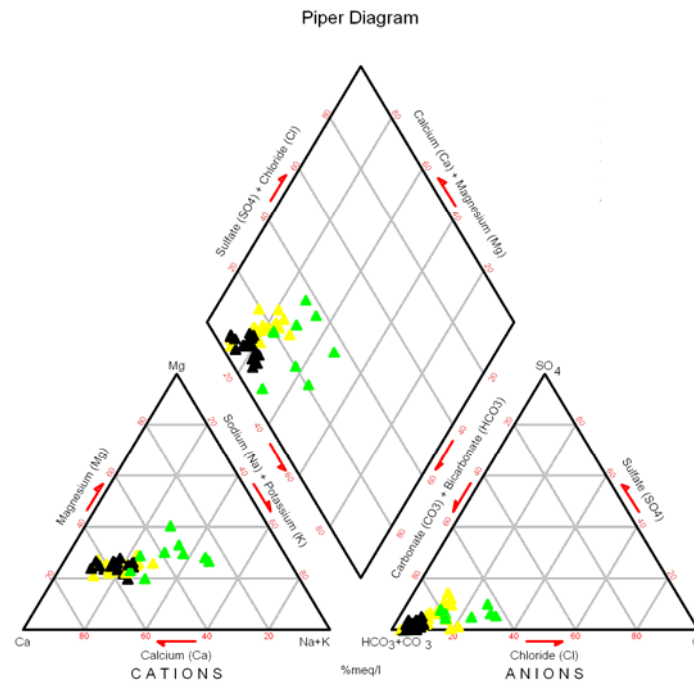


Fig. 5.2.2.3. Piper diagram, showing the determination of major cations and anions at the study area, divided in 3 groups: Group I (green): HCO_3^- is dominant, chloride is increased; the Na+K ratio to Ca is about 1:1; Group II (black): dominant in Ca and HCO_3^- as well as group III, but sulphate is slightly elevated

For statistical evaluation of the major cations and anions, a hierarchical cluster analysis was performed with the statistical software Systat, version 12. The analysis, done with the Ward method, divided the 48 wells into three major groups (see appendix 3, figure 5.2.2.3). To test the dissolved elements for significance a Spearman Rank Order correlation was done with the

statistical software SigmaStat (version 3.5). The statistical significance was defined at the 5 % level. In the Bengal Basin, several authors found correlations between dissolved elements and arsenic. The influence of DOC indicates trends of variation with both As(III) and Fe(tot), as described by AHMED et al. (2004), was not found. There is no significant relationship between DOC and arsenite ($P = 0.21$) as well as total iron ($P = 0.223$). A significant relationship between phosphorus and arsenic, as reported by MCARTHUR et al. (2000), may be evidenced ($P \leq 0.05$, $n = 56$; see figure 5.2.2.5). This can be explained by a shared diagenetic origin for both arsenic and phosphorus (RAVENSCROFT et al., 2001). Moreover, both arsenic and phosphorus form anions that sorb strongly to hydrous iron oxides, even though phosphorus was rejected as a displacement for arsenic by several authors (RAVENSCROFT et al., 2001; HANRAHAN et al., 2004; ACHARYYA et al., 2000). According to MCARTHUR et al. (2000), phosphorus enrichment parallels the distribution of arsenic enrichment and is concentrated mostly in northeast and southeast Bangladesh, presentable at the study area (see figure 5.2.2.2a).

As figure 5.2.2.4 suggests, a significant dependency between ammonia and As(tot) ($P \leq 0.05$, $n = 56$) as well as arsenite ($P \leq 0.05$, $n = 56$) has been proven for the investigation area (AHMED et al. 2004). However, an inverse relationship, as suggested by RAVENSCROFT et al. (2005) was not detectable (see figure 5.2.2.4). If ammonia is increased, this may be an indication for decomposition of high amounts of organic matter. High amounts of organic residuals from nearby peat cause much FeOOH reduction, the release of large amounts of arsenic and so high arsenic concentrations (RAVENSCROFT et al., 2001). This could explain the correlation between arsenic and ammonia.

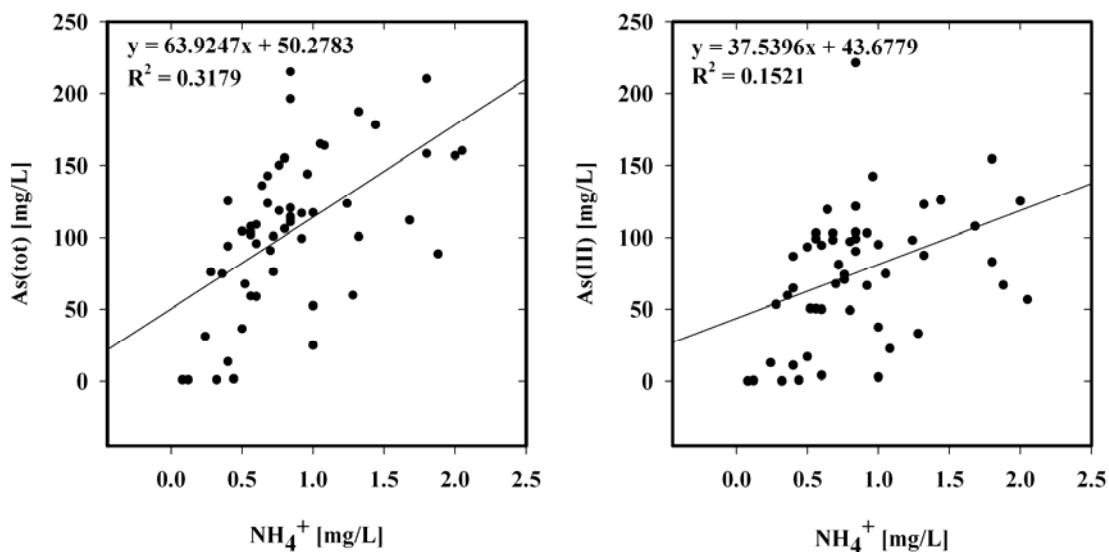


Fig. 5.2.2.4. Ammonia vs. As(tot) as well as As(III)

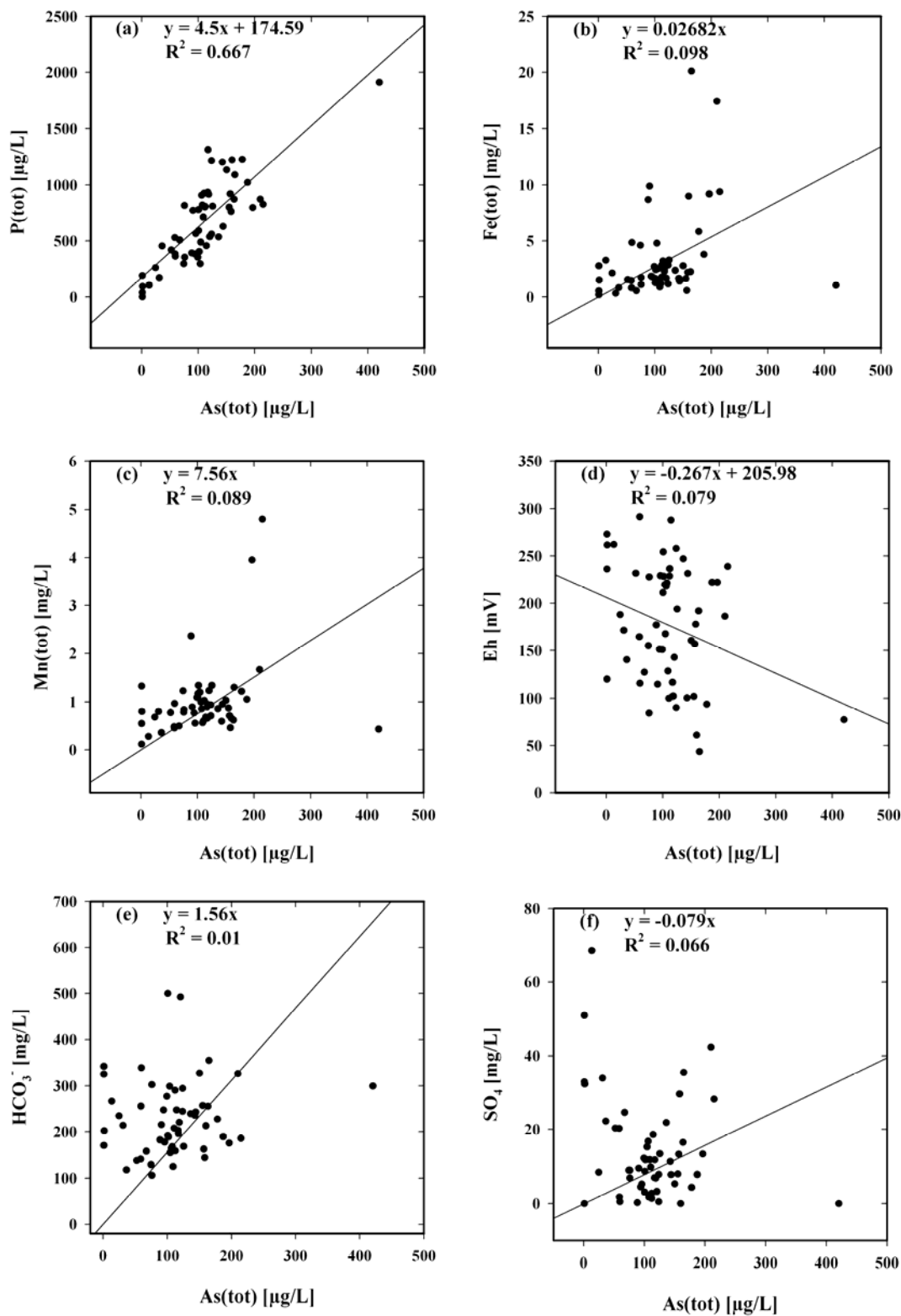


Fig 5.2.2.5. As(tot) vs. P(tot), Fe(tot), Mn(tot), Eh, HCO_3^- and SO_4

HASAN et al. (2008) reported correlations between arsenic and total iron, RAVENSCROFT et al. (2005) mentioned an inverse relationship. This can be rejected for the study area ($P = 0.061$, $n = 56$), as described in previous publications (AHMED et al., 2004;

MCARTHUR et al., 2000; NICKSON et al., 2000; SMEDLEY and KINNIBURGH, 2002; VAN GEEN et al., 2004; see figure 5.2.2.5). An inverse relationship between Eh and arsenic ($P = 0.104$, $n = 56$) as well as iron (GAULT et al., 2005) was not detectable. Correlations between arsenic and manganese (HASAN et al., 2008) were not found ($P = 0.342$, $n = 56$).

A negative correlation between arsenic and sulphate (AHMED et al., 2004; RAVENSCROFT et al., 2001; SMEDLEY and KINNIBURGH, 2002, HARVEY et al., 2006) can be excluded for the study area (see figure 5.2.2.5; $P = 0.08$, $n = 56$). A relation between HCO_3^- and arsenic (NICKSON et al., 2000; HARVEY et al., 2006) was not found.

However, where good correlations with As are found at the Bengal Basin, these are only applicable locally and are of limited value for quantitative prediction of arsenic concentrations (SMEDLEY and KINNIBURGH, 2002). For example the positive correlation between As and Fe, as described by AHMED et al. (2004), is not true for Bangladesh as a whole, as suggested by SMEDLEY and KINNIBURGH (2002). This is also the case at the study area. As aforementioned at chapter 2, non correlated data could arise from re-precipitation of iron, re-adsorption of arsenic onto fresh hydrous iron oxides (FeOOH) or precipitation of Fe^{2+} as siderite FeCO_3 (WELCH and LICO, 1998).

At the newly drilled test field, situated in the centre of the study area (see figure 5.2.2.2), monitoring wells were installed at depths of 9 m (30 ft), 15 m (50 ft), 21 m (70 ft), 26 m (85 ft), 27 m (90 ft), 35 m (115 ft), and 85 m (280 ft) (see figure 4.1.1.1). Also there, a correlation between arsenic and phosphorus was found ($P \leq 0.05$, $n = 140$). A connection between dissolved iron and arsenic can be negated for the whole depth profile, but is true for individual sections, as explained in chapter 5.2.3. However, section I and II on their own show a significant dependency between arsenic and iron ($P \leq 0.05$, $n = 100$). Furthermore, an inverse relation of dissolved sulphate with arsenic was detected at the test field, but was not found in the surrounding area. In the main, the test field can be seen as representative for Comilla due to the fact that the hydrochemical features are similar at both the test field and the mapping site.

As aforementioned, the maximum arsenic concentrations occur at depths between 20 and 50 m, whereas samples shallower than 10 m and deeper than 150 m are basically As free. This is in accordance with findings of previous investigations (RAVENSCROFT et al., 2001; SMEDLEY and KINNIBURGH, 2001; HASAN et al., 2008; ZAHID et al., 2007; ZHENG et al., 2004; RAVENSCROFT et al., 2001; RAVENSCROFT et al., 2005). At depths less than 10 m, both mapping wells and monitoring wells are below the local drinking water standard of $50 \mu\text{g/L}$ (see figure 5.2.2.6). At depths between 12 and 35 m, the mean concentrations of

arsenic are increased with a maximum peak at 35 m in the test field and 21 m in the surrounding area (see figure 5.2.2.6).

At a depth of 85 m (BGL TF 280), mean concentrations for arsenic were measured at a level just above the local drinking water standard (see figure 5.2.2.6). At the deepest well (275 m) in the study area, BGL MAP 03, arsenic was not detected, or was rather below the detection limit of 0.2 µg/L.

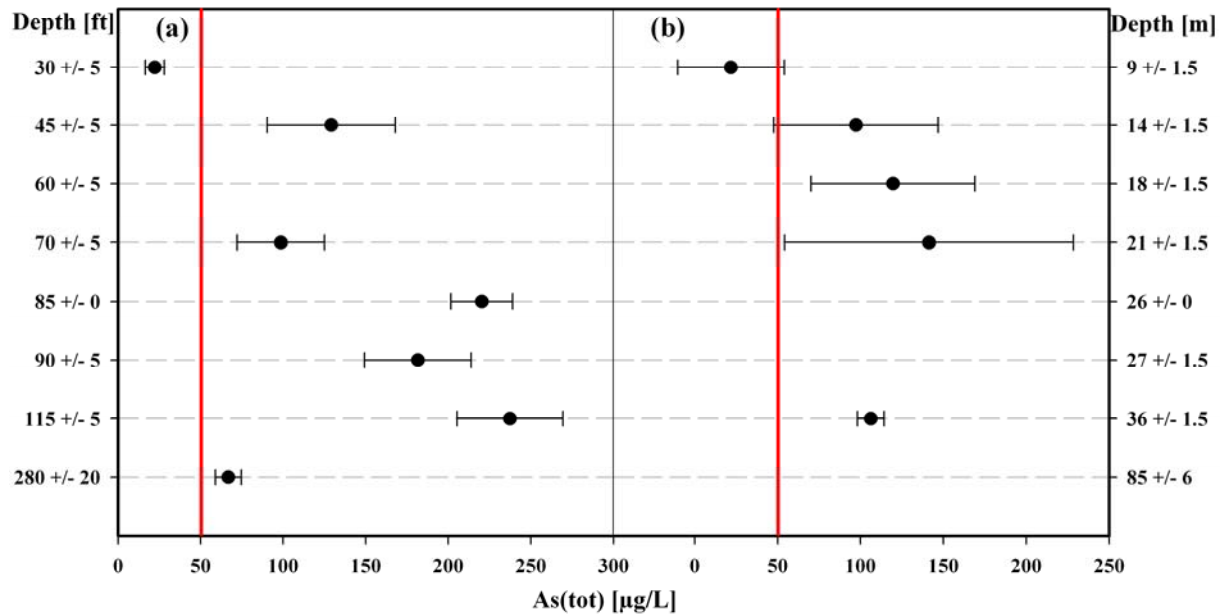


Fig. 5.2.2.6. Comparison of mean As(tot) + standard deviation for the (a) test field and (b) mapping wells against the depth; the red line describes the local drinking water standard (50 µg/L)

Summarizing the above, the newly drilled test field can be seen as representative for the arsenic problem in Bangladesh. Almost 94 % of all measured wells are above the local drinking water standard of 50 µg/L, which was reported as typically for shallow wells at the south-east of Bangladesh (SMEDLEY and KINNBURGH, 2001). However, in comparison to the highest affected regions in Bangladesh (e.g. Chandpur) with arsenic-levels above 300 µg/L (SMEDLEY and KINNBURGH, 2001), the study area at Titas, Daudkandi Upzilla, Comilla District can be seen as moderate affected. Nearly all wells are dominated by inorganic, trivalent arsenite ($\text{H}_3\text{As}^{\text{III}}\text{O}_3^0$) due to mildly oxidising conditions (100 – 350 mV) confirming previous studies in the vicinity (ZHENG et al., 2004; BHATTACHARYA et al., 2002; AHMED et al., 2004). The groundwater type and composition at the study area can be seen as typical for Bangladesh as mentioned in several studies (e.g. SMEDLEY and KINNBURGH, 2002; MC ARTHUR et al., 2000; RAVENSCROFT et al., 2003; NATH et al., 2007; ZAHID et al., 2007; HASAN et al., 2008). As reported for the Bengal Basin, the

arsenic distribution against the depth is representative at the test field as well as the surrounding area. Relations were found between arsenic and phosphorus as well as ammonia. Several authors (e.g. KINNIBURGH et al., 2003; MCARTHUR et al., 2004) reported correlations between the well age and arsenic content, based on the assumption that arsenic concentrations may rise after a well is installed. The main idea is that irrigation wells, which have much greater effects on the local groundwater system, are installed in the region at the same time as the house wells where arsenic is measured. Arsenic concentrations may rise after pumping commences.

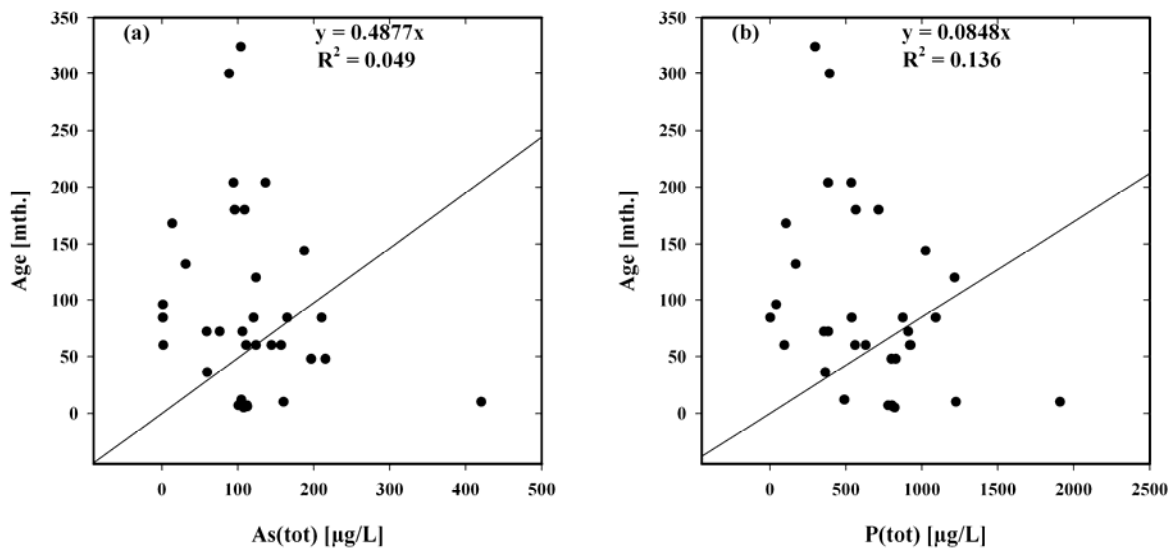


Fig. 5.2.2.7. Total arsenic (a) and total phosphorus (b) vs. well-age

As figure 5.2.2.7 suggests, increasing arsenic-concentrations at shallow tube wells are not related to the well-age at the study area ($P = 0.728$, $n = 48$). This statement is based on the deliverables from mapping, but with the addition, that the comparison between arsenic and well-age was combined from different wells, sampled only one-time, in some cases twice. This leads into a limitation of its significance. However, it would be more meaningful to do a continuous monitoring ($>5a$) at selected wells, but this was not possible within these project.

5.2.3 Depth dependent hydrochemical changes

The study-site is located in the south-east of the capital Dhaka at Titas, Daudkandi Upzilla, Comilla District, close to the main river channel of the Meghna River. As described in chapter 4.1, a core drilling was constructed to retrieve undisturbed samples at intervals of 3 m for further detailed classification and sorption tests in laboratory setups and to acquire stratigraphical information (see figure 4.1.1.1). On the basis of the litholog, five main stratigraphical units are to distinguish (LISSNER, 2008):

0. 0 – 3 m: filling material;
- I. 3 – 6 m: sandy silt and grey to brown fine sand;
- II. 6 – 27 m reduced grey fine sand and silt, in 26 m peat fragments (Holocene aquifer);
- III. 27 – 79 m silty clay to clay, in 61 to 73 m peat fragments, lens of coarser sediment (fine sand) in 34 m;
- IV. 79 – 83 m channel of oxidised brown fine in the upper part to medium sand in the lower part of aquifer (deeper Pleistocene aquifer);
- V. > 83 m clay to heavy clay;

According to HARVEY et al. (2002), this quaternary sequence is typical for southern and south-eastern Bangladesh. The study site is thus representative for the area. The upper 3 m sediment is landfill material and thus not significant for further interpretations. Based on the litholog, 6 test-wells were constructed into the upper Holocene aquifer with depths of 9 m (30 ft), 15 m (50 ft), 21 m (70 ft), 26 m (85 ft), 27 m (90 ft), and 35 m (115 ft), and one monitoring well was constructed into the deeper, Late-Pleistocene aquifer at a depth of 85 m (280 ft) (fig. 4.1.1.1). Despite the closeness to the core drilling (approx. 55 m), the thickness of the individual layers in the test field diverged from that of the core drilling (figure 5.2.3.1). According to LISSNER (2008), the soil type of the first layer (I) is mainly silt (89 % silt with 11 % clay, no sand). It can be assumed, that the brownish sand between the silt layer and the top of the shallow aquifer is oxic, so the groundwater is (mean Eh 230 mV). The upper aquifer (layer II) is dominated by sand, silt (15 – 48 %) and clay (1 – 3 %) occurred in minor fractions. At a depth of approx. 30 m, a lens of silty clay was located, containing peat fragments. At the bottom of the Holocene aquifer (layer II) the percentage of sand within grain size distribution is increased. Texture is loose and single grained. The ensuing aquitard is mainly composed of silt (46 – 91 %) and clay (4 – 44 %). Peat beds were found in the core

drilling between a depth of 60 and 70 m and are also supposed to be at the test field. This is confirmed up to a depth of 40 m, due to the findings from the wells, constructed by the local „hand-flapping” method (see chapter 4.1.1). The deeper aquifer consists of particularly loose and single-grained material with brown sand as the main soil fraction. The deepest aquitard (layer V) was not reached at the test field.

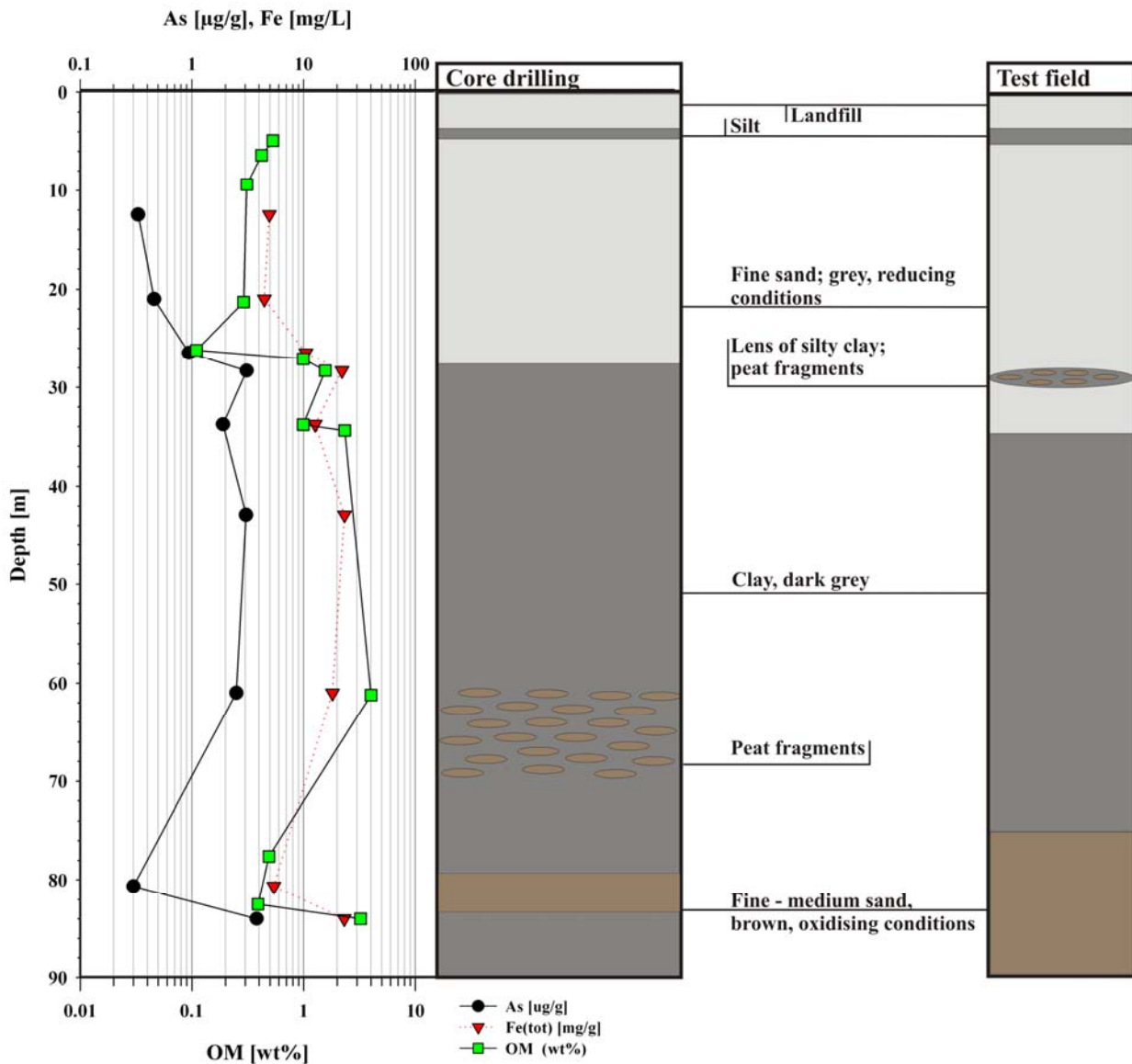


Fig. 5.2.3.1. Depth profile of the core drilling and the test field (in approx. 55 m distance) with main sediment layers at the right; solid As, Fe and OM vs. depth at the left

The brown colour of the sediment at the upper aquifer as well as the deeper aquifer derives from iron hydroxides (VAN GEEN et al., 2004; see figure 5.2.3.2). Reduction of FeOOH has occurred but it has not been completed, as the brown colour of sediment suggests (MCATHUR et al, 2004).

The role played by FeOOH within the contaminated grey sediments (figure 5.2.3.2) of the Holocene aquifer is much more complex. According to the theory, that arsenic is released from FeOOH by organic carbon, iron(oxy)hydroxides must exist in the Holocene aquifers or have existed recently (HARVEY et al., 2006). It is believed that as the brown colour derives from the presence of FeOOH, the grey colour of the subjacent Holocene aquifer-sand occurs when these oxides have been more or less completely destroyed (VAN GEEN et al., 2003). However, FeOOH has not been definitely documented in the grey sediment (HARVEY et al., 2002). So, the aquifer sediments must be poised in a geochemical state where the inventory of FeOOH is nearly (or recently) exhausted, yet arsenic has not been flushed away by flowing groundwater (HARVEY et al., 2006).



Fig. 5.2.3.2. Reduced sediment from the upper aquifer on the right (I) and oxidised, brown sand (II) from the deeper aquifer on the left

High arsenic concentrations were found in the clay layers at the study area, which mainly consist of smectite, kaolinite, chlorite, and mica as determined by XRD. These clay-minerals can act as active sorption sites for arsenic.

Arsenic concentrations associated with quartz and feldspar, from which the sandy aquifer is mainly composed, are generally relatively low (SMEDLEY and KINNIBURGH, 2002). In the sediments from the core drilling, LISSNER (2008) found As-concentrations with a maximum of 0.9 $\mu\text{g/g}$ in sandy sediment and 3.8 $\mu\text{g/g}$ in clays and peats.

Hydrochemical features (see chapter 4.1.2) were monitored from February to July, altogether 20 campaigns. Due to the findings, the depth profile can be divided in four sections:

- **Section I** (<10 m; upper aquifer): groundwater with low concentrations of As (22 µg/L), low to medium iron, ammonia and organic carbon (figure 5.2.3.3); from Ca - HCO₃-type (see appendix 6);
- **Section II** (< 26 m, upper aquifer): groundwater with high concentrations of As > 100 µg/L, low to medium iron, ammonia and organic carbon (figure 5.2.3.3); from Ca - HCO₃-type (see appendix 6); HCO₃⁻ ranges between 170 and 290 mg/L increasing with depth;
- **Section III** (> 26 m, upper aquifer): high As, P, NH₄, and DOC concentrations (figure 5.2.3.3); high mineralized groundwater from Na (350 mg/L) – HCO₃(710 mg/L)-type (see appendix 6); Chloride is high (335 mg/L), Bromide was detected (2.1 mg/L);
- **Section IV** (85 m, lower aquifer): moderate As, high NH₄, Fe(tot) and DOC concentrations (figure 5.2.3.3); high mineralized groundwater from Na (270 mg/L) – HCO₃ (370 mg/L)-type (see appendix 6), which is typical for brown and oxidised sediments (RAVENS-CROFT et al., 2001); Chloride is high (528 mg/L) as well as Bromide (3.6 mg/L);

The pH in the upper aquifers is near neutral while the pH in the lower aquifer is slightly lower with 6.3. The higher pH may be due to the higher exchange capacity of the fine-grained clayey sediments, which are enriched in clay, chlorite, mica and OM (LISSNER 2008). Except for section I (230 mV), Eh was measured with values between 170 and 200 mV, indicating partially reducing conditions. Sulphide was generally low (< 0.1 mg/L), a reason to exclude pyrite degradation as main mechanism for arsenic accumulation at our study site comparable to what has been described for Bangladesh's aquifers previously (e.g. SMEDLEY and KINNIBURGH, 2001; MCARTHUR et al., 2001; RAVENS-CROFT et al., 2001). SO₄ was measured at each well, ranging between 5.1 mg/L at the shallowest well and less than 1 mg/L at the deeper piezometers (see figure 5.2.3.3).

Nitrate (< 0.6 mg/L) and Nitrite (< 0.01 mg/L) are generally low. Furthermore, Manganese was measured at each depth showing concentrations between 0.3 mg/L and 0.7 mg/L. This might be an indication for presence and reduction of MnO_2 (MCARTHUR et al., 2004).

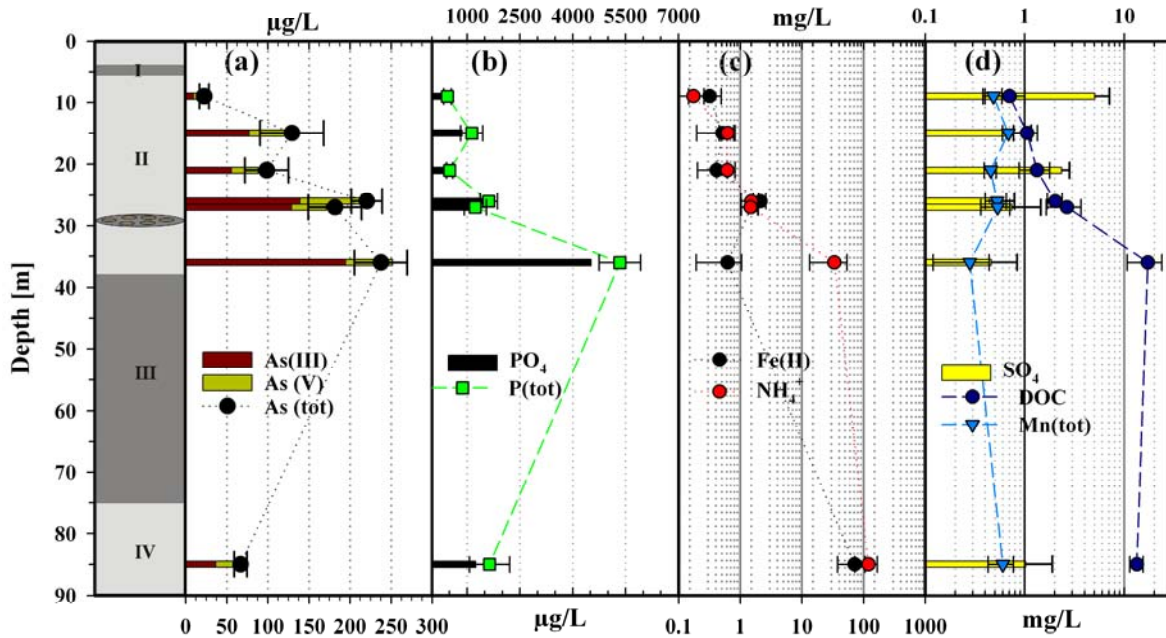


Fig. 5.2.3.3. Vertical profile of hydrochemical mean characteristics at the test field. (a) dissolved total As and As-species; (b) dissolved total P and phosphorus; (c) Fe(II) and NH_4^+ ; (d) DOC and total manganese

Apart from depths less than 10 m (section I), all wells exceed the local drinking water standard for arsenic of 50 $\mu\text{g/L}$ with a maximum peak at a depth of 36 m (section III). The dominant species is arsenite. This was also found in several previous studies (ZHENG et al., 2004; BHATTACHARYA et al., 2002; AHMED et al., 2004, MCARTHUR et al., 2004). At a depth of 10 m (section I), arsenic was found in lower concentrations ($\bar{\theta} = 22$ $\mu\text{g/L}$; see figure 5.2.3.3), which was reported as typical for Bangladesh by several authors (SMEDLEY and KINNIBURGH, 2001; HASAN et al., 2008; ZAHID et al., 2007; ZHENG et al., 2004; RAVENSCROFT et al., 2001; RAVENSCROFT et al., 2005); the arsenate/arsenite ratio is nearly 1:1. This corresponds to the deliverables from mapping, as described in chapter 5.2.2.

Groundwaters in the upper aquifers contained dissolved Fe in slight concentrations (> 1 mg/L) at depths < 21 m to medium concentrations in depths between 21 and 36 m (2 – 3 mg/L). In the lower aquifer, dissolved iron was extremely elevated (> 100 mg/L), so the groundwaters are anoxic because they contain dissolved Fe (MCARHTUR et al., 2004). As described in chapter 4.1.2.2, total iron as well as Fe(II) was determined by photometry with a detection range between 0.03 and 3.00 mg/L. Due to this, high dilutions at field site with a

ratio of 1:50 were necessary, which had adverse effects to the accuracy of measurement. However, dissolved iron, mainly available as Fe(II), is high at the Late-Pleistocene aquifer (see figure 5.2.3.3).

Dissolved organic carbon is low (< 1 mg/L) at section I and the upper part of section II. At the lower part of section II (< 26 m), medium concentrations of dissolved organic carbon (DOC) were determined with between 2 and 3 mg C/L. At section III, directly beneath the lens of silty clay, mean DOC-concentrations of 17 mg C/L were determined. Ammonia is elevated at section III (33 mg/L) as well as phosphorus (5400 $\mu\text{g/L}$). According to RAVENSCROFT et al. (2001), an indicator of the degradation of much organic matter is the presence of high ammonia and phosphorus in the mg/L range, but this will be discussed later at this section. However, the high values for ammonia at section III as well as section IV have to be handled with care, based on the fact that interferences with other dissolved elements might appear, especially iron at all levels (see chapter 4.1.2.2). Due to the upper detection limit of 0.5 mg/L for ammonia, determined by photometry, high dilutions at field site with a ratio of 1:400 were necessary which had adverse effects to the accuracy of measurement.

Section I and section II on their own show a significant correlation between arsenite and phosphorus ($P \leq 0.05$, $n = 100$; see figure 5.2.3.4) as well as section-III and section-IV ($P \leq 0.05$; $n = 40$, not plotted). This is also valid for the whole sequence as shown in figure 5.2.3.4b ($P \leq 0.05$, $n = 140$), even if the dependency is not linear.

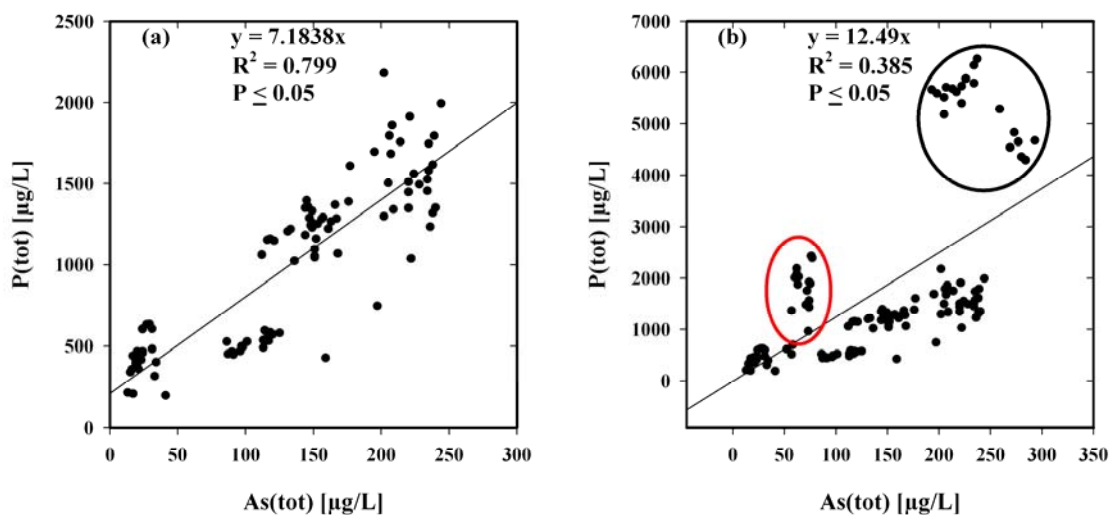


Fig. 5.2.3.4. Total As vs. total phosphorus at (a) depths less than 26 m (sections I, II) and (b) for the whole depth-profile (section III [black circle], S-IV [red circle]). Data-points derive from the monitoring between February and July

As figure 5.2.3.3 suggests, the distribution curve for phosphorus and arsenic is similar in the sections I and II. The mean As/P ratio at these sections I and II ranges from 1:7 to 1:9, but is elevated at section III as well as section IV with a ratio of approximately 1:24, so phosphate increases with the depth.

Based on the fact, that reduction of FeOOH desorbs most of the surface-sorbed As(V), which becomes reduced to As(III), a good correlation between dissolved iron and arsenic would be expectable (MCARTHUR et al., 2001), but that's not true for whole Bangladesh and is a regional phenomenon (AHMED et al., 2004; NICKSON et al., 2000; SMEDLEY and KINNIBURGH, 2002; VAN GEEN et al., 2004). This is also the case for all sections at the test field ($P = 0.201$, $n = 140$, see appendix 7a) as well as the surrounding area (see chapter 5.2.2). However, section I and II on their own show a significant dependency between arsenic and iron ($P \leq 0.05$, $n = 100$, see appendix 7b). According to MCARTHUR et al. (2001), poor correlations of arsenic with iron may arise because of resorption of arsenic onto fresh FeOOH exposed by dissolution. This may occur when the groundwater moves away from areas with complete reduction to areas with incomplete reduction, whereas As and Fe reduction get decoupled (MCARTHUR et al., 2004; RAVENSCROFT et al., 2001). Supplementary, another source of error may result from filtering of the water sample (see chapter 4.1.2.3), which reduces the amount of arsenic in sample water as well as iron (RAVENSCROFT et al. 2001). The iron oxyhydroxide precipitated on the filter may scavenge arsenic during filtration. Between ammonium and phosphorus, a strong correlation was found ($P \leq 0.05$; $n = 120$), see figure 5.2.3.5). According to RAVENSCROFT et al. (2001), this is a further indicator of the degradation of high amounts of organic matter (OM).

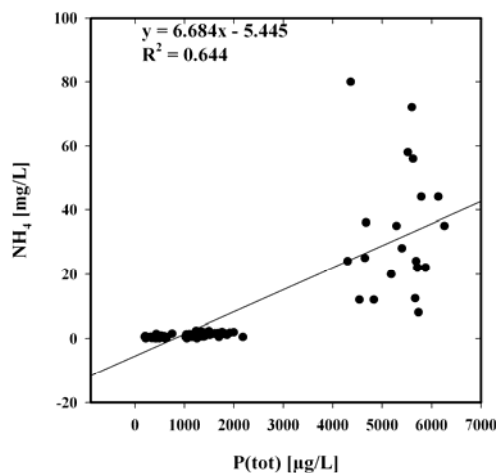


Fig. 5.2.3.5. Total phosphorus vs. NH_4 (at sections I, II, III); Data-points derive from monitoring between February and July

Furthermore, the obviously inverse relation of dissolved sulphate (see figure 5.2.3.6) with arsenic in the groundwater suggest that oxidative dissolution of pyrite has not liberated arsenic.

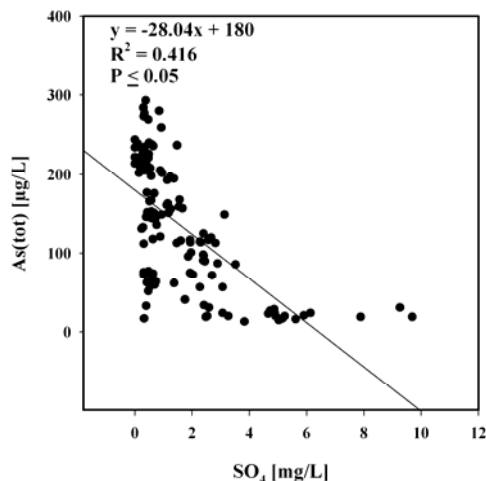


Fig. 5.2.3.6. Total arsenic vs. SO_4 (at all sections); Data-points derive from monitoring between February and July

As explained in chapter 2, reduction of ironhydroxide (FeOOH) and release of its sorbed arsenic load to solution is seen as the main mechanism by which groundwater in the Bengal Basin becomes polluted with arsenic (e.g. MCATHUR et al., 2000; RAVENSCROFT et al., 2001; SMEDLEY and KINNIBURGH, 2002). Based on this theory arsenic accumulation at the test field will be explained in the following.

According to MCATHUR et al. (2001), peat is the main redox driver and its biodegradation drives extreme degrees of FeOOH reduction and supplies high concentrations of arsenic to the groundwater. The distribution of peat and arsenic can be related to Late Pleistocene and Holocene aquifers, just as the upper and lower aquifer at the test field area. RAVENSCROFT et al. (2001) reported that reduction of FeOOH is accompanied by reduction of arsenate to arsenite. As aforementioned, this fact is observable at the test field in each depth (except < section I) and is an indication for reduction of FeOOH , as shown in figure 5.2.3.3.

Biodegradation of peat releases short-chain carboxylic acids and methylated amines that will drive FeOOH reduction and ammonium production (RAVENSCROFT et al., 2001). Due to the fact that these molecules do not migrate far from their peat source, this might be an explanation that arsenic concentrations are so strongly dependent on depth. In the following, a schematic of the process of how arsenic pollution affects individual wells will be related to the monitoring wells from the test field, as shown in figure 5.2.3.7.

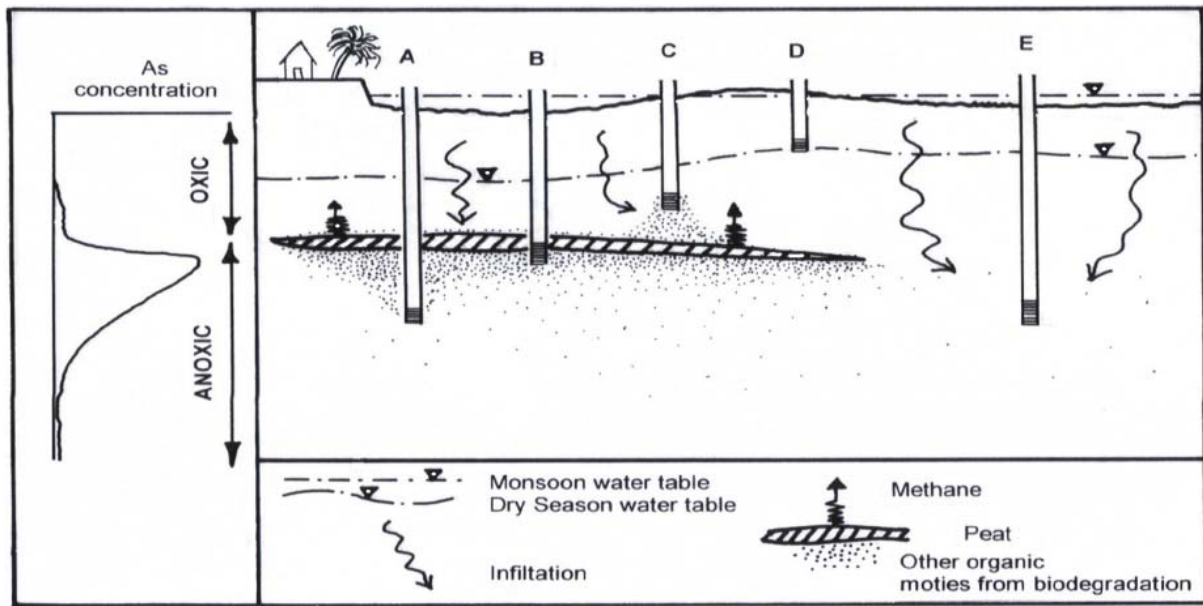


Fig. 5.2.3.7. Model of how arsenic pollution occurs in shallow wells in the Bengal Basin. Hydraulic gradients cause downward movement of water during the wet season. (RAVENSCROFT et al., 2001)

Adopting the model of RAVENSCROFT et al. (2001), the case D can be related to the well BGL MAP 30 (section I), which is only slightly contaminated with arsenic, as it was expected due to several reports (SMEDLEY and KINNIBURGH, 2001; HASAN et al., 2008; ZAHID et al., 2007; ZHENG et al., 2004; RAVENSCROFT et al., 2001; RAVENSCROFT et al., 2005). The recharging groundwaters are oxic, which will prevent redox processes except oxic degradation. A layer of brown, oxidised sand was found in the top of the aquifer.

Even if the As concentration is low in the upper part of the Holocene aquifer, the slight As-content derives from a slight degree of reduction of FeOOH. This may be due to organic matter migration downwards, which is the driving force of reduction of FeOOH (e.g. MCATHUR et al., 2001; MCATHUR et al., 2004; RAVENSCROFT et al., 2001; SMEDLEY and KINNIBURGH, 2002). The content of organic matter (OM) in solid phase was measured with approx. 0.3 wt% (LISSNER 2008). Dissolved organic carbon (DOC), an indication for microbial processes, is around 0.7 mg C/L. A further explanation for the absence of high As concentrations is that sorbed As was flushed from the sediment, due to the fact that groundwater circulation is highest at these parts of the aquifer.

The case C might be the reason for the moderate to high dissolved arsenic contents above the peat layer at depths between >10 and 27 m (see figure 5.2.3.7). As mentioned before, high concentrations of As prevailed over the whole thickness (>10 m – 36 m, sections I - III) of the grey Holocene aquifer with a maximum at 36 m (see figure 5.2.3.3). The concentrations of As

in the lower part (> 26 m) of the aquifer are higher (> 200 µg/L) than they are in the upper part (around 100 µg/L).

The arsenic pollution above a peat layer caused due to migration of arsenic in response to strong pumping. However, due to the fact that the water samples were taken by low-flow sampling, an explanation might be the intense irrigation at the surrounding agricultural crops. Furthermore, migration of organic residuals upwards cause local FeOOH reduction and additional arsenic release. According to LISSNER (2008), the content of organic matter (OM) ranged between 0.5 wt% and 2 wt%, increasing with closeness to the silty and peaty lens of clay (see figure 5.2.3.1), as well as dissolved organic carbon (DOC), ranging between 1 and 2.7 mg C/L (see figure 5.2.3.3). Supplementary, the presence of SO₄ is localised where organic matter is present (MCARTHUR et al., 2004; see figure 5.2.3.3).

The case B gives an explanation for the high arsenic concentrations at section III, screened directly beneath the lens of organic rich clay. High amounts of organic residuals from nearby peat cause an intense FeOOH reduction, the release of large amounts of arsenic and so high arsenic concentrations (RAVENSCROFT et al., 2001). As mentioned before, dissolved organic carbon and also ammonia is increased, an indication for decomposition of high amounts of organic matter. Elevated concentrations of phosphorus in the mg/L range are released to groundwater from the fermentation of buried peat deposits, as confirmed by several authors (MCARTHUR et al., 2000; RAVENSCROFT et al., 2001). This is also the case at section III, overlain by a peaty and silty lens of clay (see figure 5.2.3.3). According to MCARTHUR et al. (2000), phosphorus enrichment parallels the distribution of arsenic enrichment and is concentrated mostly in northeast and southeast Bangladesh, presentable at the study area (see figure 5.2.2.2a).

The same case might be responsible for high amounts of ammonia as well as iron at section IV, even if arsenic is moderate and oxic circumstances are dominant. However, high dissolved Fe concentrations in the deeper aquifer are associated with the brown coloured sand from the top of the aquifer (LISSNER 2008), which implicate the incomplete dissolution of iron(hydr)oxides and the release of Fe and As in the groundwater (MCARTHUR et al., 2004) (see figure 5.2.3.3). Additionally, LISSNER (2008) extracted high amounts of Fe (24 µg/g) from the sediment which suggests the occurrence of iron(hydr)oxides in the deeper aquifer (see figure 4.2.3.1).

The incomplete dissolution of FeOOH and the brown colour results from a long termed period of oxidative weathering during the lowering of sea-level that occurred between 125 and 18 ka (MCARTHUR et al., 2004). This weathering must have generated FeOOH by oxidation of

biotite and other Fe-bearing minerals in the sediment. So, the main difference between the Holocene (sections I - III) and the Late-Pleistocene aquifer (section IV) is the higher content of FeOOH in the deeper aquifer. An explanation for the absence of high As concentrations is that sorbed As was flushed from the deep aquifer during the lowering of the sea-level, as mentioned before (MCARTHUR et al., 2001; MCARTHUR et al., 2004; RAVENSCROFT et al., 2001; SMEDLEY and KINNIBURGH, 2002). Supplementary, dissolved arsenic is presumably low in these sediments because of the capacity of iron(oxy)hydroxides to adsorb arsenic (HARVEY et al., 2006).

Certainly, the schematic at figure 5.2.3.7 is simplified. Migration processes in Bangladesh's aquifers are influenced by numerous factors such as low regional hydraulic gradients, micro-topographic effects, surface water bodies, deep rooted vegetation, seasonal flooding and water logging (RAVENSCROFT et al., 2001). The behaviour of groundwater flow and migration processes were not the subject of this project but will be presented elsewhere (HÄRTIG 2008).

It has long been known that the formation of soluble arsenic sulphur complexes plays an important role in aquatic reducing environments. Worldwide investigations at reducing environments have been proven that arsenic has a high affinity to sulphur compounds. The geochemical interaction between arsenic and reduced sulphur species may play an important role for the mobility and toxicity of arsenic in sulphate reducing environments. This fact was not proven for groundwater in Bangladesh yet (GAULT et al., 2005).

Beside the already mentioned arsenic species arsenate and arsenite, a third species was detected at the test field at BGL TF 90: Monothioarsenate (H_3AsSO_3) was measured with a maximum level of $32\mu\text{g/L}$ in the dry season (February). Monothioarsenate was generally highest at BGL TF 90 whereas Monothioarsenate was not detected at BGL TF 30 as well as 280. A seasonal trend was not detectable, but it seems that the concentrations decrease during the monitoring.

The formation of H_3AsSO_3 is strongly dependent on pH and dissolved oxygen. The occurrence of thioarsenic species is limited to a pH ranging from near neutral to alkaline. Additionally, their formation depends on the arsenic:sulphur ratio in the solution. Either they can be formed by reaction of arsenite with elemental sulphur under alkaline conditions or by alkaline dissolution of As bearing sulphide minerals, e.g. Orpiment and Realgar.

5.2.4 Seasonal hydrochemical changes

As described in chapter 4.1.2, hydrochemical mapping was done at the study area at Titas, Daudkandi Upzilla, Comilla District to put the region into context of the whole arsenic problem in Bangladesh. Additionally, a weekly monitoring (see chapter 4.2.1) was done to collect data over a period of one year to find out seasonal changes in the arsenic distribution at the newly drilled test field tapping different aquifers. Altogether, 20 campaigns were arranged at an interval of approximately one week to capture hydrochemical changes resulting from the annual heavy rainfall in the end of April, the onset of the rainy season due to monsoonal precipitation as well as the influence of intensive irrigation in the surrounding area. During the 20 campaigns, 140 water samples and several additional replicates of the same sample for quality control were taken. The water table was measured at the piezometers using a light indicator. Data acquisition was carried out over a period from February to end of July. No water tables were measured at the second, sixth and fourteenth campaign. The water table between the 10th and 11th as well as the 13th and 14th campaign was measured within a two-week time period, other than the common period of one week. For this reason, potential temporary groundwater table variations were not recorded.

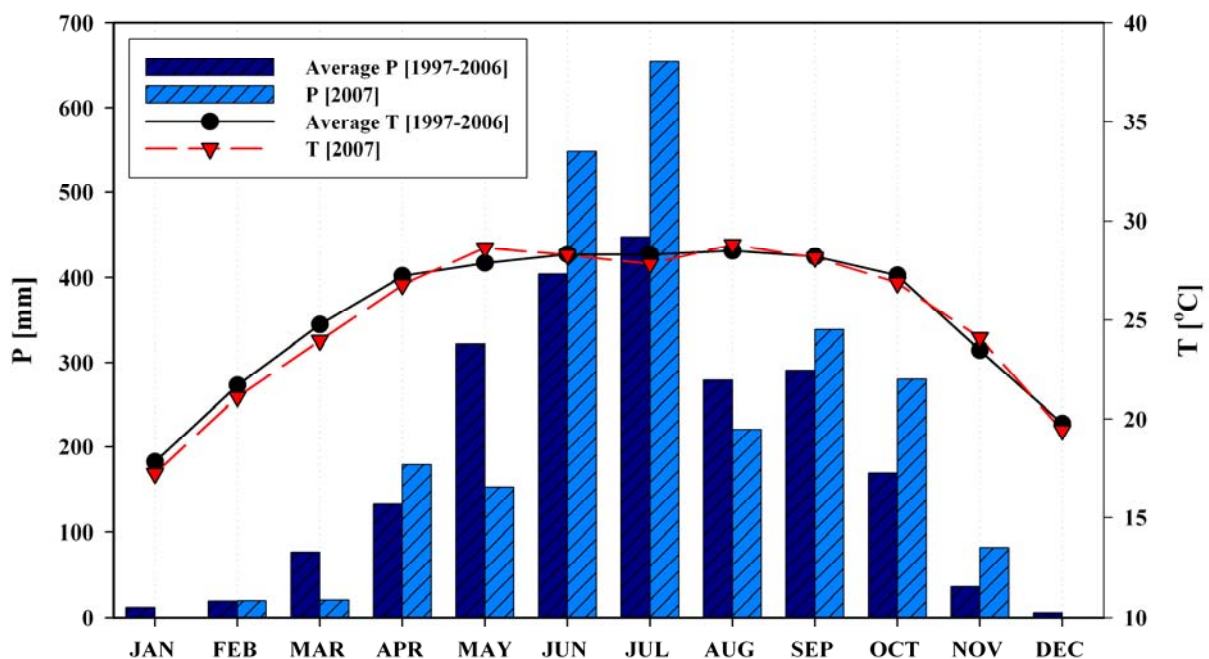


Fig. 5.2.4.1. Mean monthly precipitation and temperature over the last 10 years (1997 – 2006) in comparison to the mean monthly precipitation and temperature during the period of investigation (2007)

Meteorological data over a period of 10 years, consisting of daily rainfall, temperature, and evaporation derived from the Bangladesh Meteorological Department. In figure 5.2.4.1, the year 2007 is compared to the deposition and temperature from the last 10 years (1997 – 2006). Therefore, deposition in the year 2007 can be characterized as above averaged in comparison to the last decade. The annual rainfall in 2007 was 2497mm whereas the average of the last decade was 2197mm. Especially the monsoonal rains in the main rainy season in June (approx. 550 mm/month) and July (approx. 650mm/month) were notably heavier than the years before (see figure 5.2.4.1), whereas the May can be characterised as exceptionally hot and dry. Generally, the initiation of the monsoonal rains in 2007 was later than the average from the previous decade. The period between January and March was inconspicuous, instead of subtly lower temperatures and lower rainfall in March (see figure 5.2.4.1).

According to the Bangladesh Meteorological Department, the annual potential evaporation was measured with 13404 mm/a. To get an estimation of the amount of infiltration and run off from annual deposition, the real evaporation (ETR) was calculated by a simplified equation adapted from TURC. The choice of this equation is owed to the fact, that it is generally applicable worldwide and limited to the annual sum of deposition and average annual temperature as constituents.

$$ETR_{TURC} = \frac{P}{[0.9 + (P / I_T)^2]^{0.5}} \quad (\text{eq.6})$$

$$I_T = 300 + 25 \bullet T + 0.05 \bullet T^3 \quad (\text{eq.7})$$

ETR_{TURC} = annual value of real evaporation after TURC [mm/a]

P = annual sum of uncorrected deposition [mm/a]

T = average annual temperature [°C]

The sum of annual deposition at 2007 is 2497mm; the average annual temperature in 2007 is 25.1°C. Therefore, the real evaporation was estimated with 1439 mm/a. Consequently, 1058mm became infiltrated or ran off respectively. But as mentioned before, the calculation adapted from TURC is an imprecise method and is used merely for estimation of annual total amounts of evaporation. It does not account location, natural cover, soil composition, etc. were unaccounted for calculation and are undocumented within the study.

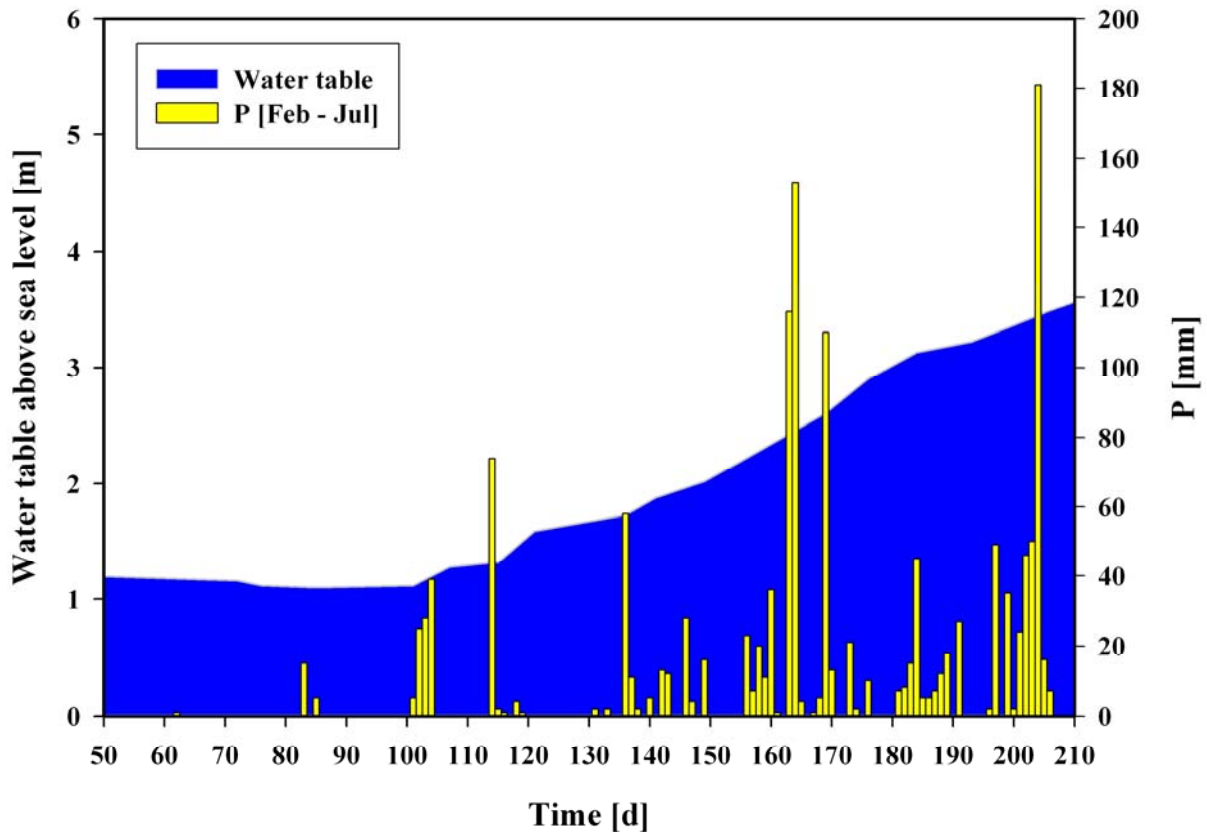


Fig. 5.2.4.2. Mean groundwater table from upper aquifer in comparison to the daily rainfall; the groundwater table was measured at the test field from February (18.02.2007) to July (25.07.2007); depths were taken by light indicator; values are averaged from all wells

As mentioned before, water tables were measured at the piezometers in addition to hydrochemical determinations. In figure 5.2.4.2, the water table above sea level is composed by the daily rainfall within the period of data acquisition from February to July. Due to the fact, that ETR according to TURC is calculable only as annual sum, it was not possible to adjust daily rainfall and evaporation.

Within the dry season, the water table at the test wells was measured with approximately 1.2 m above sea level, showing a slight decline over the months between February to April (see figure 5.2.4.2). This might be due to the intense irrigation of the surrounding crops as a consequence of low deposition during this period. In the middle of April, a distinct rise of the water table appeared due to heavy rainfalls from the so called “Nor’Westers”. Approximately 8 % of the precipitation occurred during this heavy spring-time storms and caused a water table rise of approximately 0.5 m. The first half of May is characterised by low deposition whereas the continuous monsoonal rains set in at the second half of May. Between May and

July alone, 55 % (1355 mm) of the annual deposition were released during this period and led to a rise of the water table of almost 2.1 m up to the end of the data acquisition (see figure 5.2.4.2).

To estimate the infiltration time of deposition into the upper aquifer, the kf-value was calculated based on the grain size distribution taken from sieve analysis. For this purpose, the infiltration behaviour was assumed to be vertical and the aquifer is simplified as saturated zone over the whole thickness. To estimate the kf-value from grain size distribution, the method according to HAZEN seems to be most suitable (eq.8).

$$k_{f_{HAZEN}} = 0.0116 \cdot (d_{10})^2 \quad (\text{eq.8})$$

Table 5.2.4.1. Infiltration time of deposition into the upper aquifer, estimated according to HAZEN

m/sec	m/min	m/h	m/d	m/week
1.98E-06	1.19E-04	7.12E-03	0.17	1.20

Kf-values were calculated for several zones of the aquifer, averaged and summed up to a total value (see appendix 8). Regarding the deliverables from table 5.2.4.1, infiltration water from the surface should require approximately 8 to 10 weeks before arriving a depth of 10 m. Furthermore, it should take more than half a year to influence BGL TF 115 at a depth of 36 m. But as aforementioned, the method according to HAZEN is extremely simplified with no consideration to flow conditions, distinction of saturated and unsaturated zones, rooting, etc.

As described in chapter 5.2.3, arsenic concentrations are strongly dependent on depth. But due to the fact, that Bangladesh's groundwaters are influenced by such extreme changes (as described before in this chapter) between dryness in connection with excessive irrigation and heavy monsoonal rainfalls with extensive flooding, changes in the hydrochemistry might be expectable. Figure 5.2.4.3 represents the depth and seasonal dependent distribution of total arsenic in the monitoring wells.

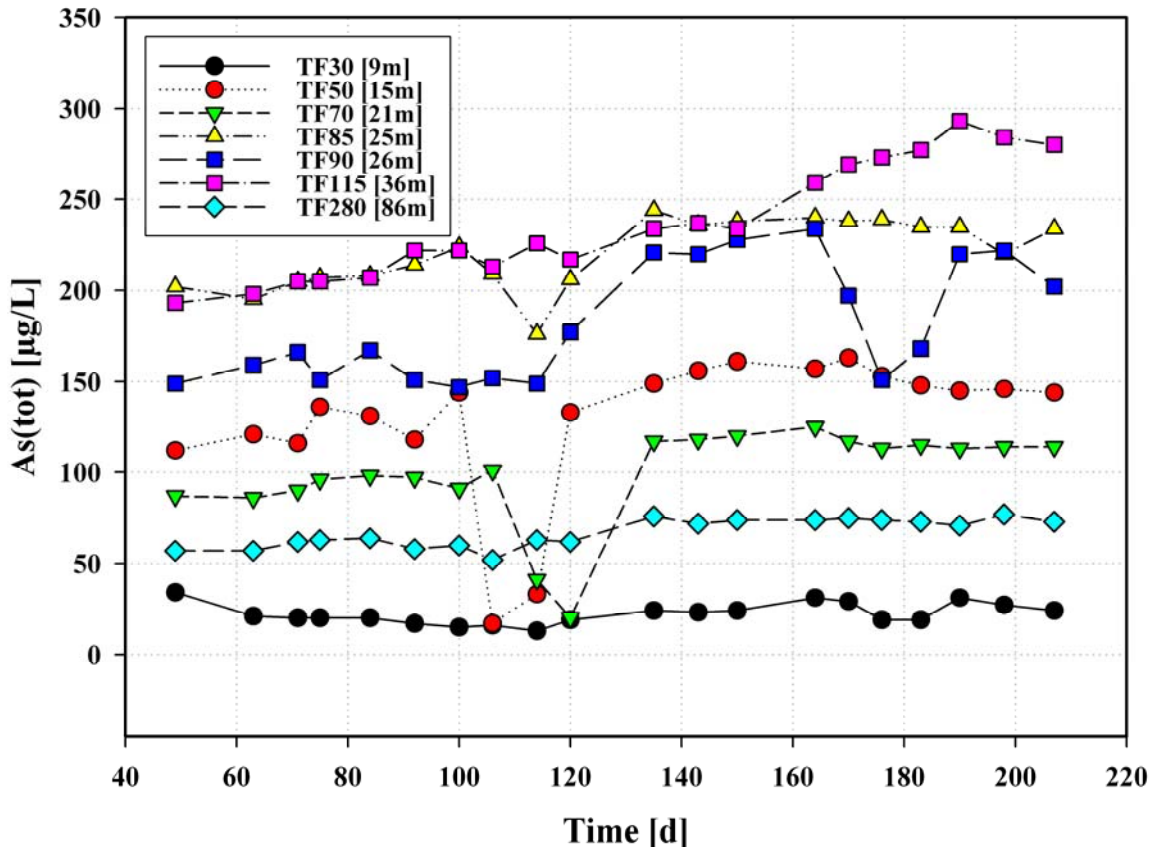


Fig. 5.2.4.3. Seasonal changes of total arsenic concentrations in different depths of the test field

It is obvious, that changing weather conditions have strong effects on arsenic concentrations. As mentioned before, heavy rainfalls appeared in the second half of April (see figure 5.2.4.2). In conjunction with this short timed storm event, a considerable degradation of the arsenic concentrations can be observed at depths between 15 and 25 m. The same downward movement is observable for phosphorus (see appendix 9). Errors in the detection of total arsenic can be excluded due to the fact that the sums of the arsenic species (measured independently from the totals) show the same decline (see appendix 2a). This gives the suggestion that dissolved arsenic has been temporary flushed away due to the infiltration of

deposition water. Noticeable changes in the mineralisation have not been detected (see appendix 10), so dilution effects can be excluded.

The intensity of degradation of the arsenic concentrations is decreasing with depth. In a depth of 15m, the arsenic concentration decreases temporary to a level of 20 µg/L, a deficit of approximately 130 µg/L. At BGL TF 70 (21 m), arsenic decreases with a delay of one monitoring campaign to a level of 20 µg/L, a deficit of 80 µg/L. Supplementary, BGL TF 85 (25 m) shows a deficit of still 50 µg/L, but increases shortly after to its maximum of 250 µg/L (see figure 5.2.4.3). Also BGL TF 50 and 70 drop back rapidly to their previous levels. At the same time, arsenic increases at BGL TF 90 from a value of 150 µg/L to 230 µg/L. It seems to be obvious that arsenic is getting vertically flushed from shallower into deeper regions of the aquifer. In comparison to the estimated infiltration time from kf, the effective infiltration time seems to be much higher.

Within the period between May (the onset of the monsoonal rains) and the end of data acquisition in July, a continuous increase in the arsenic concentrations was detected at the depths with the highest concentrations (25 – 36 m). A considerable degradation of the arsenic concentrations can be observed at BGL TF 90 between the second half of June and the second half of July. This phenomenon cannot be noticed at the other depths and the investigation of causes would be too speculative. But it seems that arsenic is getting locally flushed by horizontal groundwater flows, especially enforced in the rainy season. Therefore, it would be essential to understand the annual cycle of groundwater flow, controlled by irrigation and the groundwater recharge by rainfall.

The monitoring wells in shallower depths (21 m) have more balanced arsenic concentrations, even if the values at the rainy season are slightly increased in comparison to the dry season (see figure 5.2.4.3). BGL TF 30 is characterised by continuous low arsenic concentrations. Also BGL TF 280 shows only slight changes in arsenic concentrations over the whole monitoring campaign. This can be explained by the fact, that the recharging groundwaters are oxic, which will prevent redox processes except oxic degradation. Nevertheless, this is not true for the groundwaters from the grey Holocene fine sand. The deeper the well the higher is the arsenic concentration as well as the seasonal fluctuations.

However, these changes in the arsenic concentrations become even more apparent by consideration of arsenite. As figure 5.2.4.4 suggests, especially the deeper wells between 25 and 36 m show an obvious increase in arsenite with the beginning of the rainy season. As described in chapter 5.2.3, these depths are strongly influenced by organic matter due to a lens of silty and peaty clay. The increase in dissolved arsenite is an evidence for seasonally

occurring stronger reducing conditions, due to the massive rise of the water table. Additionally, it seems that sedimentary bounded arsenic is getting mobilised which explains the increase in total arsenic in the groundwater. As a reminder: according to the theory of reduction of arsenic-rich hydrous iron oxides (FeOOH), peat is the main redox driver and its biodegradation drives extreme degrees of FeOOH reduction and supplies high concentrations of arsenic to the groundwater. The reduction of FeOOH is accompanied by reduction of arsenate to arsenite, which explains the rise of arsenite and therefore total arsenic.

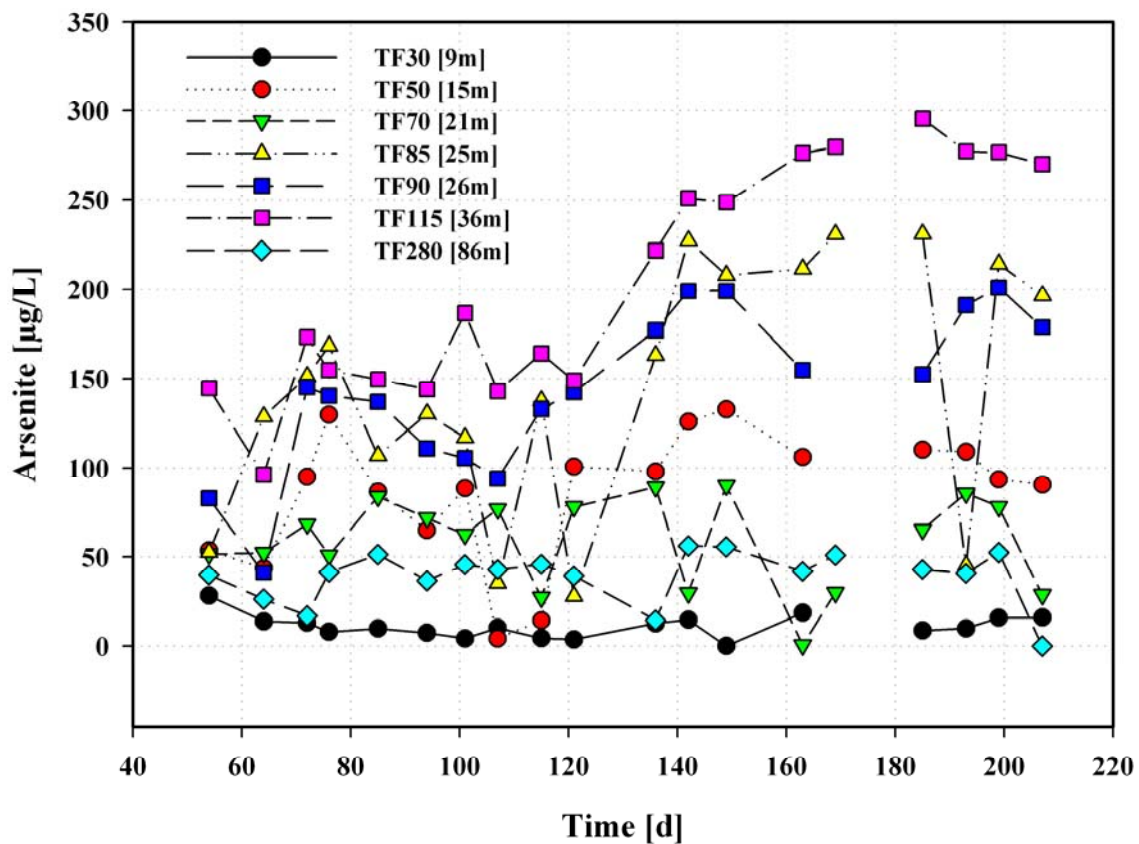


Fig. 5.2.4.4. Seasonal changes of total arsenite concentrations in different depths of the test field

In connection with an increased biodegradation of peat as the main redox driver, several authors (MCARTHUR et al., 2000; RAVENSCROFT et al., 2001) reported increased concentrations of ammonia as well as dissolved organic carbon. Additionally, increased concentrations of phosphorus in the mg/L range are released to the groundwater from the fermentation of buried peat deposits. It is not possible to give a general statement about the seasonal behaviour of dissolved phosphorus in relation to arsenic. At the shallowest well between 9 and 21 m, a significant positive correlation between arsenic and phosphorus was determined (see table 5.2.4.1). But this is not true for each depth, as table 5.2.4.1 clarifies.

Therefore, no relation between both arsenic and phosphorus was measurable at BGL TF 85, 90 and 280. BGL TF 115 (which is highest affected by arsenic), shows an inverse relation between both arsenic and phosphorus. The process behind is not yet understood clear (RAVENSCROFT et al., 2001). But it seems that the reduction of FeOOH is accompanied by a supply of high concentrations of arsenic and a displacement of phosphorus respectively. This phenomenon is not occurring in wells with low rates of biodegradation of organic matter.

Table 5.2.4.1. Well by well correlation between total arsenic and total phosphorus (P = value for statistical significance, r = correlation coefficient, n = number of samples)

	TF30	TF50	TF70	TF85	TF90	TF115	TF280
P	0.000	0.000	0.000	0.538	0.056	0.0285	0.0584
r	0.747	0.742	0.844	-0.144	0.433	-0.689	0.428
n	20	20	20	20	20	20	20

An inverse correlation was also detected between arsenic and dissolved organic carbon at BGL TF 115 ($P < 0.05$, $n = 20$; not plotted). According to RAVENSCROFT et al. (2001), dissolved organic is being degraded by driving redox processes. Due to the seasonal affective stronger reducing conditions and consequently the enlarged biodegradation of organic matter (OM), this can be an explanation for the inverse correlation.

As described in previous chapters, the concentrations for ammonia at BGL TF 115 and 280 are not representative for statements about seasonal changes. Interferences with other dissolved elements might appear, especially iron at all levels (see chapter 4.1.2.2). Since there is an detection limit of 0.5 mg/L for ammonia, determined by photometry, high dilutions at field site with a ratio of 1:400 were necessary which had adverse effects to the accuracy of measurement. However, ammonia is extremely high at BGL 115 and 280, an obvious indicator for an increased biodegradation of peat.

6. Recommendations

The present report is based on field works in Bangladesh from February to July 2007. The field work was divided mainly in two sections: a weekly monitoring at the newly drilled test wells and mapping works at the surrounding area. During the long termed data acquisition of six month, various problems and errors occurred and new ideas evolved for following studies. Therefore, some recommendations will be given in the following.

- Within a multiplicity of previous studies, shallow tube wells were tested for arsenic in Bangladesh, just as performed in this study. A fractional amount of these wells is lithological logged. It can be assumed that arsenic contaminations in the groundwater are in close connection with the sedimentary composition of the underground. Therefore, geophysical methods provide an opportunity to detect peat and clay lenses and to determine the thickness of aquifers as well as aquicludes. Both geoelectric and seismic are suitable methods for subsurface survey. Therefore, geoelectric is particularly suitable to locate clay as well as peat lenses whereas seismic is probably better suited for determining continuous layers.
- In chapter 5.2.4, the k_f -value was calculated from the grain size distribution of the samples in order to estimate the infiltration time of rain water into the upper aquifer. Therefore, the infiltration behaviour was simplified as vertical. To specify the model of groundwater circulation, it is unavoidable to perform more specific aquifer tests. Suitable methods are pumping and tracer tests in conjunction with the deliverables from sediment analysis.
- During the monsoonal rainfalls large parts of Bangladesh are flooded. However, the degree of flooding is intensified by the Ganges-Brahmaputra-Meghna river system bringing large amounts of water from India and the Himalayas and therefore large amounts of sedimentary load. Due to this fact, it could be revealing to determine the floodwater as well as its deposits for arsenic loads.

- Several authors reported good correlations between arsenic concentrations in shallow tube wells and the age of the wells. This cannot be confirmed within the recent study but it would be more meaningful to do a continuous monitoring (>5a) at selected wells.
- For hydrochemistry, redoxsensitive elements (Fe^{2+} , Mn^{2+} , NO_3^- , NO_2^- , NH_3^- , and S^{2-}) were measured by photometry at the field site. As described in previous chapters, some wells had high concentrations of dissolved iron as well as ammonia, especially BGL TF 115 and BGL TF 280. First of all, high dilutions were necessary (ammonia approx. 1:400; iron approx. 1:50), which leads to inaccuracies, due to the fact that the field equipment is exposed to a multitude of strains. This can be seen in the inhomogeneity of the values for iron and ammonia. To decrease the dilution factor (and thus inaccuracies), it is possible to use photometry programs with higher ranges (e.g. HACH method 10023 for ammonia). As described in chapter 4.1.2.2, ammonia detection can be disturbed by iron at all levels. Laboratory investigations at laboratory are necessary to determine the influence of iron on ammonia.
- The detection of fluoride and nitrite by ion chromatography can be disturbed by chloride due to similar retention times of the three anions. A shift of the retention times could therefore help to avoid these interferences and can be achieved by an eluent adjustment.

7. Acknowledgements

I like to thank the following people:

- My first supervisor Prof. Dr. Broder J. Merkel who supported this work by professional suggestions (especially at statistical problems), during the whole editing time. I also like to thank him for proofreading
- Special thanks go to Dr. Britta Planer-Friedrich for involving me in her DFG-project and for the opportunity to work abroad and to complete my study with such an impression. Her engagement, experience in the field and laboratory, availability for my asking as well as proofreading was essential for finishing my thesis
- Prof. Dr. Qumrul Hassan, Dr. Anwar Zahid and Masud Khan for my stay in Bangladesh and on-site support at Dhaka University
- Special thanks go to Rashed and Tanvir who welcomed me with amity and made my residence in Bangladesh to a unique experience. I would also like to thank their families for their kindness and hospitableness
- I like to thank my parents, who gave me the mental and financial support
- H.J. Peter and Sascha Kummer for their support at the laboratory in Freiberg (Germany)
- My friends for their support
- My fellow students for helpful suggestions

8. References

- Acharyya S. K., Lahiri S., Raymahashay B. C., and Bhowmik A.** (1999) Arsenic toxicity of groundwater in parts of the Bengal basin in India and Bangladesh: the role of Quaternary stratigraphy and Holocene sea-level fluctuation. *Environmental Geology* **39**(10), 1127-1137.
- Ahmed K. M., Bhattacharya P., Hasan M. A., Akhter S. H., Alam S. M. M., Bhuyian M. A. H., Imam M. B., Khan A. A., and Sracek O.** (2004) Arsenic enrichment in groundwater of the alluvial aquifers in Bangladesh: an overview. *Applied Geochemistry* **19**(2), 181-200.
- Alam M., Alam M. M., Curray J. R., Chowdhury A. L. R., and Gani M. R.** (2003) An overview of the sedimentary geology of the Bengal Basin in relation to the regional tectonic framework and basin-fill history. *Sedimentary Geology* **155**(3-4), 179-208.
- Alauddin M. and Quiggin J.** (2008) Agricultural intensification, irrigation and the environment in South Asia: Issues and policy options. *Ecological Economics* **65**(1), pp. 111-124
- Bhattacharya P., Jacks G., Ahmed K. M., Routh J., Khan A. A.** (2002) Arsenic in Groundwater of the Bengal Delta Plain Aquifers in Bangladesh. *Bull. Environ. Contam. Toxicol.* **69**, 538–545
- Breit G. N., Whitney J., Foster A., Welch A. H., Yount J., Sanzolone R., Islam M. K., Islam M. S., Islam M. M., Sutton S., and Newville M.** (2001) Preliminary Evaluation of Arsenic Cycling in the Sediments of Bangladesh. *USGS Report*, 4.
- DPHE** (1999) Groundwater studies for arsenic contamination in Bangladesh. Final Report. Rapid Investigation Phase. Department of Public Health Engineering, Government of Bangladesh. Mott MacDonald.
- Gault A.G., Jana J., Chakraborty S., Mukherjee P., Sarkar M., Nath B., Polya D.A., Chatterjee D.** (2004) Preservation strategies for inorganic arsenic species in high iron, low-Eh groundwater from West Bengal, India. *Anal Bioanal Chem* **381**, 347–353
- Hanrahan G., Salmassi T. M., Khachikian C. S., Foster K. L.** (2005) Reduced inorganic phosphorus in the natural environment: significance, speciation and determination. *Talanta* **66**, 435–444

Harvey C. F., Ashfaq K. N., Yu W., Badruzzaman A. B. M., Ali M. A., Oates P. M., Michael H. A., Neumann R. B., Beckie R., Islam S., Ahmed M. F. (2006) Groundwater Dynamics and Arsenic Contamination in Bangladesh. *Chemical Geology* 228 (1-3 SPEC. ISS.), pp. 112-136

Hasan M. A., v. Brömsen M., Bhattacharya P., Ahmed K. M., Sikder A. M., Jacks G., Sracek O. (2008) Geochemistry and mineralogy of shallow alluvial aquifers in Daudkandi upazila in the Meghna flood plain, Bangladesh. *Environ Geol*

Kinniburgh D. G. and Smedley P. L. (2001) Arsenic contamination of groundwater in Bangladesh. British Geological Survey & Department of Public Health Engineering.

Kinniburgh D. G. and Smedley P. L. (2002) A review of the source, behaviour and distribution of arsenic in natural waters. *Applied Geochemistry* 17, 517-568.

Kinniburgh D. G. and Smedley P. L., Davies J., Milne C.J., Gaus I., Trafford J.M., Burden S., Huq S.M.I., Ahmed N., Ahmed M.K. (2003) The scale and causes of the groundwater arsenic problem in Bangladesh. Arsenic in groundwater: geochemistry and occurrence. *Kluwer Academic Publishers*, 211-257.

Lißner H. (2008) Column experiments simulating various scenarios for arsenic mobilization in Bangladesh.- *Freiberg Online Geoscience FOG* Vol. 18, ISSN 1434-7512 (<http://www.geo.tu-freiberg.de/fog/issues.html>)

Manning B. A. and Goldberg S. (1996) Modeling competitive adsorption of arsenate with phosphate and molybdate on oxide minerals. *Soil Science Society of America Journal* 60(1), 121-131.

McArthur J. M., Ravenscroft P., Safiullah S., Thirlwall M. F. (2000) Arsenic in groundwater: testing mechanisms for sedimentary aquifers in Bangladesh. *Water Resources Research* 37(1), 109-117

McArthur J. M., Banerjee D. M., Hudson-Edwards K. A., Mishra R., Purohit R., Ravenscroft P., Cronin A., Howarth R. J., Chatterjee A., Talukder T., Lowry D., Houghton S., and Chadha D. K. (2004) Natural organic matter in sedimentary basins and its relation to arsenic in anoxic ground water: the example of West Bengal and its worldwide implications. *Applied Geochemistry* 19(8), 1255-1293.

Nath B., Sahu S.J., Jana J., Mukherjee-Goswami A., Roy S., Sarkar M.J., Chatterjee S. (2007) Hydrochemistry of arsenic-enriched aquifer from rural West Bengal, India: A study of the arsenic exposure and mitigation option. *Water Air Soil Pollut* **190**, 95–113

Nickson R., McArthur J., Burgess W., Ahmed K. M., Ravenscroft P., and Rahman M. (1998) Arsenic poisoning of Bangladesh groundwater. *Nature* **395**(6700), 338-338.

Nickson R. T., McArthur J. M., Ravenscroft P., Burgess W. G., and Ahmed K. M. (2000) Mechanism of arsenic release to groundwater, Bangladesh and West Bengal. *Applied Geochemistry* **15**(4), 403-413.

Parkhurst, D.L. (1995): Public health and regulatory aspects of inorganic nitrogen compounds in drinking water –International workshop, *Inorganic Nitrogen Compounds and Water Supply*, Hamburg

Planer-Friedrich B., London J., McCleskey R. B., Nordstrom D. K., and Wallschlaeger D. (2007) Thioarsenates in geothermal waters – determination, preservation, and geochemical role. *Environmental Science and Technology* **41**(15), 5245-5251.

Ravenscroft P., Burgess W. G., Ahmed K. M., Burren M., and Perrin J. (2005) Arsenic in groundwater of the Bengal Basin, Bangladesh: Distribution, field relations, and hydrogeological setting. *Hydrogeology Journal* **13**(5-6), 727-751.

Ravenscroft P., McArthur J., and Hoque B. (2001) Geochemical and Palaeohydrological Controls on Pollution of Groundwater by Arsenic. *Arsenic exposure and health effects* (ed. W. R. Chappell, C. O. Abernathy, and R. L. Calderon), pp. 53-78. Elsevier Science Ltd.

Rahman MM, Chowdhury UK, Mukherjee SC, Mondal BK, Paul K, Lodh D, Biswas BK, Chanda CR, Basu GK, Saha KC, Roy S, Das R, Palit SK, Quamruzzaman Q, Chakraborti D (2001) Chronic Arsenic Toxicity in Bangladesh and West Bengal, India – A Review and Commentary. *Clinical Toxicology* **39**(7), 683-700

Reimann K. U., (1993): Geology of Bangladesh – Beiträge zur regionalen Geologie der Erde. Gebrüder Bornträger, Berlin – Stuttgart

Rossum J.R. (1975) Checking the accuracy of water analysis through the use of conductivity.-J. *American Water Works Association* **67**(4), 204-205

van Geen A., Rose J., Thorai S., Garnier J., Zheng Y., and Bottero J. (2004) Decoupling of As and Fe release to Bangladesh groundwater under reducing conditions. Part II: Evidence from sediment incubations. *Geochimica et Cosmochimica Acta* **68**(17), 3475-3486.

Wallschläger D. and Staley C. J. (2007) Determination of (Oxy)thioarsenates in Sulfidic Waters. *Analytical Chemistry* **79**, 3873-3880.

Welch A.H., Lico M.S. (1998) Factors controlling As and U in shallow ground water, southern Carson Desert, Nevada. *Applied Geochemistry* **13**(4), 521-539

Zahid A., Hassan M.Q., Balke K.D., Flegr M., Clark D.W. (2007) Groundwater chemistry and occurrence of arsenic in the Meghna floodplain aquifer, southeastern Bangladesh. *Environ Geol* **54**, 1247–1260

Zheng Y., Stute M., van Geen A., Gavrieli I., Dhar R., Simpson H. J., Schlosser P., and Ahmed K. M. (2004) Redox control of arsenic mobilization in Bangladesh groundwater. *Applied Geochemistry* **19**(2), 201-214.

9. Appendix

Appendix 1a: Comparison of both measured conductivity and calculated conductivity for mapped wells (MAP) and monitoring wells from test field (TF). The percent error derive from difference between EC measured and EC calculated

Soln	Sample code	EC measured	EC calculated	deviation [EC rec - Eccalc]	Percent error	Soln	Sample code	EC measured	EC calculated	deviation [EC rec - Eccalc]	Percent error
1	TF3001	252.0	185.0	67.0	26.6	99	TF9019	460.6	309.0	151.6	32.9
2	TF3002	259.5	186.0	73.5	28.3	100	TF9020	480.0	296.0	184.0	38.3
3	TF3003	286.2	194.0	92.2	32.2	101	TF11501	2558.0	2681.0	-123.0	-4.8
4	TF3004	279.6	207.0	72.6	26.0	102	TF11502	3201.0	2620.0	581.0	18.2
5	TF3005	255.5	180.0	75.5	29.5	103	TF11503	2056.0	1803.0	253.0	12.3
6	TF3006	309.6	211.0	98.6	31.8	104	TF11504	2430.0	1844.0	586.0	24.1
7	TF3007	384.0	210.0	174.0	45.3	105	TF11505	3381.0	2564.0	817.0	24.2
8	TF3008	372.8	224.0	148.8	39.9	106	TF11506	2540.0	1856.0	684.0	26.9
9	TF3009	333.2	206.0	127.2	38.2	107	TF11507	3006.0	1919.0	1087.0	36.2
10	TF3010	243.3	175.0	68.3	28.1	108	TF11508	3840.0	2611.0	1229.0	32.0
11	TF3011	328.3	233.0	95.3	29.0	109	TF11509	1896.0	1429.0	467.0	24.6
12	TF3012	315.6	198.0	117.6	37.3	110	TF11510	2964.0	2105.0	859.0	29.0
13	TF3013	269.8	181.0	88.8	32.9	111	TF11511	3283.0	2501.0	782.0	23.8
14	TF3014	200.8	142.0	58.8	29.3	112	TF11512	3168.0	1830.0	1338.0	42.2
15	TF3015	209.8	152.0	57.8	27.6	113	TF11513	2705.0	1730.0	975.0	36.0
16	TF3016	237.5	171.0	66.5	28.0	114	TF11514	1956.0	1678.0	278.0	14.2
17	TF3017	244.5	189.0	55.5	22.7	115	TF11515	1434.0	1399.0	35.0	2.4
18	TF3018	269.5	188.0	81.5	30.2	116	TF11516	1001.0	1045.0	-44.0	-4.4
19	TF3019	236.0	158.0	78.0	33.1	117	TF11517	1130.0	1158.0	-28.0	-2.5
20	TF3020	215.2	164.0	51.2	23.8	118	TF11518	1419.0	1335.0	84.0	5.9
21	TF5001	300.6	239.0	61.6	20.5	119	TF11519	1192.0	1063.0	129.0	10.8
22	TF5002	308.4	246.0	62.4	20.2	120	TF11520	1082.0	963.0	119.0	11.0
23	TF5003	317.4	234.0	83.4	26.3	121	TF28001	2390.0	1825.0	565.0	23.6
24	TF5004	326.2	238.0	88.2	27.0	122	TF28002	2635.0	1848.0	787.0	29.9
25	TF5005	318.0	221.0	97.0	30.5	123	TF28003	2733.0	1840.0	893.0	32.7
26	TF5006	325.5	241.0	84.5	26.0	124	TF28004	2766.0	1780.0	986.0	35.6
27	TF5007	357.0	231.0	126.0	35.3	125	TF28005	2605.0	1833.0	772.0	29.6
28	TF5008	354.9	227.0	127.9	36.0	126	TF28006	2814.0	1821.0	993.0	35.3
29	TF5009	348.6	235.0	113.6	32.6	127	TF28007	2805.0	1844.0	961.0	34.3
30	TF5010	333.9	231.0	102.9	30.8	128	TF28008	3150.0	1863.0	1287.0	40.9
31	TF5011	312.0	232.0	80.0	25.6	129	TF28009	2802.0	1862.0	940.0	33.5
32	TF5012	331.1	239.0	92.1	27.8	130	TF28010	2850.0	1851.0	999.0	35.1
33	TF5013	335.4	235.0	100.4	29.9	131	TF28011	2820.0	1811.0	1009.0	35.8
34	TF5014	311.7	228.0	83.7	26.9	132	TF28012	2710.0	1834.0	876.0	32.3
35	TF5015	319.8	227.0	92.8	29.0	133	TF28013	2937.0	1845.0	1092.0	37.2
36	TF5016	292.5	218.0	74.5	25.5	134	TF28014	2892.0	1865.0	1027.0	35.5
37	TF5017	298.2	225.0	73.2	24.5	135	TF28015	2620.0	1343.0	1277.0	48.7
38	TF5018	309.0	219.0	90.0	29.1	136	TF28016	2540.0	1852.0	688.0	27.1
39	TF5019	327.3	225.0	102.3	31.3	137	TF28017	2558.0	1888.0	670.0	26.2
40	TF5020	313.5	217.0	96.5	30.8	138	TF28018	2700.0	1902.0	798.0	29.6
41	TF7001	292.2	228.0	64.2	22.0	139	TF28019	2713.8	1872.0	841.8	31.0
42	TF7002	301.0	236.0	65.0	21.6	140	TF28020	2787.0	1842.0	945.0	33.9
43	TF7003	309.6	236.0	73.6	23.8	141	MAP0101	367.5	267.0	100.5	27.3
44	TF7004	315.3	233.0	82.3	26.1	142	MAP0201	255.0	190.0	65.0	25.5
45	TF7005	315.0	228.0	87.0	27.6	143	MAP0301	298.8	235.0	63.8	21.4
46	TF7006	315.6	253.0	62.6	19.8	144	MAP0401	1084.0	890.0	194.0	17.9
47	TF7007	337.4	240.0	97.4	28.9	145	MAP0501	470.0	340.0	130.0	27.7

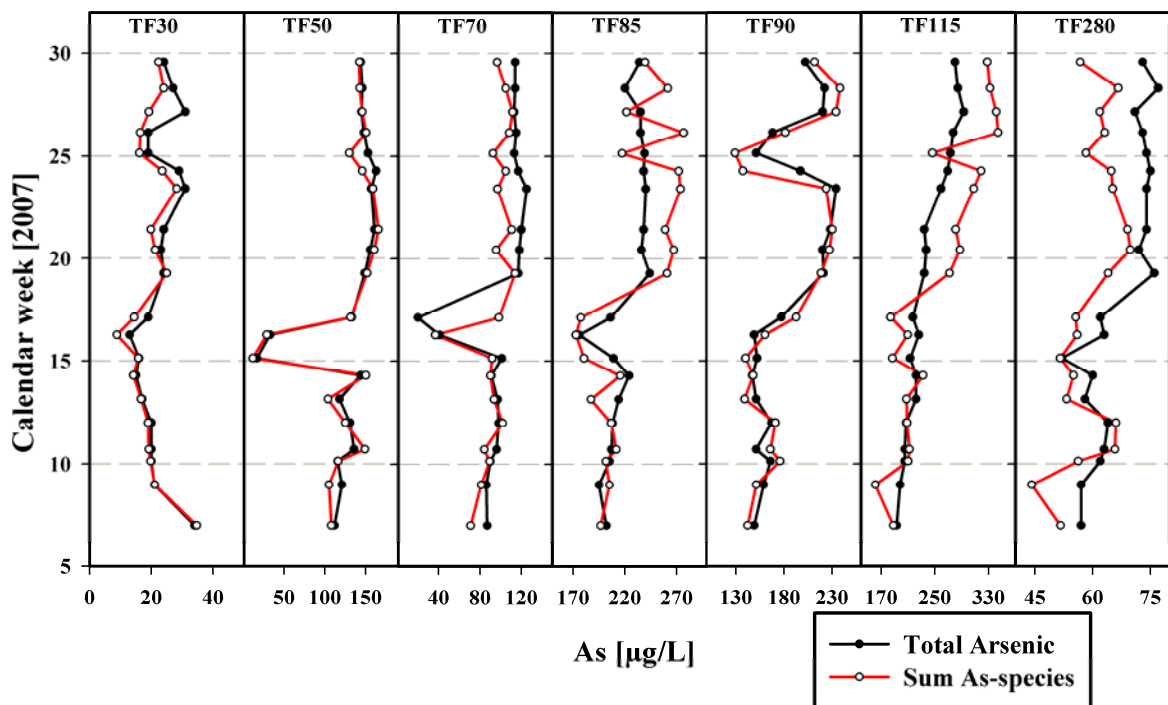
Appendix 1a (continued)

Soln	Sample code	EC measured	EC calculated	deviation [EC rec - Eccalc]	Percent error	Soln	Sample code	EC measured	EC calculated	deviation [EC rec - Eccalc]	Percent error
48	TF7008	330.4	246.0	84.4	25.5	146	MAP0601	343.0	243.0	100.0	29.2
49	TF7009	342.3	239.0	103.3	30.2	147	MAP0701	470.0	341.0	129.0	27.4
50	TF7010	320.4	227.0	93.4	29.2	148	MAP0801	380.8	292.0	88.8	23.3
51	TF7011	307.5	227.0	80.5	26.2	149	MAP0901	498.0	394.0	104.0	20.9
52	TF7012	324.6	225.0	99.6	30.7	150	MAP1001	367.5	267.0	100.5	27.3
53	TF7013	340.9	230.0	110.9	32.5	151	MAP1101	376.0	290.0	86.0	22.9
54	TF7014	316.8	212.0	104.8	33.1	152	MAP1201	934.0	753.0	181.0	19.4
55	TF7015	326.9	231.0	95.9	29.3	153	MAP1301	481.0	386.0	95.0	19.8
56	TF7016	307.8	232.0	75.8	24.6	154	MAP1401	305.1	225.0	80.1	26.3
57	TF7017	301.8	224.0	77.8	25.8	155	MAP1501	260.5	199.0	61.5	23.6
58	TF7018	305.4	217.0	88.4	28.9	156	MAP1601	308.0	244.0	64.0	20.8
59	TF7019	309.0	213.0	96.0	31.1	157	MAP1701	413.0	307.0	106.0	25.7
60	TF7020	316.2	217.0	99.2	31.4	158	MAP1801	456.0	342.0	114.0	25.0
61	TF8501	419.0	300.0	119.0	28.4	159	MAP1901	300.3	235.0	65.3	21.7
62	TF8502	436.0	312.0	124.0	28.4	160	MAP2001	270.0	203.0	67.0	24.8
63	TF8503	465.0	323.0	142.0	30.5	161	MAP2101	395.2	282.0	113.2	28.6
64	TF8504	437.0	313.0	124.0	28.4	162	MAP2201	284.4	225.0	59.4	20.9
65	TF8505	481.0	321.0	160.0	33.3	163	MAP2301	345.1	272.0	73.1	21.2
66	TF8506	471.0	329.0	142.0	30.1	164	MAP2401	309.0	240.0	69.0	22.3
67	TF8507	543.0	315.0	228.0	42.0	165	MAP2501	460.0	350.0	110.0	23.9
68	TF8508	528.0	316.0	212.0	40.2	166	MAP2601	755.0	612.0	143.0	18.9
69	TF8509	474.0	333.0	141.0	29.7	167	MAP2701	364.7	243.0	121.7	33.4
70	TF8510	501.0	326.0	175.0	34.9	168	MAP2801	353.9	233.0	120.9	34.2
71	TF8511	487.0	317.0	170.0	34.9	169	MAP2901	437.0	305.0	132.0	30.2
72	TF8512	481.0	319.0	162.0	33.7	170	MAP3001	508.0	376.0	132.0	26.0
73	TF8513	508.0	323.0	185.0	36.4	171	MAP3101	1158.0	950.0	208.0	18.0
74	TF8514	490.0	307.0	183.0	37.3	172	MAP3201	398.4	283.0	115.4	29.0
75	TF8515	478.0	309.0	169.0	35.4	173	MAP3301	331.8	244.0	87.8	26.5
76	TF8516	425.0	291.0	134.0	31.5	174	MAP3401	616.0	395.0	221.0	35.9
77	TF8517	439.0	311.0	128.0	29.2	175	MAP3501	584.0	409.0	175.0	30.0
78	TF8518	469.0	308.0	161.0	34.3	176	MAP3601	486.0	342.0	144.0	29.6
79	TF8519	435.9	301.0	134.9	30.9	177	MAP3701	388.0	241.0	147.0	37.9
80	TF8520	478.0	308.0	170.0	35.6	178	MAP3801	567.0	406.0	161.0	28.4
81	TF9001	396.8	310.0	86.8	21.9	179	MAP3901	350.0	233.0	117.0	33.4
82	TF9002	439.0	314.0	125.0	28.5	180	MAP4001	531.0	376.0	155.0	29.2
83	TF9003	419.0	308.0	111.0	26.5	181	MAP4101	389.6	275.0	114.6	29.4
84	TF9004	443.0	308.0	135.0	30.5	182	MAP4201	808.0	523.0	285.0	35.3
85	TF9005	461.0	313.0	148.0	32.1	183	MAP4301	237.0	175.0	62.0	26.2
86	TF9006	455.0	305.0	150.0	33.0	184	MAP4401	958.0	701.0	257.0	26.8
87	TF9007	482.0	310.0	172.0	35.7	185	MAP4501	581.0	404.0	177.0	30.5
88	TF9008	485.0	308.0	177.0	36.5	186	MAP4601	356.3	237.0	119.3	33.5
89	TF9009	495.0	309.0	186.0	37.6	187	MAP4701	385.6	261.0	124.6	32.3
90	TF9010	459.0	302.0	157.0	34.2	188	MAP4801	380.0	262.0	118.0	31.1
91	TF9011	491.0	333.0	158.0	32.2	189	MAP0102	383.6	278.0	105.6	27.5
92	TF9012	492.0	314.0	178.0	36.2	190	MAP0402	798.0	627.0	171.0	21.4
93	TF9013	502.0	311.0	191.0	38.0	191	MAP2502	506.0	356.0	150.0	29.6
94	TF9014	484.0	304.0	180.0	37.2	192	MAP2702	380.0	254.0	126.0	33.2
95	TF9015	475.0	298.0	177.0	37.3	193	MAP2902	499.0	350.0	149.0	29.9
96	TF9016	378.4	276.0	102.4	27.1	194	MAP4102	373.1	273.0	100.1	26.8
97	TF9017	414.0	299.0	115.0	27.8	195	MAP4202	768.0	539.0	229.0	29.8
98	TF9018	472.0	304.0	168.0	35.6	196	MAP4302	231.5	166.0	65.5	28.3

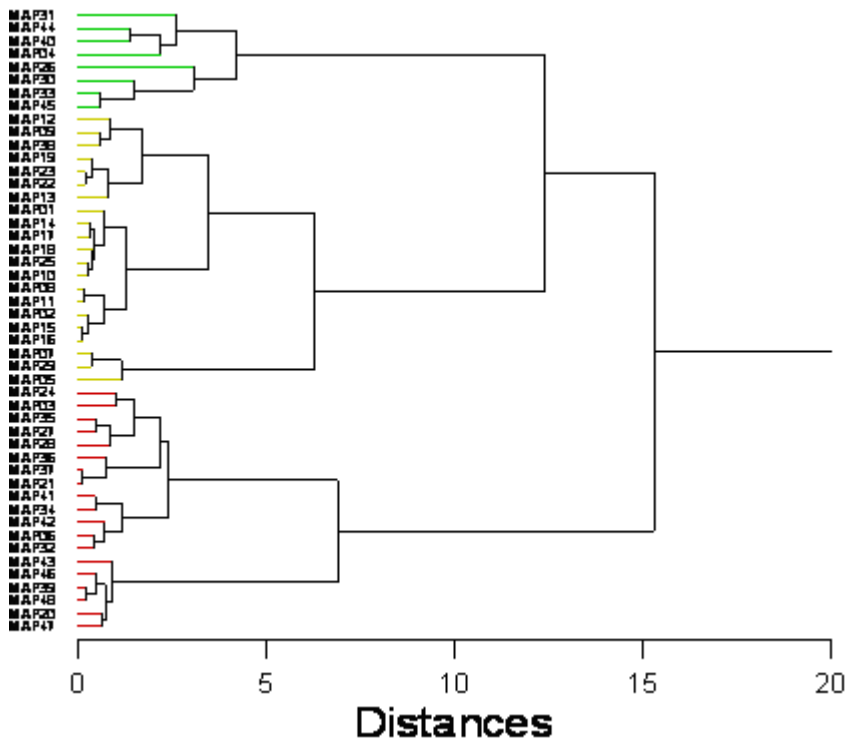
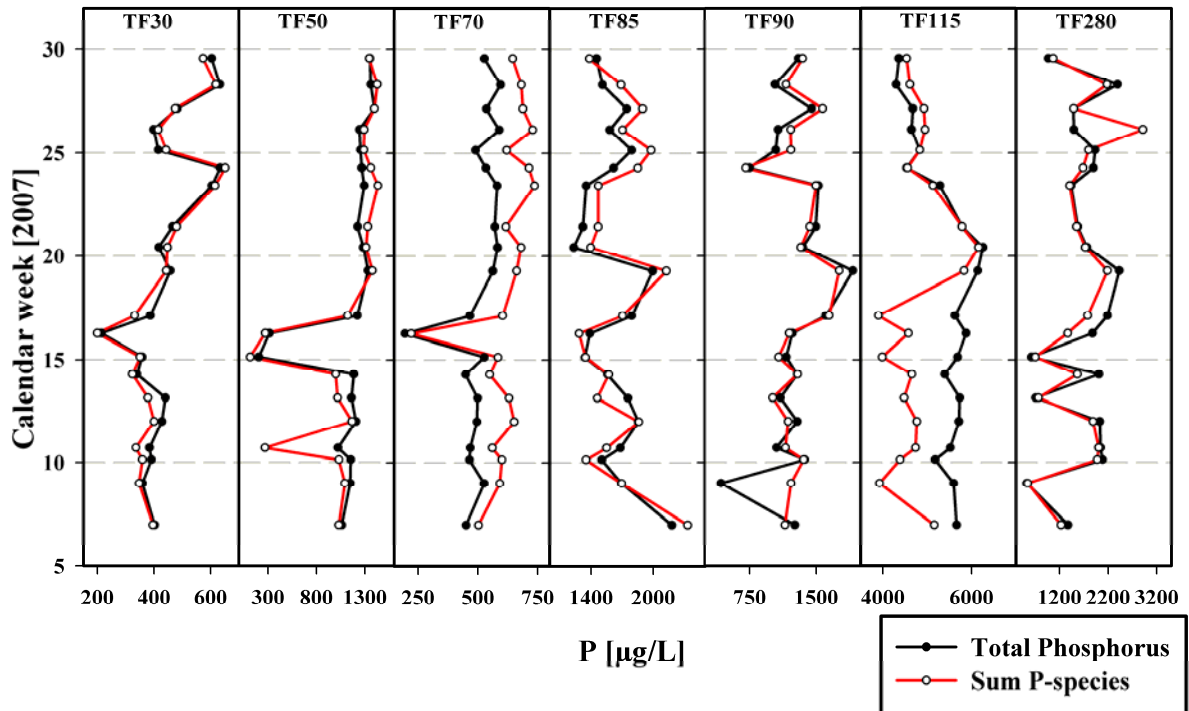
Appendix 1b: Mean percent error and mean deviation between measured and calculated conductance

Sample code	Mean percent error	Mean deviation [$\mu\text{S/cm}$]	Mean conductivity [$\mu\text{S/cm}$]
TF30	31.0	87.4	275.1
TF50	28.3	91.7	322.1
TF70	27.4	87.1	316.8
TF85	33.3	158.2	472.3
TF90	32.9	152.6	459.2
TF115	18.1	505.4	2312.1
TF280	33.4	920.3	2741.4
MAP	26.9	124.2	469.6

Appendix 2a: Comparison of total arsenic with sum of arsenic species for each monitoring well at test field



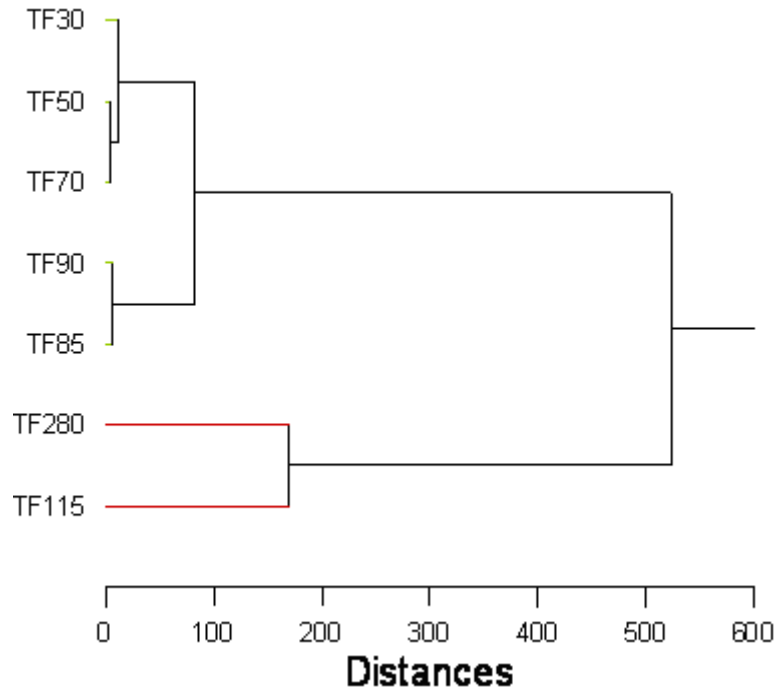
Appendix 2b: Comparison of total phosphorus with sum of phosphorus species for each monitoring well at test field



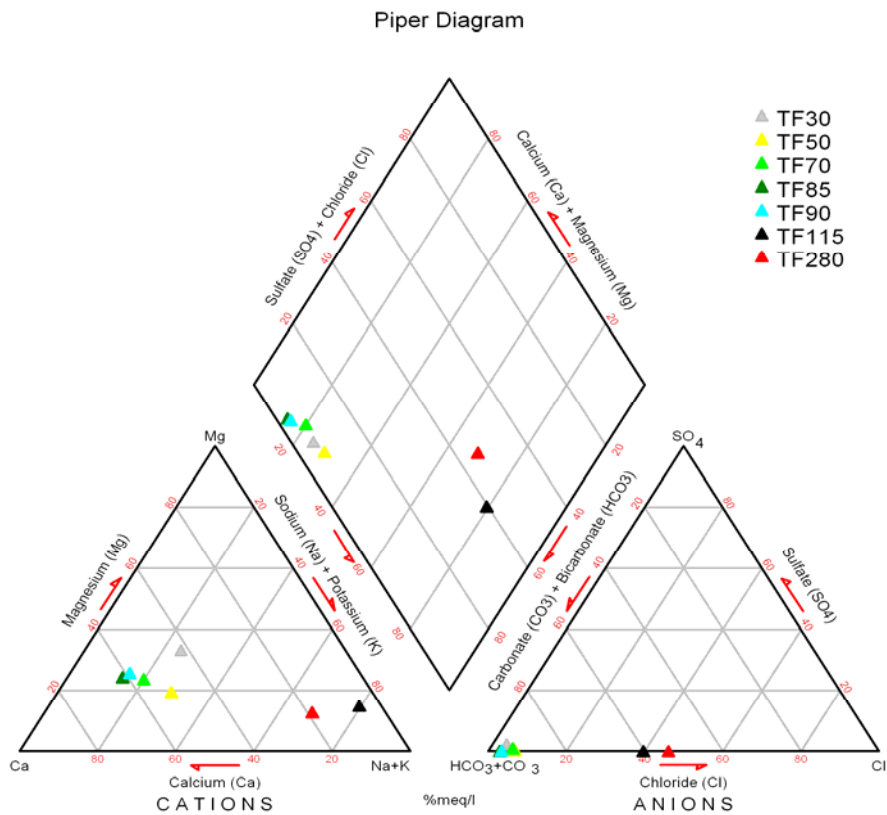
Appendix 3: Dendrogram of the hierarchical cluster analysis using the ward method showing three major groups for surrounding wells

Appendix 4: Distribution of total phosphorus and P-species at mapping wells; Rate phosphate of total phosphorus

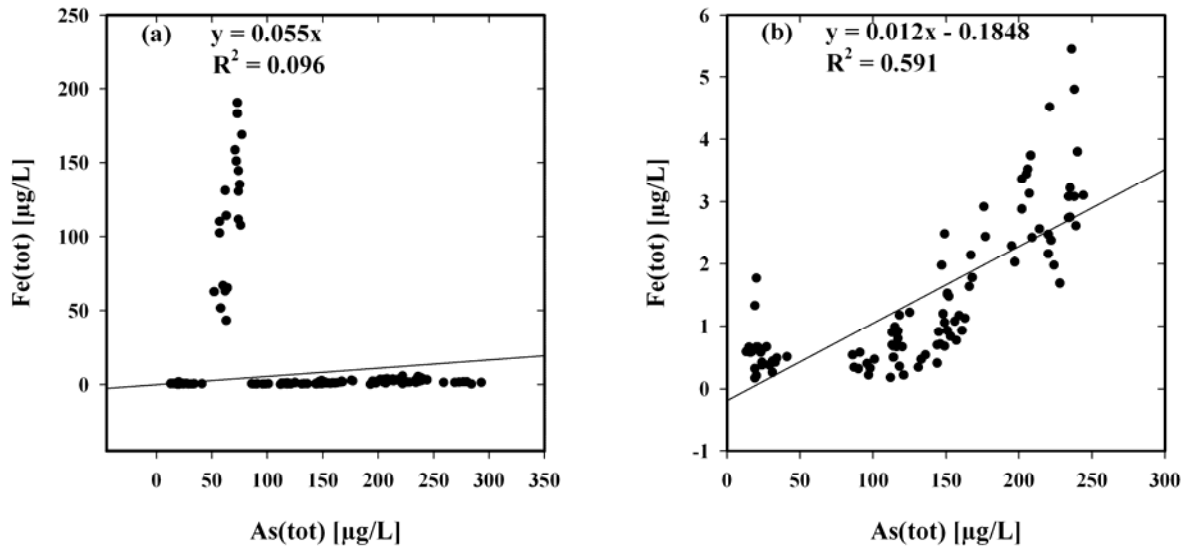
Sample code	Unidentified P-species [µg/L]	PO ₄ ³⁻ [µg/L]	Total P [µg/L]	% rate PO ₄ ³⁻ of P(tot)	Sample code	Unidentified P-species [µg/L]	PO ₄ ³⁻ [µg/L]	Total P [µg/L]	% rate PO ₄ ³⁻ of P(tot)
MAP0101	228.5	0.0	489.1	0.0	MAP2901	220.0	320.0	383.1	83.5
MAP0201	164.9	630.0	817.1	77.1	MAP3001	185.0	51.0	94.0	54.2
MAP0301	348.3	69.5	189.3	36.7	MAP3101	190.9	50.8	0.0	24.9
MAP0401	122.5	866.8	1090.7	79.5	MAP3201	13.1	231.5	260.1	-4.4
MAP0501	128.6	1815.0	1910.0	95.0	MAP3301	22.7	67.2	528.0	12.7
MAP0601	181.3	1082.5	1223.2	88.5	MAP3401	72.3	276.0	362.6	76.1
MAP0701	194.0	1111.0	1215.3	91.4	MAP3501	193.2	861.9	1133.8	76.0
MAP0801	194.2	875.0	935.7	93.5	MAP3601	205.9	185.2	353.4	52.4
MAP0901	146.8	919.7	1226.5	75.0	MAP3701	253.1	395.4	591.4	66.9
MAP1001	182.0	1317.5	1313.3	100.3	MAP3801	27.5	166.9	871.6	19.1
MAP1101	179.3	750.7	925.5	81.1	MAP3901	281.9	632.0	809.2	78.1
MAP1201	220.2	411.0	536.9	76.6	MAP4001	207.8	706.6	908.7	77.8
MAP1301	141.7	114.2	169.6	67.3	MAP4101	248.1	421.9	560.4	75.3
MAP1401	211.0	756.9	921.0	82.2	MAP4201	199.9	551.3	778.3	70.8
MAP1501	195.2	591.5	714.0	82.8	MAP4301	355.2	770.8	819.7	94.0
MAP1601	159.8	601.5	763.1	78.8	MAP4401	263.9	136.0	104.8	129.9
MAP1701	242.6	743.5	915.7	81.2	MAP4501	389.4	479.4	534.3	89.7
MAP1801	215.5	602.4	801.0	75.2	MAP4601	320.1	529.2	564.7	93.7
MAP1901	166.3	310.5	418.6	74.2	MAP4701	423.7	913.6	1023.6	89.3
MAP2001	225.0	177.0	295.2	60.0	MAP4801	336.0	394.5	405.2	97.4
MAP2101	215.0	583.8	772.9	75.5	MAP0102	379.4	373.2	456.1	81.8
MAP2201	131.1	290.8	454.0	64.1	MAP0402	208.4	780.8	873.5	89.4
MAP2301	183.3	413.5	506.8	81.6	MAP2502	284.3	291.4	296.2	98.4
MAP2401	246.1	1151.5	1204.8	95.6	MAP2702	407.5	740.5	827.3	89.5
MAP2501	177.1	216.6	382.3	56.7	MAP2902	323.4	326.1	354.2	92.1
MAP2601	173.8	73.1	40.2	181.6	MAP4102	325.9	552.1	629.3	87.7
MAP2701	264.2	579.6	798.2	72.6	MAP4202	254.5	602.3	801.5	75.1
MAP2801	44.0	359.2	391.5	91.7	MAP4302	397.8	696.8	807.2	86.3



Appendix 5: Dendrogram of the hierarchical cluster analysis using the ward method showing two major groups for the major ions from monitoring wells



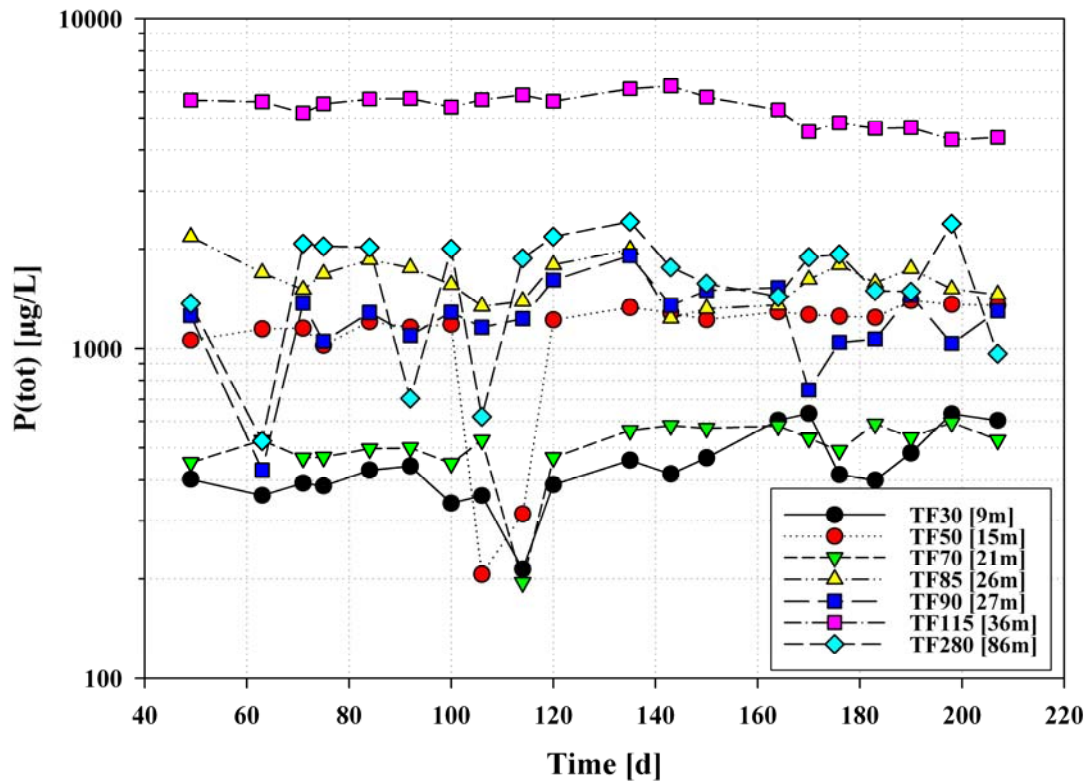
Appendix 6: Piper diagram, showing the determination of major cations and anions at the monitoring wells in different depths, divided in 2 major groups: Group I (TF30, TF50, TF70, TF85, TF90): Ca and HCO_3^- dominated; Group II (TF115, TF280): Na and HCO_3^- dominated



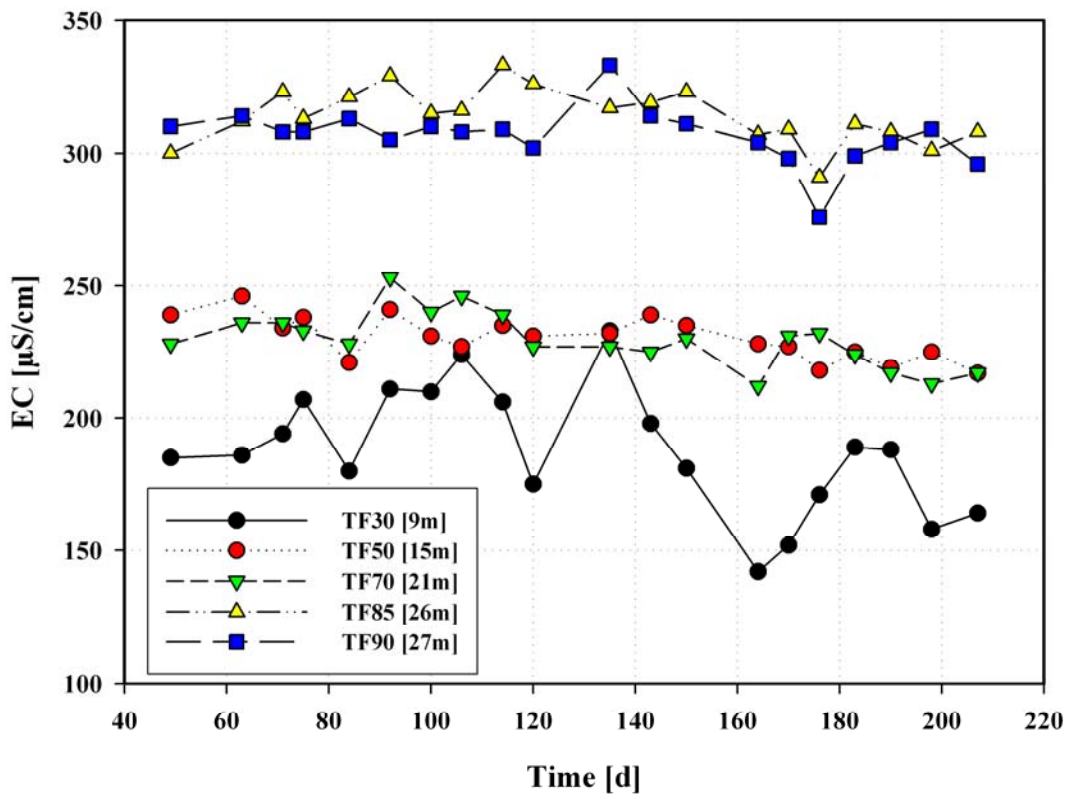
Appendix 7: Total arsenic vs. (a) total iron (at the sections I – IV; n = 140), (b) total iron (at section I and II; n = 100) Data-points derive from monitoring between February and July

Appendix 8: Averaged kf for the upper aquifer at the core drilling at hospital ground, depending on the method after HAZEN. Grain size distribution was done by sieve analysis

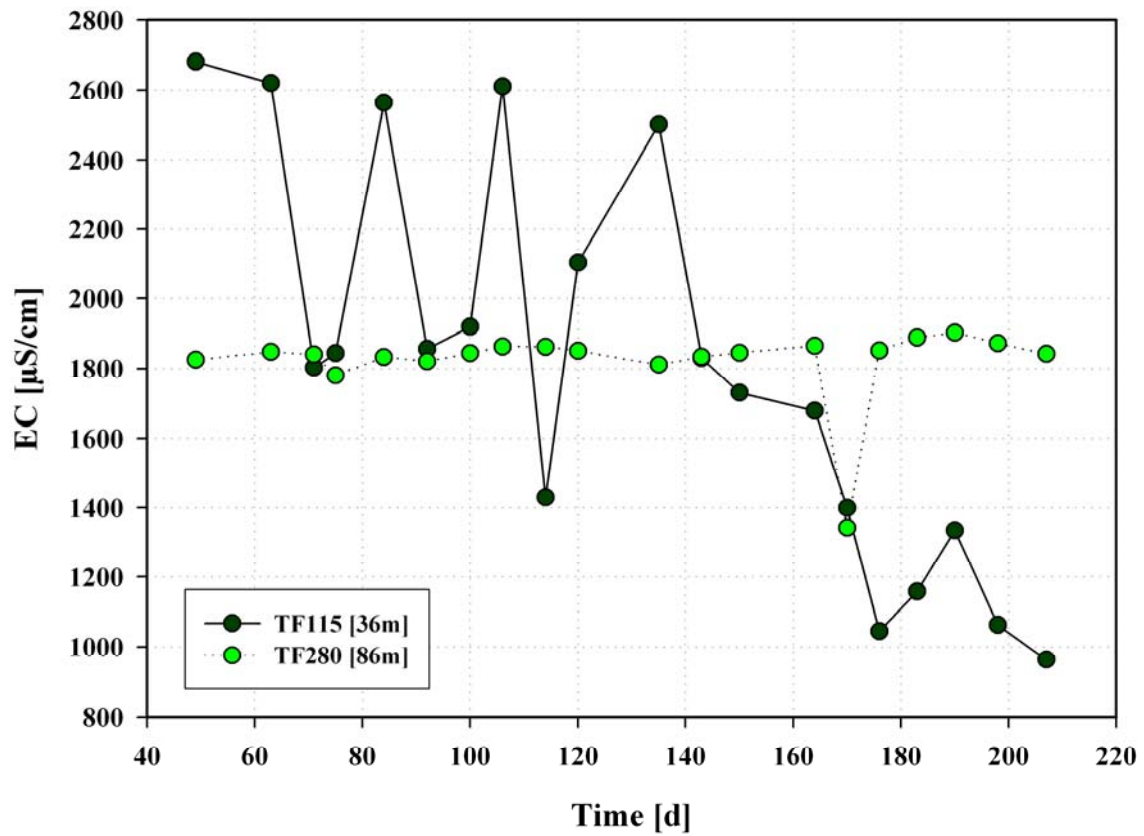
Sample-code	d10 [mm]	d60 [mm]	HAZEN kf = $0.0116 \cdot (d10)^2$	from [m]	to [m]
BAN-3	0.010	0.10	1.16E-06	0.0	6.7
BAN-4	0.015	0.12	2.61E-06	7.6	8.2
BAN-5	0.010	0.13	1.16E-06	9.1	9.8
BAN-6	0.008	0.08	7.42E-07	10.7	11.3
BAN-7	0.010	0.16	1.16E-06	12.2	12.8
BAN-8	0.012	0.15	1.67E-06	13.7	14.3
BAN-9	0.010	0.15	1.16E-06	15.2	15.8
BAN-10	0.012	0.15	1.67E-06	16.8	17.4
BAN-11	0.009	0.15	9.40E-07	17.4	18.9
BAN-12	0.015	0.12	2.61E-06	18.9	19.5
BAN-13	0.015	0.12	2.61E-06	19.5	20.1
BAN-14	0.013	0.13	1.96E-06	20.1	20.7
BAN-15	0.013	0.13	1.96E-06	20.7	21.3
BAN-16	0.011	0.12	1.40E-06	21.3	21.9
BAN-17	0.012	0.10	1.67E-06	21.9	22.6
BAN-18	0.012	0.10	1.67E-06	22.6	23.2
BAN-19	0.010	0.09	1.16E-06	23.2	23.8
BAN-20	0.010	0.09	1.16E-06	23.8	24.4
BAN-22	0.018	0.19	3.76E-06	24.4	25.0
BAN-23	0.020	0.30	4.64E-06	25.0	25.6
BAN-24	0.020	0.30	4.64E-06	25.6	26.2
Mean:	0.013	0.14	1.977E-06		



Appendix 9: Seasonal changes of total phosphorus concentrations in different depths of the test field



Appendix 10a: Seasonal changes of EC in different depths (9 – 27 m) of the test field



Appendix 10b: Seasonal changes of EC in different depths (115 – 280 m) of the test field